1-1-2003

Bond of reinforcement in concrete with different types of corroded bars

Assem Adel Abdel Aal Hassan
Ryerson University

NOTE TO USERS

This reproduction is the best copy available.

UMI®

BOND OF REINFORCEMENT IN CONCRETE WITH DIFFERENT TYPES OF CORRODED BARS

By

Assem Adel Abdel Aal Hassan
Master of Science in Structural Engineering,
Ain Shams University, Cairo, Egypt 1999

A Thesis

presented to Ryerson University

in partial fulfillment of the

requirements for the degree of

Master of Applied Science

in

Civil Engineering

Toronto, Ontario, Canada, 2003

©(Assem Hassan) 2003

UMI Number: EC52875

INFORMATION TO USERS

The quality of this reproduction is dependent upon the quality of the copy submitted. Broken or indistinct print, colored or poor quality illustrations and photographs, print bleed-through, substandard margins, and improper alignment can adversely affect reproduction.

In the unlikely event that the author did not send a complete manuscript and there are missing pages, these will be noted. Also, if unauthorized copyright material had to be removed, a note will indicate the deletion.

Borrower's Page

No.	Borrower's Name	Address	Phone No.	Date	Signature
1					
2					
3					
4					
5					
6					
7					
8					
9					
10					
11					
12					
13					
14					
15					
16					
17					
18					
19					
20					
21					
22					
23					
24					
25					
26					
27					
28					
29					
30					

BOND OF REINFORCEMENT IN CONCRETE WITH DIFFERENT TYPES OF CORRODED BARS

By

© Assem Adel Abdel Aal Hassan 2003

Master of Applied Science
in
Civil Engineering
Ryerson University
Toronto, Ontario, Canada

ABSTRACT

Repair and rehabilitation of existing structures is becoming a major part of the present construction activities. Corrosion of reinforcement is a major contributing factor to the deterioration of reinforced concrete steel structure. Corrosion of reinforcing steel severely influences the bond at the steel-concrete interface.

The aim of this research is to study the effect of corrosion on bond strength using pullout specimens and four different types of concrete having three different types of steel embedded. The study is conducted for four levels of corrosion ranging from uncorroded to severely corroded specimens. The four concrete types used were fly ash concrete mixture, silica fume concrete mixture, normal Portland cement (NPC) concrete mixture with a water/cement ratio (w/c) of 0.32, and a 0.52 w/c ratio concrete mixture. Each type of these concretes has three different types of steel embedded in them: regular carbon, stainless, and epoxy coated steel bars. The relationship between the bond strength, weight loss and the rib profile loss is studied. The results showed preference for using regular carbon steel bars than stainless steel bars, stainless steel bars exhibited badly damaged shape with lots of voids compared to the regular carbon steel bars. Also, the bond strength for corroded and un-corroded stainless steel bars was lower than that of the regular carbon steel bars. Low levels of corrosion (about 0.5 to 1 % of mass loss) were noted to improve the bond strength slightly when using either regular carbon steel bars or stainless steel bars

embedded in any type of the concrete mixtures. However, bond strength decreases rapidly with an increase in the corrosion level for both regular carbon and stainless steel bars in any type of the concrete mixtures used. The use of supplementary cementing materials (SCM) such as fly ash and silica fume was very effective in delaying the corrosion process compared to that of NPC concrete with no SCM. Also, the bond performance of any steel bars embedded in NPC concrete with low w/c (0.32) was found to be superior to that of a concrete mixture with high w/c (0.52). However, the bond strength for F.A and S.F concrete was slightly lower than that of the NPC concrete with 0.32 w/c ratio.

ACKNOWLEDGMENT

I would like to express my deepest gratitude and appreciation to Dr. Lamya Amleh for her continuous advise through the whole research, her support and valuable remarks was greatly useful and helpful to achieve effective and beneficial results.

The experimental work was carried out at the Ryerson University Civil Engineering Department concrete laboratory. The great help of the department and the laboratory technical staff is highly appreciated.

The contribution of the Ministry of Transportation concrete section engineer Franc Pianca for permitting to use of the ministry concrete labs to perform some specialized tests, was extremely helpful in completion the research in high performance manner.

My worm and sincere thanks to my mother and father for their valuable support, assistance, and endless help, throughout all the stages of the research. A special thanks is also for my sister and my brothers for their support and constant encouragement.

A special gratitude is owed to my wife sherine for her infinite love and tender, without her support, patience, and encouragement, the completion of this research would not have been possible to me. Therefore, I embrace the opportunity to dedicate this thesis to her.

To My Wife

Sherine

TABLE OF CONTENTS

CHAPTER 3: BOND PERFORMANCE

CHAPTER 4: MATERIALS AND EXPERIMENTAL PROGRAM

CHAPTER 5: TEST RESULTS

CHAPTER 6: CONCLUSIONS AND RECOMMENDATIONS

LIST OF FIGURES

LIST OF TABLES

LIST OF SYMBOLS

HPC   High performance concrete

SCM   Supplementary cementing material

CH   Calcium hydroxide

NaCl   Sodium chloride

NPC   Normal Portland cement

C-S-H   Calcium silicate hydrate

S.F   Silica fume

F.A   Fly ash concrete

w/c   Water-to-cement ratio

w/cm   Water-to- cementitious materials ratio

f_c concrete compressive strength

f_t splitting tensile strength

RCS   Regular carbon steel

CHAPTER 1

INTRODUCTION

1.1 General

Recently the aspects of concrete durability and performance have become a major subject of discussion especially when the concrete is subjected to a severe environment. Corrosion of steel bars is the main factor influencing both the concrete durability and strength. The corrosion products of the steel reinforcement expand up to seven times the original size, developing high pressures within the concrete, which cause cracking and spalling of the concrete cover and expose the rebar to further corrosion activity.

"In the United States, there are more than 581,000 bridges in the national highway infrastructure system. Nearly 32% of these bridges are listed as structurally deficient or functionally obsolete. The cost of repairing and replacing these bridges is estimated at $100 billion, and approximately 20 percent of the total estimated cost is due to the corrosion deterioration of concrete bridges. Based on the information provided by the Strategic Highway Research Program (SHRP), it is estimated that the cost of the corrosion damage in the United States transportation system now stands at over $20 billion, and it is increasing at the rate of $500 million per year. From a survey of collapsed buildings in England from 1974 to 1978, eight concrete building structures collapsed because of the corrosion of the steel reinforcement. In 1975, the U.S. Interstate Highway System alone reported the need for US $6 billion for repair and replacement of reinforced concrete bridge decks. In addition, it was reported that at least 4800 of the 25000 bridges in the State of Pennsylvania were found to be in dire need of repair" (Amleh 2000).

Bond stress is the shear stress over the surface of the bar, and is defined as the change in the force within the reinforcing bar divided by the area of that bar surface over which the change in the force takes place. Bond stress initially comes from weak chemical bonds between steel and hardened hydrated cement paste in the concrete, but

1

this resistance is broken at a very low stress. Once slip occurs, friction contributes to the bond, but with increasing slip between bar and concrete, bond comes to depend principally on the bearing of the lugs on the concrete, or mechanical interlock of the ribs rolled on the surface of the bar with the concrete. In this stage, the reinforcing bar generates bursting force tends to split the surrounding concrete. However the resistance provided by the concrete cover and the confining reinforcement may limit the failure load. Many researchers have investigated the effect of reinforcement corrosion on the bond strength and noted a significant decrease in the bond strength with the increase in the level of corrosion. They attribute the degradation of the bond strength to the formation of weak and friable material between the bar and the concrete. They also found that the increases in the diameter of the corroded bar develops a longitudinal cracks which reduce the resistance to the bursting forces generated by bond action and cause a great bond degradation.

Corrosion could be expected to affect bond strength between the steel reinforcement and concrete. the expansion due to the corrosion products at first increases radial stresses between bar and concrete and hence increase the frictional component of bond. However, further corrosion develops longitudinal cracking and reduction in the resistance to the bursting forces generated around the steel bar. Some researchers suggest that a firmly adherent layer of rust may contribute to an enhancement in bond strength at early stages of corrosion (Al- Sulaimani et al 1990), but at more advanced stages of corrosion, weak and friable material between bar and concrete will certainly be at least partially responsible for the reduction in bond strength (Cabrera and Ghodussi 1992).

Corrosion reduces the ribs height of the deformed bar which causes reduction in the contact area between the ribs and the concrete leading to reduction in the bond strength. This is usually happened at advanced stages of corrosion. Corrosion also may affect the rib face angle in the advanced stages; moreover ribs of deformed bars will eventually be lost at high level of corrosion. Corrosion of reinforced bar is usually associated with the increase of the crack width. The increase of the corrosion products around the bar leads to increase of bursting force and tension cracking of the

2

surrounding concrete, as the corrosion increase, the cracks width becomes wider and the bond strength decreases.

1.2 Scope and objectives

The main objective of this research is to study the effect of corrosion on bond strength using four different types of concrete with three different types of steel embedded. The study is conducted for four levels of corrosion, from uncorroded bars to extreamly corroded bars. The four concrete types used were fly ash concrete mixture, silica fume concrete mixture, normal Portland concrete mixture with a water to cement ratio (w/c) of 0.32, and a high water to cement concrete mixture (0.52). Each type of these concretes has three different types of steel embedded in them: regular carbon, stainless, and epoxy-coated steel bars. The surface of the cross-sectional area of the embedded end of the epoxy-coated bars was left uncoated after cutting the bars to the required lengths. The cross-sectional area was left uncoated to study the effect of corrosion concentration in a small area on the concrete cracking.

1.3 Thesis structure

The thesis consist of six chapters, a brief description of the contents of each chapter is included.

Chapter 1: Introduction to the research

Chapter 2: The bond mechanism, This chapter deals with the following; Description of the bar-concrete interaction, the effect of bar profile, shape and geometry on the bond strength, and the effect of casting position on the bond strength.

Chapter3: Bond performance in different concrete and steel types,This chapter deals with the following; The performance of bond in high performance concrete, the performance of bond for epoxy-coated bars and the performance of bond for corroded bars

Chapter 4: Materials and test methods, This chapter deals with the following; Description of the research experimental work, the concrete mix parameters, the physical, chemical, and mechanical properties of the materials used, the properties of the concrete mixture including the test results of the fresh and hardened concrete, and description of specimens preparation and the tests setup

Chapter 5: Test results and discussion for accelerated corrosion specimens, This chapter summarize the test results of the following; The current measurements for the specimens tested and comparison of the corrosion times, the results of the pullout test for uncorroded bars and for different degrees of bars corrosion, and a comparison between the bond strength of the regular carbon steel bars and stainless steel bars in the bond strength at different degrees of corrosion as a percentage of the weight loss and the percentage of rib profile loss.

Chapter 6: Conclusions and recommendations; the conclusions are drown from the investigation, and suitable recommendation for further research are made in this chapter.

CHAPTER 2
THE BOND MECHANISM

2.1 Introduction

Bond between reinforcement and concrete is necessary to ensure composite action of the two materials. The normal assumptions of plain section behavior used in section analysis and design rely on composite interaction being achieved. Bond stress is the shear stress over the surface of the bar. which is a considerably simplified representation of the "actual" conditions. Bond stress is defined as the change in the force within the reinforcing bar divided by the area of that bar surface over which the change in the force takes place. In other words, bond stress is the shear stress transferred from the concrete to the reinforcing bar to change the bar stress from point to point which depends on the development length and the change in the bending moment along the member.

Bond stress initially comes from the weak chemical bonds between the steel and the hardened hydrated cement paste of that concrete, but with a little increase of the applied load on the steel bar this resistance is lost. Once slip occurs, friction contributes to the bond. but with increasing slip between the bar and the concrete, bond resistance is derived principally from the bearing, or mechanical interlock, of the ribs on the surface of the bar with the concrete. At this stage. the reinforcing bar generates bursting forces results from the horizontal component of the force acting between the concrete and the rib face angle. This force tends to split the surrounding concrete, and the resistance provided by the concrete cover and the confining reinforcement to these bursting forces may limit the failure load.

2.2 Bar-concrete interaction

Based on a previous study by Leroy et al (1967). the force in the steel bar that is transmitted to the surrounding concrete by bond can be classified into three components:

5

(a) Chemical adhesion, (b) Friction, (c) Mechanical interaction between the concrete and the steel.

Bond of plain bars depend primarily on the first two elements in addition to the effect of the end anchorage, although there is some mechanical interlocking due to the roughness of the bar surface. Deformed bars, however, depend primarily on mechanical interlocking for superior bond properties. This does not mean that friction and chemical adhesion are negligible in the case of deformed bars, but that they are secondary. However, the scientists, who have contributed to the knowledge of the many aspects of bond (Task group bond model 2000), agree that the interaction between the concrete and the bar subjected to a tensile force is characterized by four different stages (Fig.2.1), these stages are:

- Stage I (Uncracked stage)

- Stage II (Microcracks)

- Stage III (splitting cracking)

- Stage IVa (Bond failure of plain bars)

- Stage IVb (Bond failure of deformed bars surrounded by light confinement)

- Stage IVc (Bond failure of deformed bars surrounded by heavy confinement)
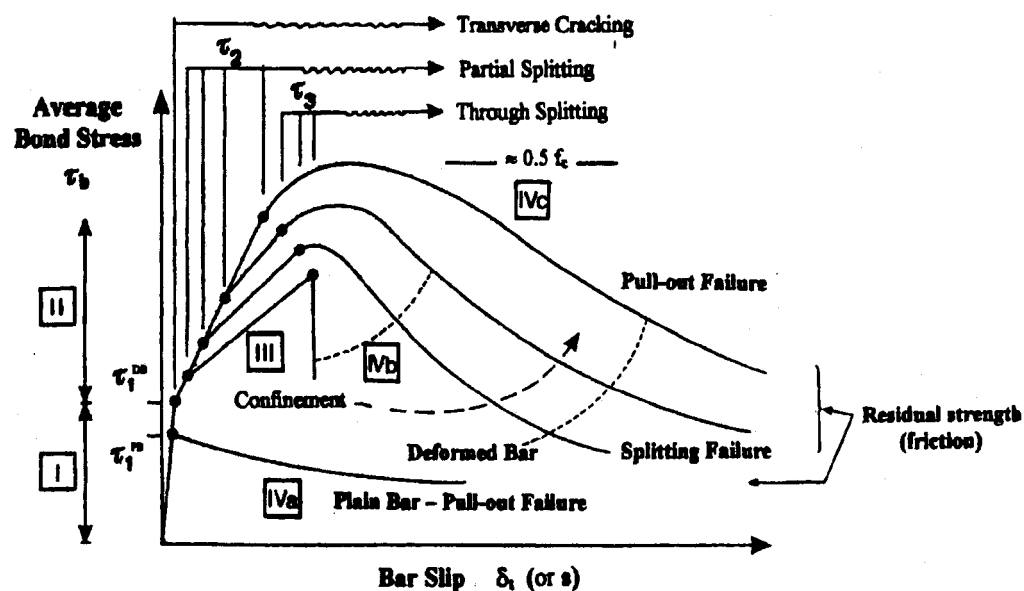
Figure 2.1: Local bond stress-slip law (Task group bond model 2000)

Stage I (Uncracked stage)

The maximum bond stress that the plain bar can resist without slipping is defined as τ_1^{ps} (Fig. 2.1). At this stage, the bond stress (τ) is less than the maximum bond stress τ_1^{ps}, and chemical adhesion is responsible for the bond efficiency, and no bar slip occurs, however localized stress occurs close to the lug tips. Choi and Lee (2002) found that adhesion ranges from 1.0 to 2.0 MPa, is appropriate for the analysis of the bond of deformed bars and concrete.

ACI Committee 408 (1991) suggested that the bond strength due to adhesion is between 0.48-1.03 MPa. Cairns and Abdulla (1994) studied the adhesion between the concrete and steel plates; they compared the bond characteristics at the interface of a steel plate with mill-scale, and the concrete with that of a fusion-bonded epoxy-concrete interface. Specimens were cast in which the concrete was sandwiched between two plates of steel and two plates of steel with epoxy coating. A normal stress of 9 MPa was applied to the specimen prior to loading it in shear until a slipping failure occurred. They observed minimal adhesion in the case of the coated plates, and the coated plates were noted to be clean after failure, while the uncoated plates were covered with a layer of crushed mortar.

Stage II (Microcracks)

The maximum bond stress that the deformed bar can resist without occurring a transverse microcracks is defined as τ_1^{DS} (Fig. 2.1). At this stage, the bond stress (τ) is higher than τ_1^{DS}, the chemical adhesion breaks down at this stage, the lugs induce large bearing stresses in the concrete p* (defined as the reaction of the bar lugs bearing against the concrete) (Fig. 2.2.a) and transverse microcracks originate at the tips of the lugs as well as compressing of the porous concrete in front of the lug (in some cases due to lack of compaction) allowing the bar to slip, but the wedging action of the lugs remain limited and there is no concrete splitting. (Fig. 2.2.b)

7

Stage III (splitting cracks)

At this stage, when continuous increase of bond stress takes place, the longitudinal cracks (splitting cracks) spread radially, owing to the wedging action, which is enhanced by the concrete crushing in front of the lugs (Fig. 2.2.c).

It was observed by Rehm (1968) that the slip resistance upon reloading is considerably higher than the slip resistance found initially, which was attributed to the ribs that are bearing against the compacted nonporous crushed concrete at the second loading compared with the porous intact concrete during the initial loading. Fig. 2.3 shows a decrease of the slip resistance for the deformed bars after reloading when the rib face angle is greater than 40 °.
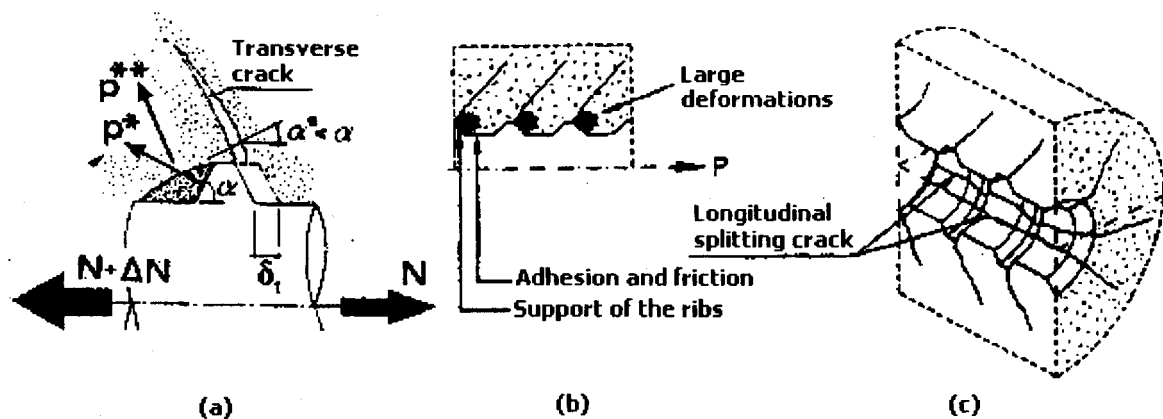
Figure 2.2: (a) Bar-concrete slipping and wedging action of the bar; (b) friction and bearing action; (c) transverse cracking and splitting (Task group bond model 2000)
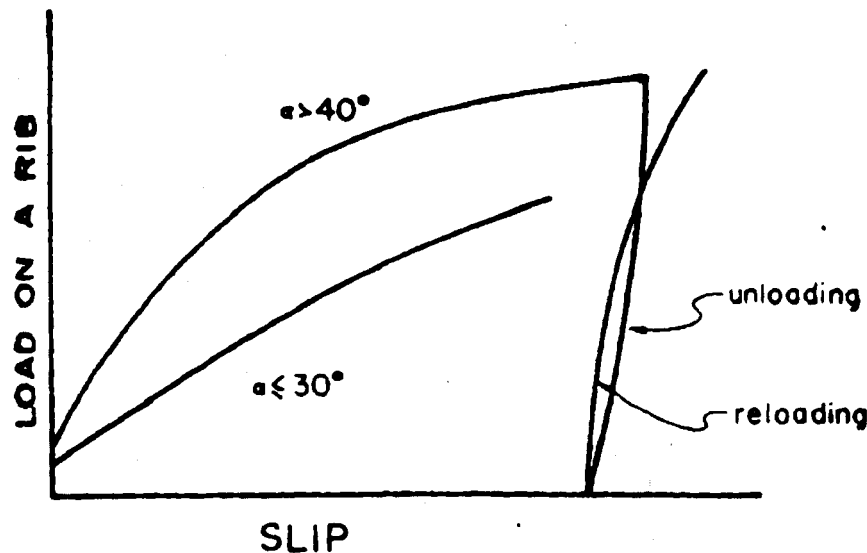
Figure 2.3: Load slip curve for the action in front of every rib

(Rehm 1968)

Stage IVa (Bond failure of plain bars)

As explained earlier, in the case of plain bars, the bond resistance is assumed to be chemical adhesion between the mortar paste and the bar surface, however, low stresses will cause sufficient slip to break the adhesion between the concrete and the steel. Once slip occurs, further bond resistance is developed only by friction and by the wedging action of small dislodged sand particles between the bar and the surrounding concrete. This stage immediately follows the depletion of adhesive bond, and failure occurs when the adhesion and friction resistance is overcome, and the bars usually pull out from the encasing concrete.

Stage IVb (Bond failure of deformed bars surrounded by light confinement)

The bond in this stage tends to fail abruptly in the case of deformed bars surrounded by light confinement; the longitudinal cracks accompanied by slip on the rib face break out through the entire cover thickness (Fig. 2.4c).

9

In the case of sufficient amount of transverse reinforcement (medium confinement) is provided, a longitudinal cracks accompanied by crushing or shearing-off in the concrete below the ribs will occur through the entire cover thickness (Fig. 2.4b). The bond stress values as high as (1/3 −1/2) f_c can be developed during this stage, with the unavoidable and often unacceptable side-effect represented by very high slip values.

Stage IVc (Bond failure of deformed bars surrounded by heavy confinement)

In the case of deformed bars surrounded by heavy confinement, splitting does not occur and bond failure is caused by bar pullout. The force transfer mechanism changes from rib bearing to friction along the vertical line between the tops of the ribs as seen in Figure 2.4a. Under continued loading, the interface is smoothed due to wear and compaction, leading to a further decrease of bond resistance.

As far as Stage III is concerned, due to the build-up of the wedging action exerted by the bars and to the propagation of the splitting cracks, all possible contribution to the confinement are mobilized: in fact, the confinement efficiency depends on the concrete cover thickness, bar spacing (Ferguson 1966; Edwards and Jannopoulos, 1978; Ferguson et al., 1954; Morita and Kaku, 1979), reinforcement, and transverse pressure.
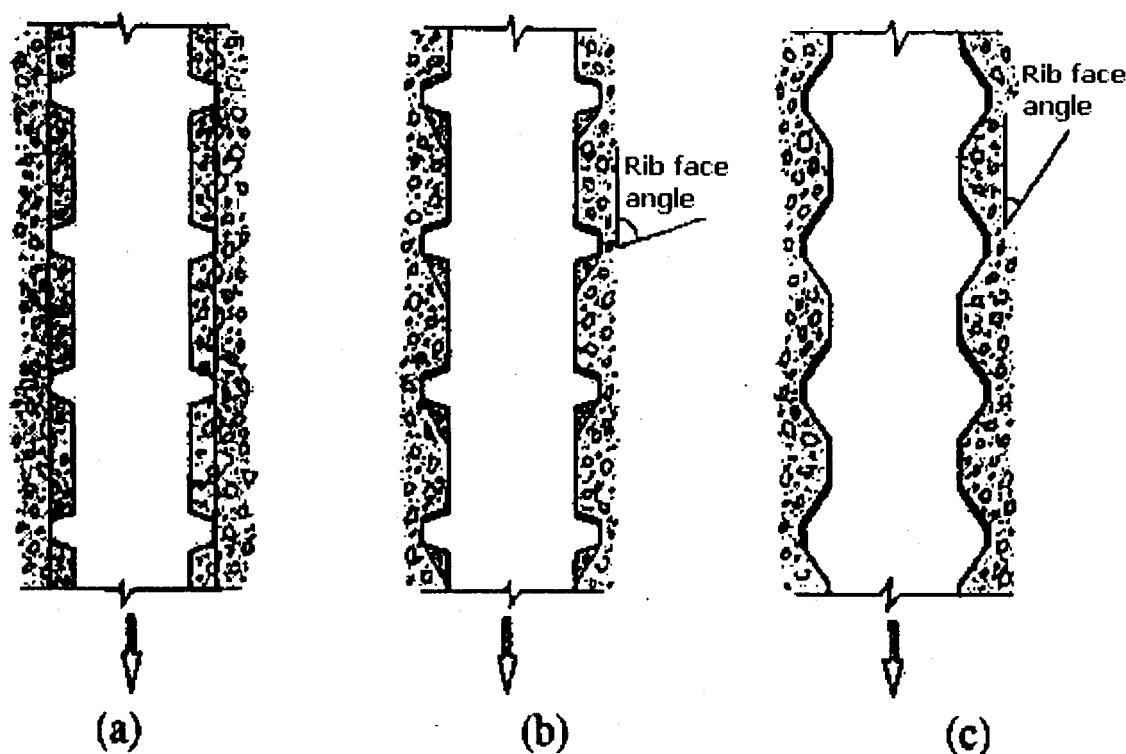
Figure 2.4: Modes of bond failure: (a) heavy confinement pull-out; (b) medium confinement, splitting induced pull-out accompanied by crushing and/or shearing-off in the concrete below the ribs; and (c) light confinement splitting accompanied by slip on the rib face (Task group bond model 2000)

2.3 Effect of bar profile on bond strength

As it is well known, the theory of reinforced concrete is based on stress transfer between the reinforcing steel bars and the surrounding concrete. This transfer of load or stress is made possible by the resistance to relative motion or slippage between the concrete and the surface of the embedded steel bar. The resistance to slippage occurs due to the bond at the steel-concrete interface.

Previous bond research (Rehm,1961; Lutz, Gergely, and Winter 1966; Soretz, and Holzenbein, 1979; Kimura, Hideka and Jirsa,1992; Darwin and Ebeneze,1993) involving

pullout and beam-end tests of regular and specially machined bars, indicates that the geometry and shape of bar deformations affect the bond strength of anchored bars. It was concluded from their studies that bond performance of deformed bars would improve with an increase in the rib height or decrease in rib spacing, an increase in rib bearing area-to-rib shearing area ratio (or approximately rib height-to-rib spacing ratio), or an increase in the rib face angle above 45 deg. Today, the ratio of rib bearing area-to-rib shearing area is alternately known as the relative rib area Rr that is the ratio of the projected rib area (normal to bar axis) to the product of the nominal bar perimeter by the center-to-center rib spacing.

Choi and Lee (2002) found that the effective rib face angel (as a result from the crushing of the concrete in front of the rib) ranges between 25 and 35 degrees which is lower than the actual rib face angel, and the relative rib area has a little effect on the bond strength of deformed bars when the bars are not confined by transverse reinforcement. Lutz, Gergely, and Winter (1966) predicted that bars with a large rib face angle would be less affected by grease or other friction-reducing agents than bars with a flatter rib face angle. If the face of the rib formed an angle of 90 degree with the axis of the bar, all of the bond strength would be produced by the direct bearing of the rib against the concrete key. In this case, friction between the concrete and steel would be unnecessary, on the other hand bars with 90 degree angle could have insufficient compaction of the concrete in front of the rib which oppositely affect the bond strength. However, for a plain bar (a rib face angle of 0 degree), friction caused by adhesion between the concrete and steel would be the only bond component, and loss of this adhesion would destroy the bond. As the rib face angle becomes larger, the contribution of the friction component parallel to the face of the rib to the bond strength becomes smaller. Therefore, the loss of adhesion becomes less significant.

2.3.1 Effect of the geometry and shape

David (1941), investigated the effect of different bar geometry on bond stress. He found that the stress transmission from the loaded end to the free end was higher in case of plain bars than in the case of ribbed bars. Also, it was observed that the stress in the ribbed steel bar was higher near the loaded end than in case of plain bars, and this may attributed to the increase of bond resistance due to the ribs action, which is not available.

Another study by Maslehuddin et al (1990) evaluated the effect of the steel surface condition on the bond with the concrete; one of their objectives was to evaluate the effect of several rust degrees on the steel surface and the corresponding bond with the concrete. The study was conducted for several bar diameters subjected to different degrees of atmosphere exposure. The results of this experimental work indicated that there was no change in the bond between concrete and 16 mm diameter samples due to atmospheric corrosion. In the case of 32 mm diameter bars, there was a slight increase in the bond resistance with increasing periods of atmospheric exposure. He attributed the results due to the filling of shallow gaps between the lugs in small size bars by the rust formed during atmospheric exposure, thus producing a plain surface effect in the case of rusted bars compared to a ribbed surface in the fresh samples. However, in larger bars, with the large size ribs, the slight increase of bond stress with the time of exposure is probably due to the increased roughness developed due to atmospheric exposure.

2.3.2 Effect of rib angle, rib spacing, and rib height

Several researches have evaluated the effect of the rib geometry on the bond performance of the steel bar. Cairns and Abdullah (1994) studied the effect of the reduction of bond stress in fusion-bonded epoxy-coating reinforcement (FBECR); they also evaluated the variation in bond stress with rib face angle for machined bars. Figure 2.5 shows the variation in rib face angle from 30 to 75, with the bond stress and the corresponding slips. At slips 0.01 and 0.1 mm, the bond stress slightly increases with the increase in the rib

13

face angle. At the failure load (slip 1 mm), the bond stress increases with the increase of rib angle from 30 to about 55 or 60. This may be attributed to the increase of bearing force due to the increase of bearing area. It should be mentioned that the large increase in the rib face angle can result in an insufficient concrete compaction below the rib and this factor should be taken in to consideration to design the rib face angle.
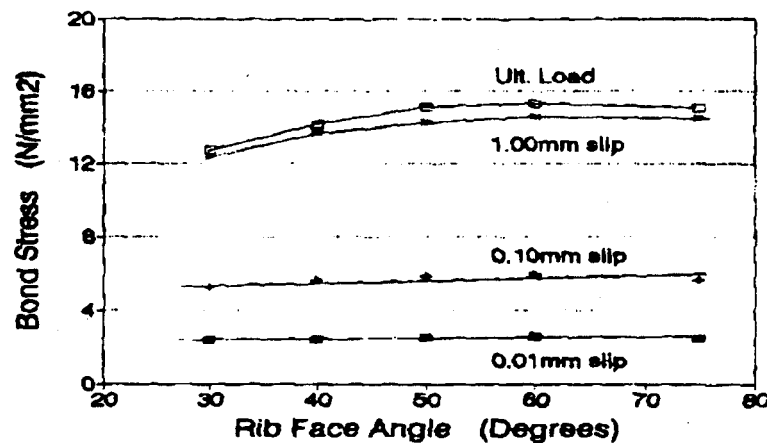
Figure 2.5: Variation in bond stress with rib face angle (Cairns an Abdullah 1994)

2.4 Effect of casting position and concrete confinement on the bond strength

According to Park and Paulay (1975), the load-bond slip relationship for deformed bars is primarily affected by the quality of the concrete in front of the bar ribs. The quality of the concrete in this region depends on its relative position of casting. Figure 2.6 shows the effect of different casting position on the bond slip relationship. Soft and spongy layer of concrete can form under the ribs in case of casting perpendicular to the bar length (number 3 Figure 2.6). This results in a higher slip (compared to the other casting positions) due to the crushing of the weak concrete under the ribs.

The effect of casting position on bond is even more severe for plain bars. Figure 2.7 shows the effect of casting position for 16 mm plain bars. The upper curves of each pair in the figure were obtained for heavily rusted and pitted bars. The lower curves of each pair is for smooth surface bars. The ultimate bond strength is drastically reduced in the case of

14

horizontal bars as compared with vertical bars. It is to be expected that the top bars in a beam will have poorer bond characteristics than the bottom bars, since the water and air gain will be greater under top bars. In addition, the relative downward movement of the surrounding concrete caused by settlement of the fresh mixture, can be large. The amount of settlement that can occur depends on the extent of bleeding of the fresh concrete and the rate of the water is permitted to escape from the formwork (Park and Paulay 1975).
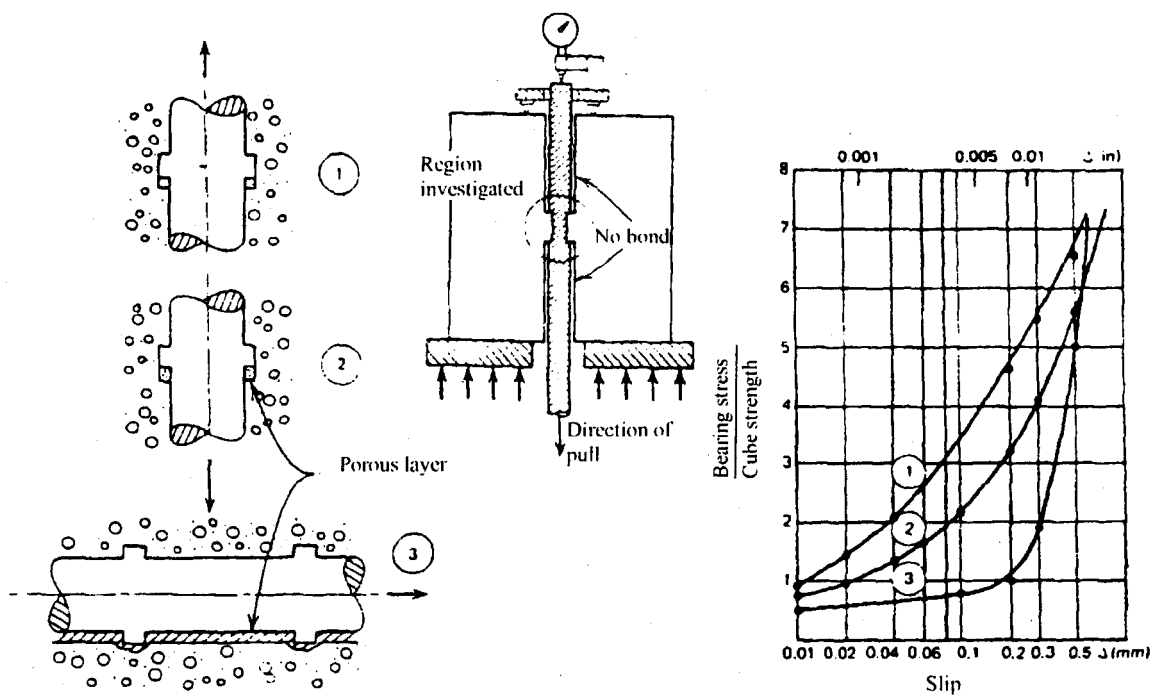
Figure 2.6: The influence of casting position on bond performance

(Park and Paulay 1975)
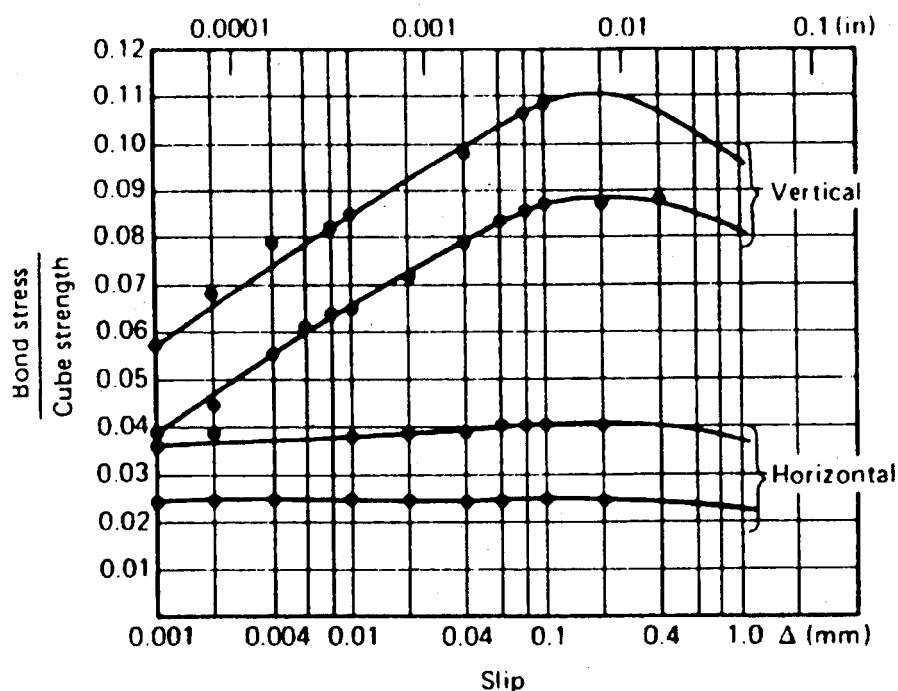
Figure 2.7: The load-slip relationship for No. 5 (16 mm) plain rounded bar in different casting positions (Park and Paulay 1975)

Welch and Patten (1967) studied this effect and compared the bond performance of bars surrounded by concrete in leaky timber molds and in well-sealed steel moulds. In the latter they also delayed the placing of the concrete by 40 minutes. Fig. 2.8 demonstrates their results, the upper two curves indicate to the delayed placing for top and bottom bars and the lower part indicates to the leaky timber mold placing for the same bars. This shows the effect of concrete settlement on bond, particularly for top bars. The ACI code recognizes this phenomenon by requiring 40% excess development length for top-cast deformed bars.

The widening of splitting cracks can be restricted if the concrete that surrounds a bar is confined in certain areas, such as at the simply supported ends of beams, transverse compression is normally available from the reaction force. Transverse compression is beneficial to the anchorage of reinforcement.

16
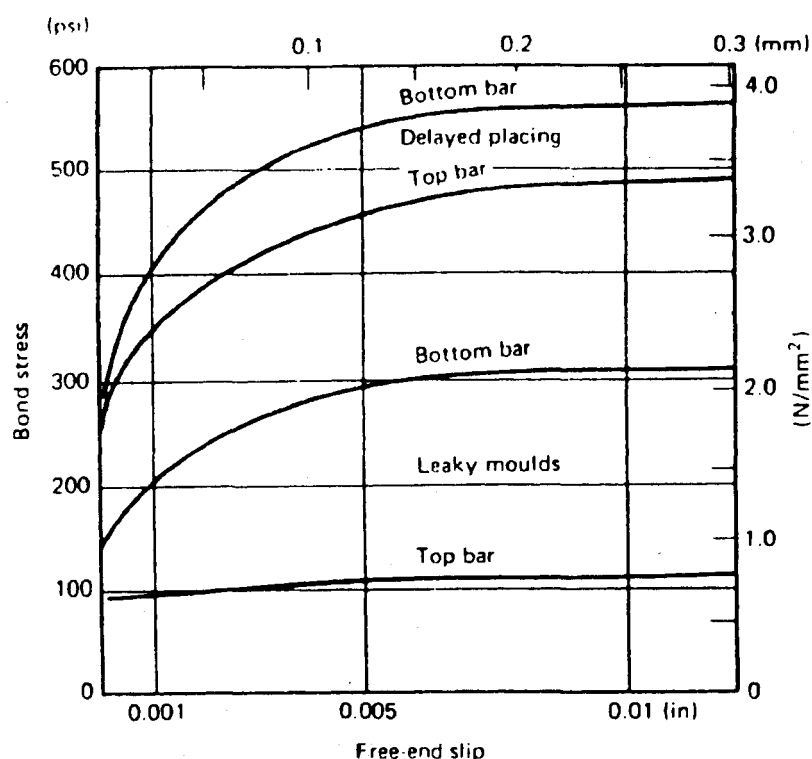
Figure 2.8: Bond stress-slip relationship for plain round barsas affected by settlement of fresh concrete. (Park and Paulay 1975)

Increased concrete cover has been found to produce some increase in the resistance against splitting however, the improved bond performance is not proportional to the additional cover thickness. For large size bars, the beneficial effect is not very significant. For these bars, as a rule, the effect on the formation and widths of cracks under service load condition is the governing criterion in selecting an appropriate value for allowable average bond stress. Extra cover does not provide protection against excessive surface crack width; medium sized top bars appear to benefit more from added cover.

Stirrups, particularly when closely spaced, prevent the opening of cracks that form along the embedded bars and enable greater bond forces to be transmitted. In many situations, this is only possible if the shearing stresses are transmitted across splitting cracks by means of aggregate interlock.

The aim of confinement by means of stirrups or transverse reinforcement is to prevent a failure along a potential splitting crack and to enforce, if necessary, a shear failure, which is associated with the maximum attainable bond strength.

CHAPTER 3
BOND PERFORMANCE

3.1 Overview of high performance concrete

Many researchers reported that the main microstructure characteristics for high performance concrete (HPC) are its dense microstructure even at the interfacial region and the strong bond between the aggregate and the matrix. Manufacture of HPC entails the use of low ratios of water to cementitious materials (w/cm) and supplementary cementing material (SCM). To understand the influence of using supplementary cementing materials like silica fume, fly ash, etc. as a partial replacement of cement, a quick overview for the properties of these materials and the effect of using them in concrete should be demonstrated.

3.1.1 Overview of supplementary cementing materials

The use of SCM's such as ground granulated blast furnace slag, fly ash, and silica fume, has become common with the production of concrete because of their economic value and other benefits.

In the case of high performance concrete (HPC), the incorporation of one or more types of the SCM, together with a low water/cement ratio (usually a superplasticizer is used in these mixes and sometimes with very high dosage to maintain adequate workability), has proved to improve greatly the microstructure over that of concrete with ordinary w/c (Mehta 1981). The SCM particles have very high surface area, which consume part of the mixing water to get their surface wet, results in a very little free water left in the mix for bleeding. Also, the SCM improves the concrete microstructure by either filler effect and/or chemical effect (pozzolanic reaction). At early ages, the filler effect of SCM is responsible for the improvement in densification of the microstructure. The SCM improves packing of the hydration products especially around the aggregate particles.

19

At later ages, the chemical effect (pozzolanic reaction) adds to the improvement of the microstructure. The pozzolanic reaction of SCM is mainly by reaction with the calcium hydroxide crystals (the main By-Product from the hydration of normal cement) that nucleated earlier around the SCM particles. The pozzolanic reaction produces more calcium silicate hydrate (C-S-H) gel, which is the main cementitious product from the hydration of normal cement. C-S-H will effectively tie together the hydration products and the unhydrated cement particles leading to more homogeneous and denser matrix.

The chemical effect of SCM is consumption calcium hydroxide (CH) crystals with time and replacing them by C-S-H gel, leading to a reduction in the concentration of CH and porosity in the transition zone as well as an increase in the bond between the aggregate and the matrix (Larbi 1993). Goldman and Bentur (1993) concluded that improving the aggregate /matrix bond will induce the "true" composite behavior of the concrete in which the aggregate acts as an active reinforcing inclusion.

Mehta (1986) referred to the process of transforming the large grains of a system into a series of smaller grains as "grain size refinement". The high performance concrete is characterized by its low content of CH crystals, which if present are not well crystallized (Sarkar and Aitcin 1987). The addition of SCM refines the pore distribution and produces a discontinuous pore structure with less permeability. This is attributed to the development of a denser structure and the replacement of CH by C-S-H gel. Figure 3.1 shows the change in the pore size distribution of cement paste with varying pozzolan content. The figure bars indicate to the size of the pore for different percentage of pozzolan (0, 10, 20 and 30% as partial replacement of cement) and after 28, 90 and 360 days of casting. The figure also shows the refinement of the pore distribution with high percentage of pozzolan (30% as a partial replacement of cement), and after longer time of casting.

20

3.1.2 Properties of concrete containing silica fume as supplementary cementing material

The addition of very fine particles to a concrete mixture tends to reduce segregation and bleeding tendencies. When very fine particles of silica fume (SF) are added to the concrete, the size of flow channels is greatly reduced because these particles are able to find their way into the empty spaces between two cement grains, causing high reduction in bleed-water flow channels and high reduction of the concrete permeability. Also, due to increase in the number of solid to solid contact point, the cohesiveness of the concrete mixture is greatly improved when SF is added (Mehta 1981). This makes the material highly attractive for use in shotcrete, and pumping.
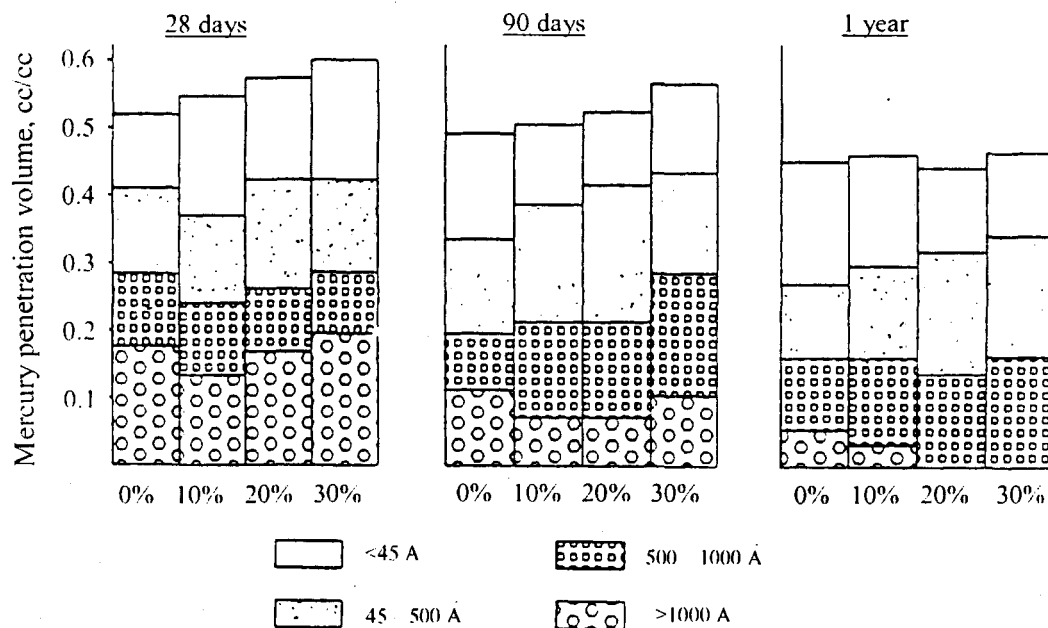
Figure 3.1: Change in pore size distribution of cement paste with varying pozzolan content (Mehta 1981).

21

Several reports confirming the sensitivity of the concrete containing silica fume to plastic-shrinkage cracking when exposed to drying conditions at an early age. Since concrete containing silica fume shows little or no bleeding, the rate of water evaporation from the surface of concrete is low and hence, a small amount of surface cracking occurs (Mehta 1981). This phenomenon generally occurs in hot weather (high ambient temperature, low humidity of the environment and windy conditions).

Creep of concrete can be defined as the increase in strain under a sustained stress. Creep of concrete is inversely proportional to its strength. Since the concrete containing S.F (as a supplementary cementing materials) is characterized by high strength, the creep for concrete containing S.F will be lower than that of the corresponding Portland cement concrete (Neville 1981).

If SF is used as a partial replacement of cement (10-15 %), there will be no deleterious effect on early strengths (i.e. 1-day and 3-day strengths), and a noticeable strength increase is recorded during the 3 to 28-days moist-curing period when most of the pozzolanic reaction takes place.

Many researchers investigated the permeability of concrete containing SF and concluded that there is a significant effect on permeability. For example, a concrete mixture containing 100 kg/m^3 portland cement, 20% SF, and a superplasticizer showed approximately the same permeability as a concrete containing 250 kg/m^3 portland cement but no SF or plasticizer. The average value of the permeability coefficient of a plasticized concrete mixture containing 250 kg/m^3 cement but without SF was 615x10^5 m/sec, compared with 17.5x10^5 m/sec when 10% SF was added to the concrete mixture (Cao and Sirivivatnanon, 1991). In addition to the large decrease in the permeability as a result of SF incorporation into concrete, a major reason for the improved resistance of concrete to acidic and sulfate waters is the reduction in the calcium hydroxide content of the cement paste. which decrease linearly with the amount of SF added.

The alkali aggregate reaction is a reaction between the active silica constituents of the aggregate and the alkalis in cement, this reaction causes expansion and visible surface cracking (Neville 1981). The cracks resulted from the alkali aggregate reaction will cause further deterioration of the concrete structure and will subject the reinforcing bars to corrosion activity. The SF concrete proved to reduce alkali-aggregate expansion. Since the amount of pozzolans needed for reducing the alkali-aggregate expansion depends on the reactivity of the pozzolans, many researchers have reported that 10% SF was found adequate to control the alkali aggregate expansion.

The ability of the concrete to protect embedded steel from corrosion also depends on its electrical resistivity (Cao and Sirivivatnanon, 1991). As shown in Figure 3.2, increasing the addition of silica fume has increased the ohmic resistance of concrete substantially. For saturated concrete without SF, the resistivity is in the 5 to 10 k-ohm cm range. With concrete containing 100 kg/m^3 cement, the resistivity was found to increase by 58% at 10% SF addition, and 190% with 20% addition. For concrete with 250-kg/m^3 cement, the increase in resistivity was 210 and 615% for 10% and 20% silica fume, respectively. For a rich concrete mixture (400 kg/m^3 Portland cement content) that is typically recommended when a serious consideration has to be given to the steel corrosion problem, the electrical resistivity was increased by 550% and 1600% for 10% and 20% SF addition to concrete, respectively. This increase in electrical resistivity was probably due to the pore refinement process caused by the pozzolanic reaction because the ionic mobility is expected to be low in a matrix, which has a fine structure.
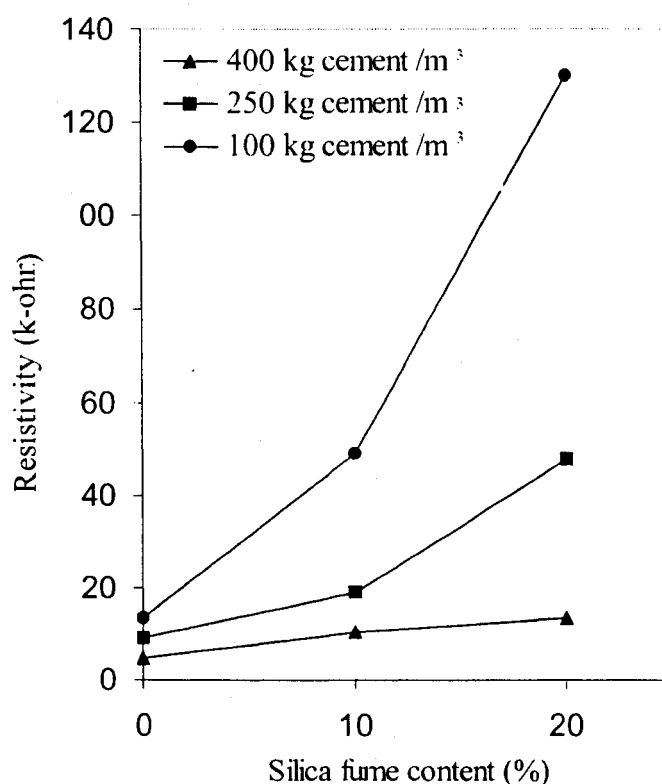
Figure 3.2: Effect of silica fume on the ohmic resistance of concrete (Cao and Sirivivatnanon, 1991)

3.1.3 Effect of silica fume concrete on bond stress

Several researchers have studied the effect of silica fume on the steel-concrete bond strength (Gjorv et al,1990, Khedr, and Abu-Zeid 1994, Aziz 1994). Gjorv et al (1990) studied the effect of silica fume on the mechanical behavior of the bond between steel and concrete by using a pullout test (ASTM C 234 1991) on concrete of varying compressive strengths and varying contents of silica fume (0% to16% by mass of cement). They concluded an improving effect on the pullout strength with the increasing additions of silica fume up to 16% by the weight of cement, especially in the high compressive strength range of the concrete. They also concluded that the presence of silica fume affected the morphology and microstructure of the steel-cement paste transition zone, thereby reducing

24

both porosity and thickness of this zone. Similar results showing the superiority of the concrete-steel bond in silica fume concrete over that in ordinary Portland cement (OPC) concrete were obtained by Khedr and Abuzeid (1994).

Abadjiev et al (1993) studied the influence of silica fume on the bond between concrete and plain and deformed reinforcing bars by using pullout tests, using cubes made of concrete of similar compressive strengths both with and without the use of silica fume. They found that the use of silica fume resulted in an increase of more than 100% in the bond between the concrete matrix and plain reinforcement bars and an increase of between 9 and 37% in the bond between the concrete matrix and deformed reinforcing bars.

This observed effect of silica fume can be attributed to several mechanisms: reduced accumulation of free water at the interface during casting, thereby increasing the contact zone between the concrete and steel, reduced preferential orientation of calcium hydroxide crystals at the steel-paste transition zone, and densification of the transition zone due to pozzolanic reaction between calcium hydroxide and silica fume (Gjorv et al 1990).

Abdulaziz et al (1997) evaluated the effect of silica fume concrete on bond failure and the slip of the steel reinforcement; they compared silica fume concrete with ordinary Portland cement concrete. They concluded that the average ultimate pull-out load sustained by OPC concrete specimens before failure was less than that of silica fume concrete.

3.2 Performance of bond for epoxy coated bars

Because one of the principal causes of deterioration in concrete structures is corrosion of steel reinforcement. Several manufacturers worldwide now supply reinforcement coated with a tough fusion-bonded epoxy to isolate bars from aggressive conditions. The surface texture of the coating is smoother than the mill-scale finish of ordinary steel reinforcement, and alters the bond behavior of the bar. Many studies report a reduction in

25

the bond strength of coated bars, although the amount of reduction varies widely, from zero to nearly 50 percent (Cairns and Abdullah 1994).

The reduction in bond strength of a coated bar relative to an uncoated bar is illustrated in Figure 3.3. Because of the loss of friction between the coated bar and the surrounding concrete, the only component of bond is the force perpendicular to the face of the rib. If the resistance to splitting of the concrete cover (the vertical component of the resultant bond force at the face of the rib) is the same for either case, then the bar without friction will have smaller bond capacity than the bar that develops friction between the concrete and the bar rib.

Bearing component / Friction

Friction
Bearing / Radial pressure
Bond strength

Bearing component

Bearing / Radial pressure
Bond strength

(a) Uncoated bar (friction on lug)   (b) Epoxy-coated bar (without friction)
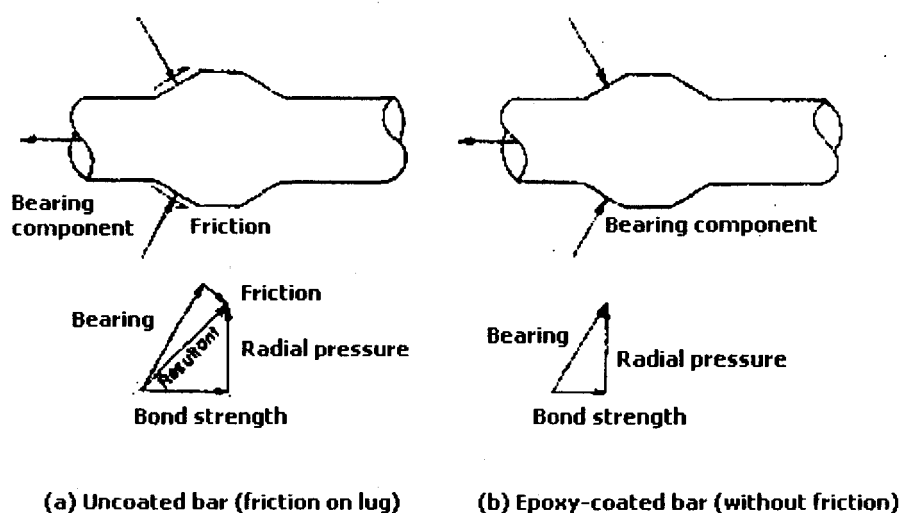
Figure 3.3: Bond strength components, coated versus uncoated bar (Hamad 1995)

Many researchers have attempted to evaluate the effect of rib geometry on the bond performance of coated and uncoated steel bar; Hamad (1995) evaluated the effect of bar parameters on the bond strength, he studied the change of ribs spacing, rib height, as well as rib angle and evaluated the optimum value for each variable. The results of this study shows that when the rib spacing and rib height for coated bar were kept constant (60 and

26

7.5 percent of the diameter of the bar respectively), the bond strength of the coated bar increased slightly as the rib face angle increased from 30 to 90 degrees. The stiffness of the load-slip curves of bars with angles of 60, 75, and 90 degrees was greater (less slip at a given load) than bars with angles of 30 and 45^s degrees. He also noted an increase in the bond strength for an increase in the rib face angle from 30 to 60 for both coated and uncoated bars, while keeping the other parameter constant.

Another study was conducted by Cairns and Abdullah (1994) to investigate the effect of fusion-bonded epoxy-coated reinforcement (FBECR) on the bond strength focused on the bond slip behavior and the variation on the rib face angle. The bond tests were conducted using the RILEM pullout specimen, illustrated in Figure 3.4. A PVC sleeve covers the bar over half the embedded length at the loaded end to minimize the pattern restraint effects. The specimen was cast with the bar horizontal). The machined bars were coated by hand spray in the laboratories of a manufacturer of epoxy powders. The uncoated machined bars were heat treated to obtain a surface condition similar to that of ordinary hot-rolled bars. To verify that results from machined bars were applicable to rolled reinforcement, a hot-rolled production bar was also included in the program.
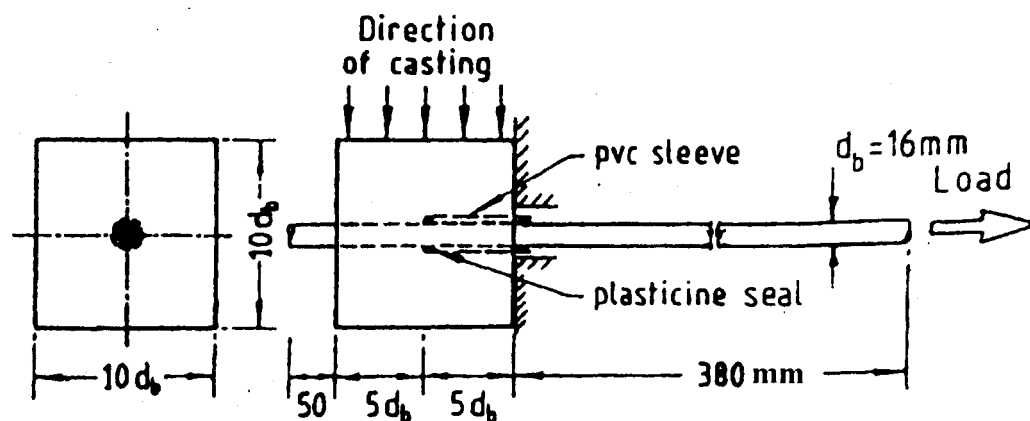
Figure 3.4: RILEM pullout bond test specimen (Cairns and Abdullah 1994)

The RILEM bond test specification requires a medium workability concrete. The measured slump was in the range of 40 to 70 mm (1.6 to 2.75 in.). The specimens were loaded in a 10-ton capacity screw- driven testing machine. The Rate of loading was around 7.5 kN/min (3.9 kip-force/min). The free-end slip was recorded throughout the test.

A plot of bond stress ratio, defined as the ratio of load carried by coated bars to that carried by un coated bars at a given slip (Fig. 3.5), shows the bond stress developed by coated bars to be initially 40 percent less than that of similar uncoated bars, but that the difference progressively reduces with increasing slip, and even reverses at slips in excess of 1.0 mm.
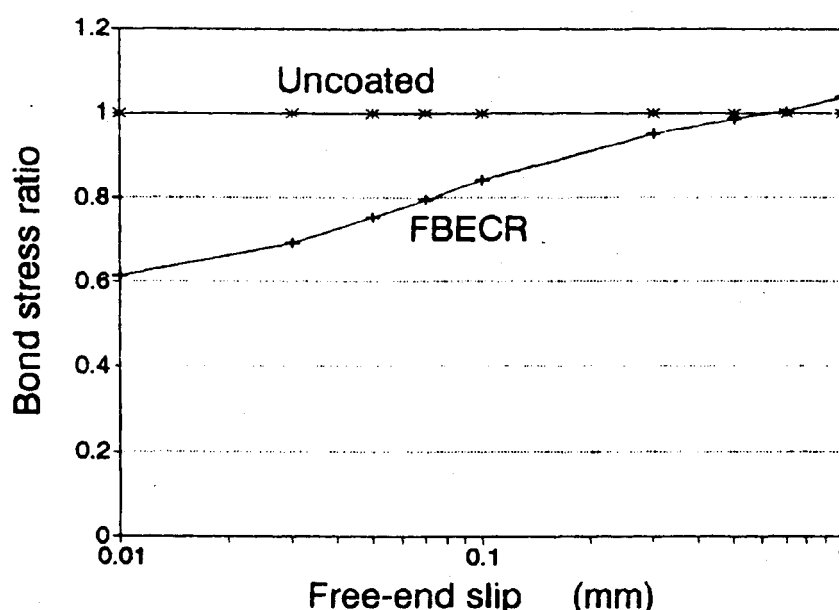
Figure 3.5: Variation in bond stress ratio with free-end slip (Cairns and Abdullah 1994)

Figure 3.6 shows the variation in bond stress with rib face angle for uncoated and coated specimens. An increase in the rib face angle produced an increase in the bond stress at a given slip at all stages. The increase was greater for coated bars. In Figure 3.7, the ratio of bond stress developed by coated bars at a specified slip to that developed by a similar uncoated bar is plotted. The figure shows that rib face angle influenced the relative

behavior of FBE and uncoated reinforcement at slips of 0.01 and 0.1 mm, but had little influence at slips of 1.0 mm or at the ultimate load.
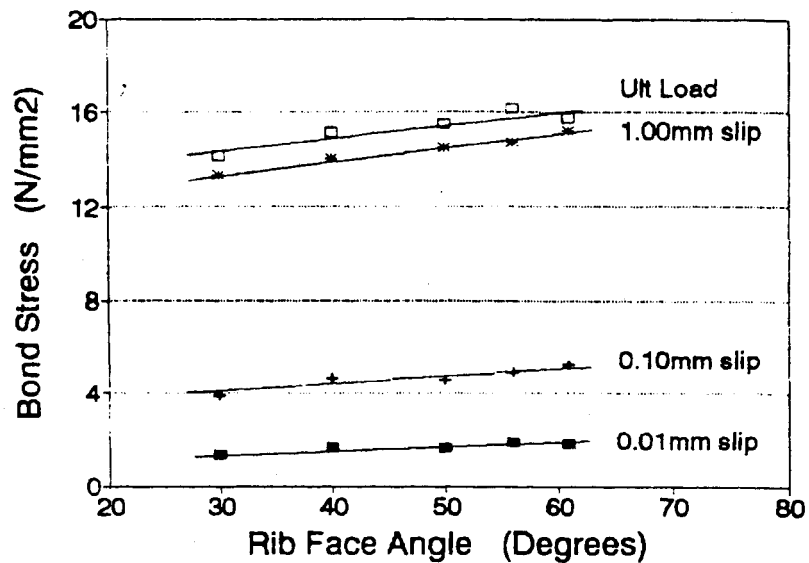
Figure 3.6: Variation in bond stress with rib face angle for coated machined bar (Cairns and Abdullah 1994)
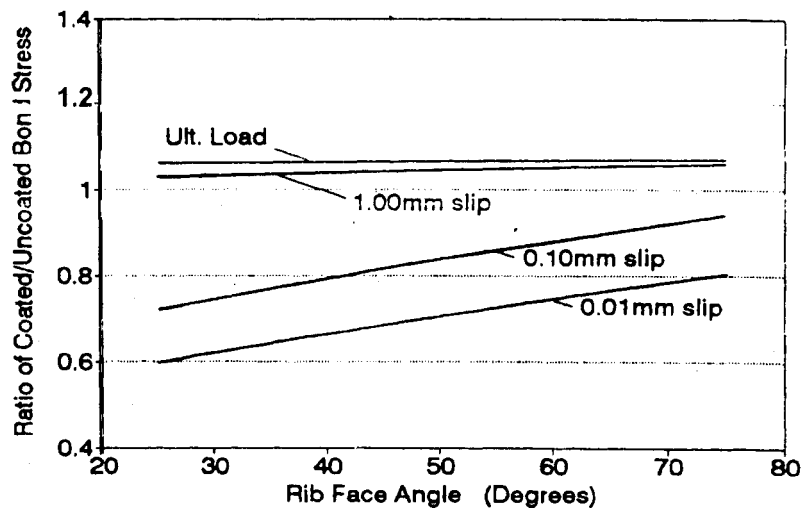
Figure 3.7: Variation in bond stress ratio with rib face angle (Cairns and Abdullah 1994)

Another study of the bond resistance of epoxy-coated reinforcements was carried out in slab-type members at Purdue University by Cleary and Ramirez (1989). Tests were conducted on four series of specimens. The slabs were approx. 4 m long, 0.6 m wide, and 203 mm deep. Reinforcement consisted of three No. 6 bars spliced at mid span. Splice lengths varied from 406 mm to 254 mm. The specimen's details are shown in Figure 3.8
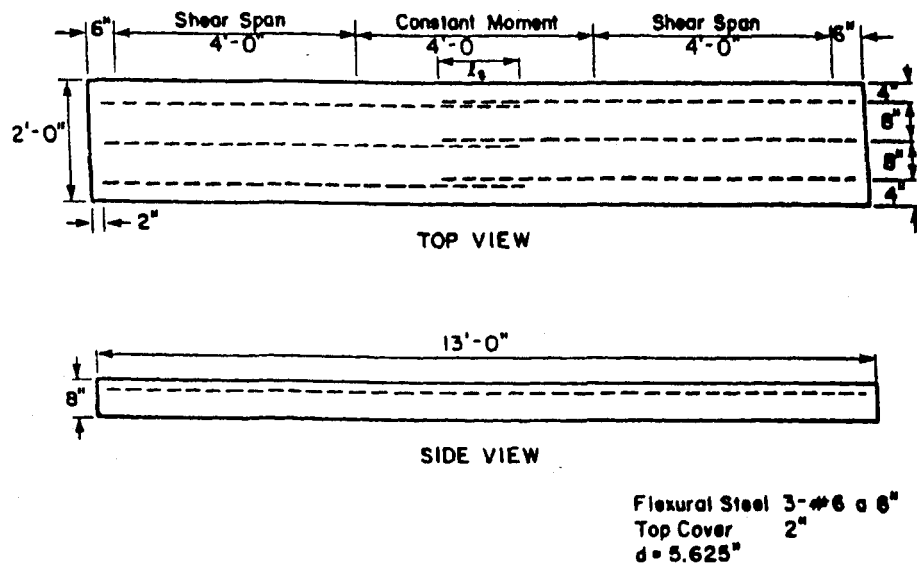
Figure 3.8: Shallow specimen details (Cleary and Ramirez 1989)

Each series of beams was cast separately. The concrete compressive strength was 58 MPa for the 254 mm splice series, 28 MPa for the 305 mm splice series, and 39 MPa for the 356 mm and 406 mm splice series. The crack widths and the end and centerline deflections were measured at each load level.

A bond ratio of 0.95 was found in the 305 mm series with 28 MPa concrete. The 254 mm series with 58 MPa concrete resulted in a bond ratio of 0.85. The average end deflections at a given load were only slightly larger for the specimens reinforced with epoxy-coated bars when compared to the specimens reinforced with uncoated bars. The specimens reinforced with epoxy-coated bars contained fewer, wider cracks than comparable

30

specimens reinforced with uncoated bars. Also, the total width of cracking is larger for the specimens reinforced with epoxy-coated than that for the specimens with uncoated reinforcing bars.

3.3 Performance of bond under corroded bars

3.3.1 Introduction

Corrosion affects bond strength, the slight formation of the corrosion product of a corroding bar at first increases radial stresses between the bar and the concrete and hence increases the frictional component of bond. However, further corrosion will lead to the development of longitudinal cracking and a reduction in the resistance to the bursting forces generated by the bond action. Some suggest that a firmly adherent layer of rust may contribute to an enhancement in bond strength at early stages of corrosion, at more advanced stages of corrosion, weak and friable material between bar and concrete will certainly be at least partially responsible for reductions in bond strength [Cabrera and Ghodussi (1992), Amleh and Mirza (1999), Al-Sulaimani et al (1990)].

Corrosion may reduce the height of the ribs of a deformed bar above the bar core, this is unlikely to be significant except at advanced stages of corrosion. Corrosion also may affect the rib face angle in the advanced stage, moreover ribs of deformed bars will eventually be lost due to corrosion.

3.3.2 Review of the previous work

Almusallam, et al (1995) assessed the effect of different degrees of reinforcement corrosion on bond degradation, they studied the free-end slip and the modes of failure in four degrees of corrosion (as a percentage of bar weight loss), as well as the effect of different crack widths and degradation of rib profile for the various degrees of corrosion.

31

The results indicated that. as the degree of corrosion increases from 0 to 4% (as a percentage of bar weight loss), the ultimate load increases from 61 to 71 kN, whereas the corresponding slip at the ultimate load decreases from 0.68 to 0.238 mm (Figure 3.9 to 3.11). The results also indicated a decrease in the ultimate bond strength with rib profile degradation (Fig. 3.12).
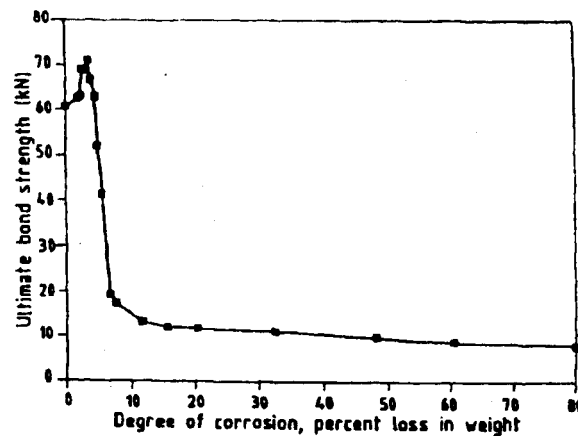
Figure 3.9: Relationship between the ultimate bond strength and different degrees of corrosion (Almusallam, et al 1995)
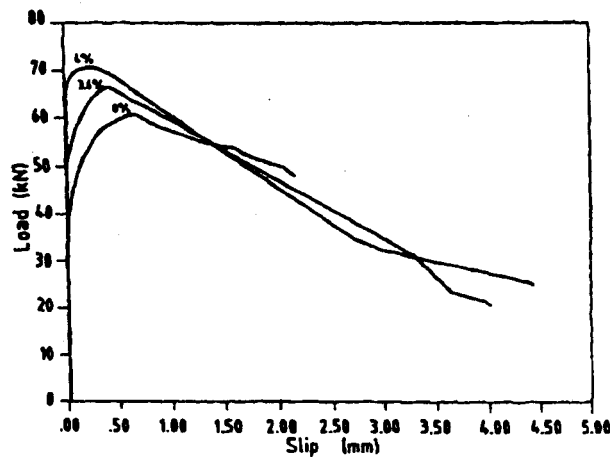
Figure 3.10: Relationship between load and slip for 0 to 6 % percentage of weight loss (Almusallam, et al 1995)
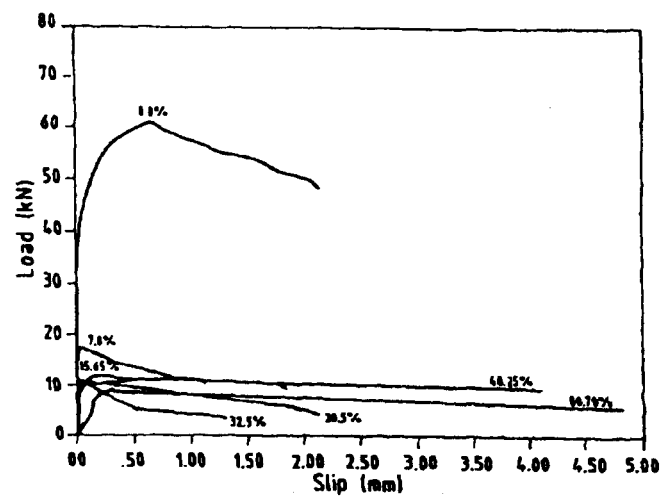
Figure 3.11: Relationship between load and slip at percentage of weight loss higher than 6% (Almusallam, et al 1995)
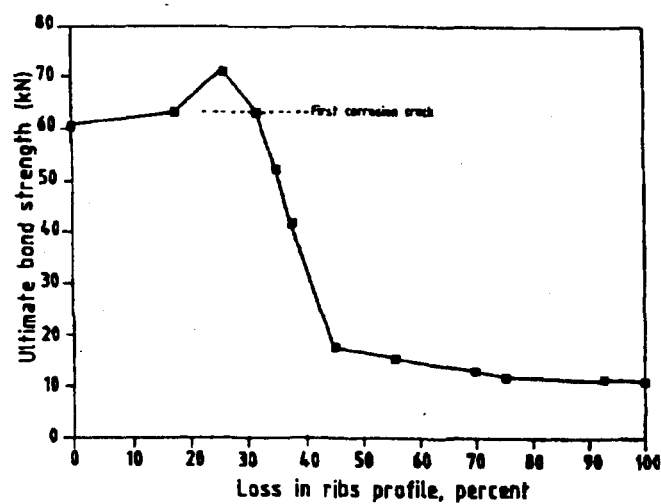
Figure 3.12: Effect of loss of rib profile on ultimate bond strength Almusallam, et al 1995)

Auyeung et al (2000), evaluated the bond strength and bond-slip behavior of reinforcement bars corroded to various levels of corrosion. They found that when the corrosion mass loss approached approximately 2%, cracks started forming along the corroded bar and once the

33

crack was formed, corrosion was accelerated due to the decrease in resistance for the liquid permeation.

Also they found that when the mass loss exceeds 1%, there was a rapid decrease in bond strength (Figure 3.13). In addition to that, the corroded bars undergo less slip until the mass loss reaches approximately 2.0%, after this mass loss, the stiffness reduces consistently (Fig. 3.14).
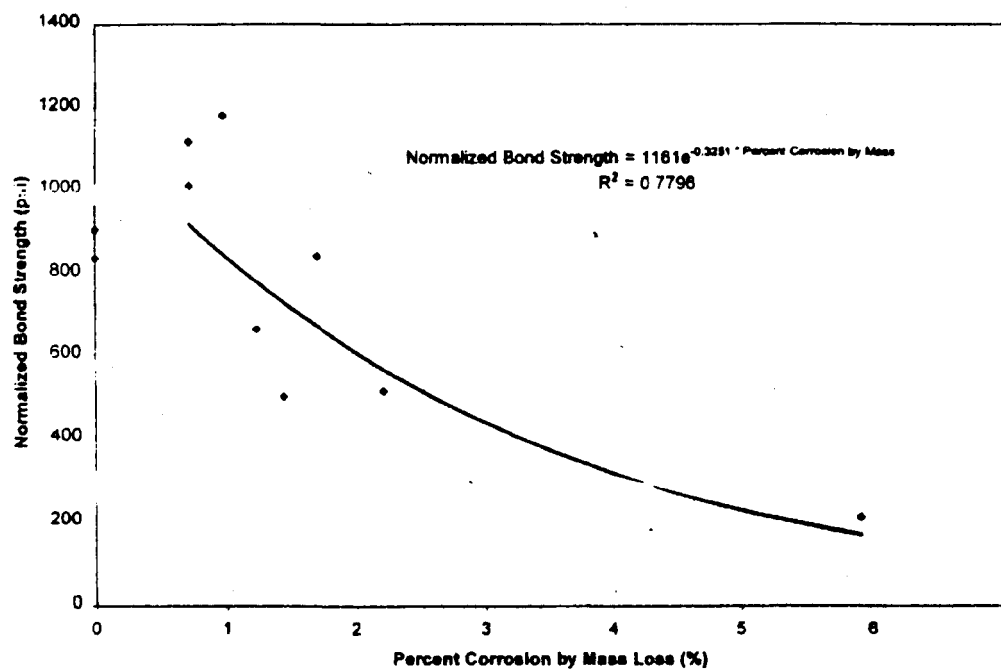
Figure 3.13: Influence of corrosion mass loss on bond strength. (Auyeung et al 2000)

34
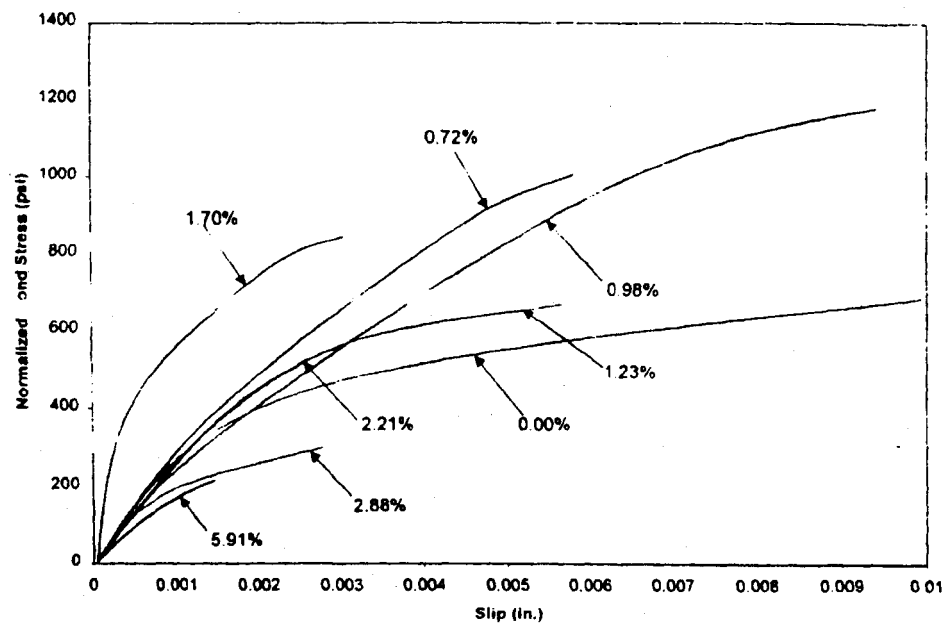
Figure 3.14: Effect of corrosion on load-slip behavior (Auyeung et al 2000)

35

CHAPTER 4

MATERIALS AND EXPERIMENTAL PROGRAM

This chapter describes the experimental test programs, it also presented the types and properties of the concrete mixtures used. A brief description of the types of the fresh and hardened concrete tests used to evaluate the concrete strength and durability is also presented. In addition, the details of the accelerated corrosion test are summarized. The compliance with several ASTM Standards with a brief description of the tests used is also introduced to ensure the highest level of performance.

4.1 Experimental program

The experimental program was designed to study the bond strength for four different concrete types, with three different reinforcing steel types after subjecting them to several degrees of corrosion.

The four concrete types used were fly ash concrete mixture (0.32 w/cm), Silica fume concrete mixture (0.32 w/cm), normal Portland cement (NPC) concrete mixture (0.32 w/c), and high w/c concrete mixture (0.52). Three different steel: regular carbon steel bars, stainless steel bars, and epoxy coated bars were used to reinforce the 100 mm diameter by 200 mm height pullout specimen, each reinforced with a single symmetrical bar.

4.2 Concrete mix parameter

Twenty concrete cylinders (100 mm diameter and 200 mm height) for each concrete type were prepared to study the compressive strength and indirect tensile strength at ages of 28 and 90 days.

Different dosages of superplasticizer were added to the fly ash, silica fume, and NPC concrete (w/c = 0.32) to obtain the same slump range for NPC concrete (w/c = 0.52). This technique was used in order to achieve the effect of introducing fly ash, silica fume, and the increase of w/c ratio, in the concrete mixtures without any other variables that might affect the mechanical properties of the concrete.

The use of such silica fume and fly ash in concrete require a low w/c together with sufficient dosage of superplasticizer (to maintain adequate workability) to improve the durability and the strength of the concrete (Mehta 1981). For this reason a low w/c of 0.32 was used with each silica fume and fly ash concrete. To study the effect of addition of silica fume and fly ash as a SCM on the mechanical properties of the concrete, the same w/c together with the same mixing proportions and materials were used with the NPC concrete. On the other hand, to study the effect of high w/c on the mechanical properties of the concrete and to study the effect of high w/c concrete in corrosion protection, a high w/c of 0.52 was used with the same mixing proportion and materials type.

The coarse aggregate used in this research is dolomite consists of two sizes, 20mm and 9mm maximum nominal sizes (mixed in ratio of 1:1). The ratio of the coarse aggregate to the fine aggregate was 3:2. The main properties of the used coarse and fine aggregate are shown in Tables 4.1 through 4.7

Ordinary Portland cement Type 10 was used in this investigation, which was produced by St. Lawrence Cement Company. A selected dosage of 375 kg/m^3 of cement was used in the four concrete mixtures. The chemical and physical properties of the selected cement are given in Tables 4.8 and 4.9

The fly ash used in this investigation is Sundance fly ash obtained from Alberta. The chemical and physical properties of the selected fly ash are given in Tables 4.10 and 4.11.

37

The silica fume used as a supplementary cementing material in this investigation, was supplied from Grace Canada under the commercial name of " FORCE 10,000 D". It is under a chemical name of Condensed Amorphous Silica Fume. The chemical and physical properties as provided by the company are listed in Table 4.12.

The poly-naphthalene sulfonic acid based superplasticizer was used for low workability concrete mixtures. The superplasticizer was manufactured by Euclid Admixture Canada Inc. with commercial name "Eucon 37", confirming to ASTM C 494 type F specifications. The physical and chemical characteristics provided by manufacturer are shown in Table 4.13

A synthetic type air-entraining admixture produced by Master Building was used in this investigation. The air-entraining admixture was used with different dosages in attempt to reach a concrete with 5-8% percentage of air per meter cube. The chemical family for this agent is Surfactant mixture, aqueous, and the physical and chemical characteristics are shown in Table 4.14

4.3 Reinforcing steel

Twenty M size reinforcing steel bars with a nominal diameter of 19.5 mm were used in this program. The regular carbon steel bars (uncoated and coated with epoxy) are manufactured locally and conformed to the ASTM Standard A615-72. The tensile test and chemical characteristics for the stainless steel bars were obtained from Ontario Ministry of Transportation and are shown in Tables 4.15 and 4.16

4.4 Properties of the concrete mixture

The fresh and hardened concrete properties were investigated. Air content and slump tests were performed during the fresh concrete stage, while compressive strength as well as

indirect tensile strength were performed after 28 and 90 days of age. Table 4.17 shows the test results of the fresh concrete as well as the mixing proportion of the four used concrete. Ten concrete cylinders (100 mm in diameter and 200 mm in height) for each concrete type were prepared, measured and tested (after 28 and 90 days of casting) in accordance with ASTM C496-96 as shown in Figure 4.1, and the splitting tensile strength (f_t) was calculated as follows

$$f_t = 2 p / \pi l d$$

Where

f_t = splitting tensile strength   (MPa)

P = Maximum applied load.   (N)

l = length of the specimen.   (mm)

d = diameter of the specimen. (mm)

The compressive strength test was carried out for ten concrete cylinders (100 mm in diameter and 200 mm in height) for each concrete type after 28 and 90 days of casting according to ASTM C39-86 using a 400 KN compressing testing machine. The results of the compressive strength test as well as the splitting tensile strength are presented in Table 4.18

4.5 Specimens preparation

In addition to the 80 concrete cylinders used to study the compressive strength and the indirect tensile strength, 27 cylindrical concrete specimens (100 mm diameter and 200 mm height reinforced axially with a single steel bar, and protruding at one end only) were prepared for each concrete type to study the bond strength under several corrosion stages.

The 27 concrete specimens for each concrete type were divided into three groups (9 specimens per group for each reinforcing steel type). Each group consist of: 3 specimens

39

tested for 0 cracking level and 2 specimens tested for each of pre-cracking, cracking, and severe corrosion levels.

The cylindrical concrete specimen has a pre-weighted No. 20 bar embedded and protruding at one end only (Fig. 4.2). The bar is 300 mm protruded out of the surface and 160 mm embedded in the bottom of the concrete cylinder

To protect the interface between the protruding steel bar and the surface of the concrete specimen from corrosion, 50 mm of the extension part of the bars along with another length of 25 mm within the specimen top, was epoxy-coated and taped with an electrical tape. For the specimens that have epoxy coated bars, it was sufficient to tape the bars with electrical tape without repainting with extra epoxy coating (Fig. 4.3)

To maintain the bar verticality during casting, a square wooden piece which had a centered hole of 21 mm in diameter, was mounted on the cylinder mold quickly after casting the concrete and the bar was then hammered until reaching the required depth (Fig. 4.4)

The concrete was mixed in a laboratory horizontal pan counter-current mixer for a total 6 minutes. The properties of the fresh concrete including the slump and air content were determined immediately after the mixing according to relevant ASTM Standards. The concrete specimens were cast in a plastic moulds. All of the specimens were compacted on a vibrating table after casting. The specimens were covered and left in the casting room for 24 hours, then they were demoulded and cured in a standard moist curing room (at $23 \pm 2°$ C and 100% relative humidity) to different stages, followed by pullout tests (Figure 4.5 and 4.6)

4.6 Accelerated corrosion

Accelerated corrosion tests are used to obtain qualitative information on corrosion behavior in a relative short period compared to the field corrosion test. Accelerated

40

corrosion tests have been used successfully to determine the susceptibility of the reinforcing and other forms of structural steel to localized attacks such as pitting corrosion, stress corrosion and other forms of corrosion.

The accelerated corrosion test in this program was terminated when the four stages of corrosion took place within the different steel types, based on the crack width; 0 corrosion stage after three month of curing and before placing the specimens in the concrete tank. pre-cracking stage considered when the current started to increases but before any crack was visible, cracking stage considered when the first crack appeared on the concrete specimen regardless the width of this crack, and severe corrosion stage considered when any crack extended up to 4 mm.

4.6.1 Test set up

After the 108 pullout specimens were cast and cured, 72 specimens were subjected to accelerate corrosion by placing them in the accelerated corrosion tanks, while the rest of the 36 specimens (3 specimens per steel type per concrete type) served as the control specimens (0 corrosion stage). .

The accelerated corrosion setup consists of 150 x 50 cm plastic tank, electrolytic solution [5% sodium chloride (NaCl) by the weight of water] and a steel mesh placed in the bottom of the tank connected to a single steel bar. The specimens were placed in the accelerated corrosion tank and partially immersed with the electrolytic solution up to two third of its height. To eliminate any change in the concentration of the NaCl and pH of the solution, the electrolyte solution was changed on a weekly basis.

The single steel bar (connected to the bottom steel mesh) and the specimen bars were connected to electrical wires by clips then connected to 12 V power supply. The direction of the current was arranged so that the single steel bar served as cathode while the

41

specimen bars served as anodes. Figures 4-7 and 4-8 illustrate the schematic drawing of the accelerated corrosion tank set-up and photograph taken during the test respectively.

The current was measured in a daily basis by means of a SMART Digital Multimeter that read both the current and the voltage. The current readings were recorded after the readings were finally stabilized.

4.7 Pull out test

The pull out test was conducted in the Ministry of Transportation Laboratory using a specially designed loading frame with manually loading hydraulic jacks (Figure 4-9). After establishing the specified levels of corrosion, the specimen was removed from the accelerated corrosion tank and a standard pullout test was performed. In order to measure the slip of the upper part of the steel bar, one LVDT was attached to the steel bar and touching the lower steel plate to measure the relative displacement between the free end steel bar and the surface of the concrete specimen. The output from the LVDT and the testing machine was connected to a data logger, where the load and the slip readings were recorded at preset intervals.

4.8 Percentage of mass loss

After the completion of the pullout test, the specimens were broken and opened then the reinforcing bar, for each specimen was cleaned and scrubbed with a stiff nonmetal brush to ensure that the bar was free from any adhering corrosion products and then cleaned with a chemical agent according to the ASTM Standard G1-90 procedure. The mass loss of the steel reinforcing bar was then obtained as the difference between the mass of the corroded bar (after the removal of the loose corrosion products) and its mass before corrosion (Amleh 2000)

$$\text{Percentage of weight loss} = \frac{[(\text{uncorroded weight} - \text{corroded weight})]}{[\text{uncorroded weight}]} \times 100$$

42

4.9 Bar profile loss

The degradation in the rib profile was determined by measuring the rib height before applying the impressed current and after the corrosion takes place in the steel bar. The percentage rib loss was determined as follows:

$$\text{Percentage of rib loss} = \frac{[(\text{rib height of uncorroded bar} - \text{rib height of corroded bar})]}{[\text{rib height of uncorroded bar}]} \times 100$$

Table 4.1: Characteristics of a sand sample

Properties	Test results
Relative density	2.7
Bulk density (t/m³)	1.79
Fineness modulus	2.5
Percentage of materials finer	1.2

Table 4.2: Sieve analysis of sand sample and the allowable limits according to ASTM standard.

Sieve No.	Opening (mm)	Percentage Passing %	Specifications	
			Min. %	Max %
¾ in.	19	100.0	-	-
½ in.	12.5	100.0	-	-
3/8 in.	9.5	100.0	100	-
No. 4	4.75	99.3	95	100
No. 8	2.36	90.1	80	100
No. 16	1.18	79.8	50	85
No. 30	0.6	56.2	25	60
No. 50	0.3	20	10	30
No. 100	0.15	4.4	2	10

Table 4.3: Characteristic of 19 mm coarse aggregate sample

Properties	Test results
Relative density	2.58
Bulk density (t/m3)	1.66
Nominal max. size (mm)	19
Water absorption %	1.77
Percentage of materials finer than sieve 200	0.46

Table 4.4: Characteristic of 12.5 mm coarse aggregate sample

44

Properties	Test results
Relative density	2.49
Bulk density (t/m3)	1.58
Nominal max. size (mm)	12.5
Water absorption %	2.92
Percentage of materials finer than sieve200	1.1

Table 4.5: Sieve analysis of size1 (19mm) coarse aggregate sample and the allowable limits according to ASTM standard.

Sieve No.	Opening (mm)	Percentage Passing %	Specifications	
			Min. %	Max %
1 in.	25	100.0	100	-
¾ in.	19	98.4	90	100
½ in.	12.5	48.7	-	-
3/8 in.	9.5	20	20	55
No. 4	4.75	.05	0	10
No. 8	2.36	0	0	5

Table 4.6: Sieve analysis of size2 (12.5mm) coarse aggregate sample and the allowable limits according to ASTM standard.

Sieve No	Opening (mm)	Percentage Passing %	Specifications	
			Min. %	Max %
¾ in	12.5	100	100	-
3/8 in.	9.5	89.3	85	100
No. 4	4.75	10	10	30
No. 8	2.36	4	0	10

45

Table 4.7: Sieve analysis of combined size1 & size2 (19mm&12.5mm) coarse aggregate sample and the allowable limits according to ASTM standard

Sieve No.	Opening (mm)	Percentage Passing %	Specifications	
			Min. %	Max %
1 in.	25	100.0	100	-
¾ in.	19	99.2	90	100
½ in.	12.5	74.3	-	-
3/8 in.	9.5	53.7	20	55
No. 4	4.75	5	0	10
No. 8	2.36	1.5	0	5

Table 4.8: Chemical properties of cement

Properties	Chemical analysis
LOI	2.46
SiO_2	19.69
Al_2O_3	5.20
Fe_2O_3	2.31
CaO	62.16
MgO	2.38
SO_3	3.83
Free Lime	1.05
Insol. (previous month)	0.28
C_3S	54.25
C_2S	15.52
C_3A	9.87
C_4AF	7.03

Table 4.9: Physical properties of cement

Properties	Values
Residue 45μm (%)	12.9
Blaine (m²/kg)	374
Air Content (%)	8.1
Initial Set (mins.)	121
Autoclave Exp. (%)	0.08
Sulfate Exp. (%)	0.010
Compressive Strength (MPa)	
1 Day	16.29
3 Days	28.30
7 Days	33.78
28 Days (previous month)	40.98

Table 4.10: Chemical properties of fly ash

Properties	Chemical analysis
Silicon dioxide, (SiO_2)	52.4
Aluminum Oxide (Al_2O_3)	23.4
Ferric Oxide (Fe_2O_3)	4.7
Calcium oxide (CaO)	13.4
Magnesium oxide (MgO)	1.3
Sodium oxide (Na_2O)	3.6
potassium oxide (K_2O)	0.6
Equivalent alkali ($Na_2O+0.658\ K_2O$)	4
Phosphorous oxide (P2O5)	0.2
Titanium oxide (TiO2)	0.8
Sulfur trioxide (SO3)	0.2
Loss on ignition	0.3

47

Table 4.11: Physical properties of fly ash

Properties	Test results
Specific gravity	2.08
Passing 45 micron %	83.6
Specific surface, Blain, cm^2/g	3060
Water requirement, %	99.2
7-day Pozzolanic activity index	94.5
28-day Pozzolanic activity index	106.9

Table 4.12: Chemical and physical properties of silica fume

Properties	Test results
Solubility in Water	Negligible
Bulk Density (#/cu. ft)	20-40
Appearance and Odor:	Light to dark gray powder
% Volatiles	None
pH	5-7 (Solution)

Table 4.13: Physical and chemical properties for superplasticizer

Physical state	Liquid
Specific gravity at 25^0C	1.21
% Of solid by weight	40.5 %
PH	8.5
Color	Dark brown
Sulfates	1.2 %
Boiling point	$100\ ^0C$ (Estimate) ($212\ ^0F$)

48

Table 4.14: Physical and chemical properties for the air entrainment agent

Physical state	Liquid
Specific gravity	1.02
Solubility in water	100%
PH	11.5
Color	Dark brown
Sulfates	1.2 %
Boiling point	105 ^{0}C
Freezing point	-2

Table 4.15: Tensile test for stainless steel bars

Ultimate tensile strength (MPa)	733
Yield strength (MPa)	421
Elongation (in 200mm manual method) %	38

Table 4.16: Chemical analysis for stainless steel bars

Carbon	0.043
Manganese	1.55
Phosphorus	0.019
Sulfur	0.002
Silicon	0.23
Chromium	17.2
Nickel	11.9
Molybdenum	2.40

Table 4.17: Properties of fresh concrete

Mix Type	W/C Ratio	Cement kg/m³	F.A kg/m³	S.F kg/m³	Water kg/m³	Coarse A.kg/m³	Fine A. kg/m³	Air en. Agent ml/m³	% S.p / m³	% Air / m³	Slump Value/ mm
N.C1	0.32	375	-	-	120	1191	794	650	1.60	5.5	160
N.C2	0.52	375	-	-	195	1073	715	500	-	8.0	175
F.A.C	0.32	157	218	-	120	1128	752	660	1.44	5.5	180
S.F.C	0.32	337.5	-	37.5	120	1183	788	650	1.92	4	150

Table 4.18: Properties of hardened concrete

Concrete Type	Compressive Strength (MPa)		Indirect Tensile Strength (MPa)	
	30 days	90 days	30 days	90 days
S.F Concrete	26	36	3.4	3.9
F.A Concrete	33	42	4.8	5.0
N. Concrete (0.32)	26	35	3.3	4.1
N. Concrete (0.52)	14	18	2.4	2.9

50
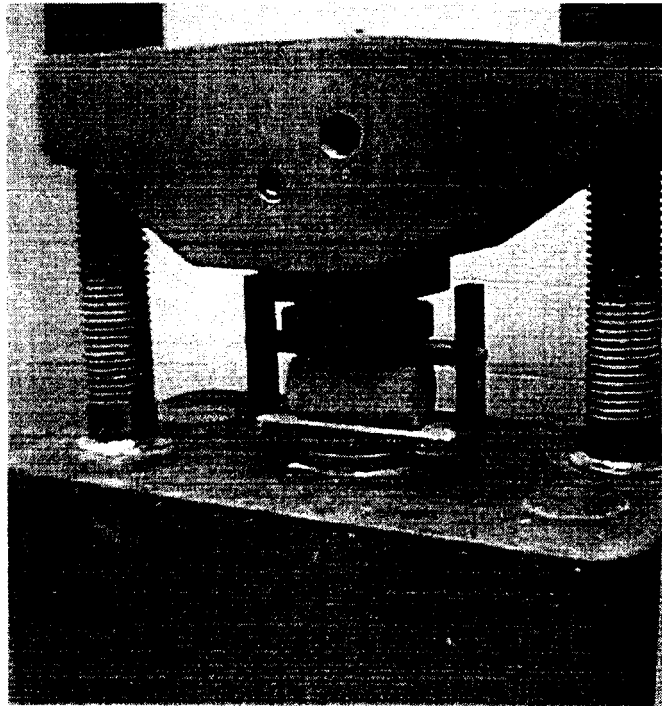
Figure 4.1: Indirect tensile test setup
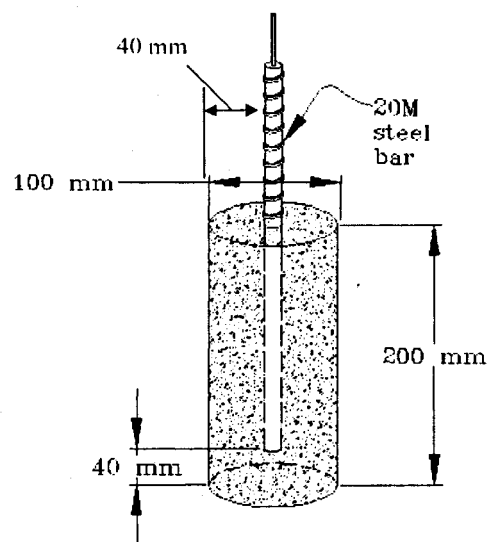
Figure 4.2: Pullout test specimen

51
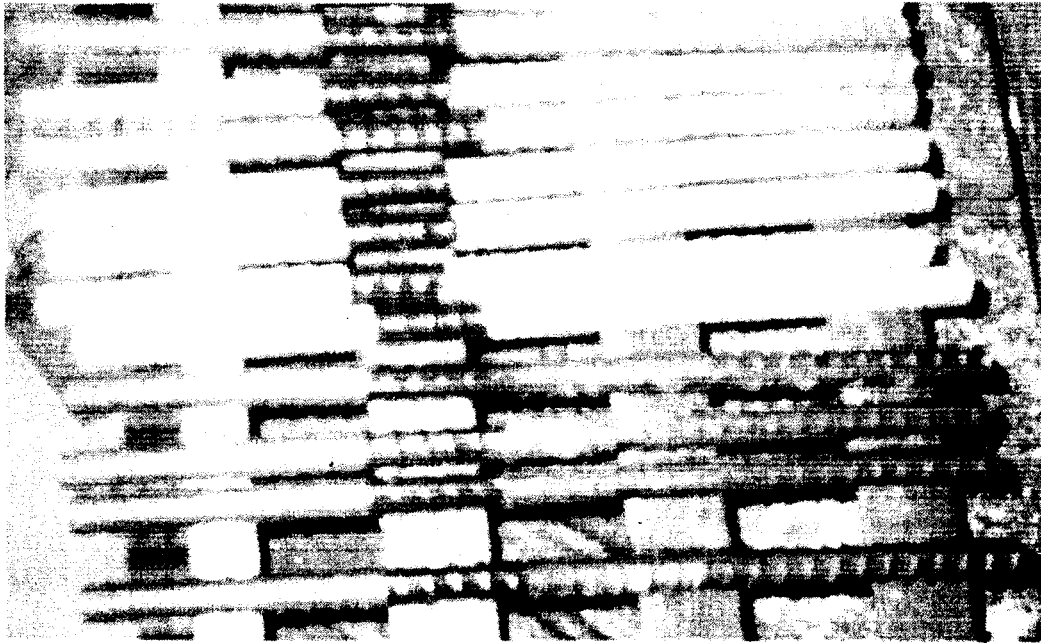
Figure 4.3: Steel bars preparation
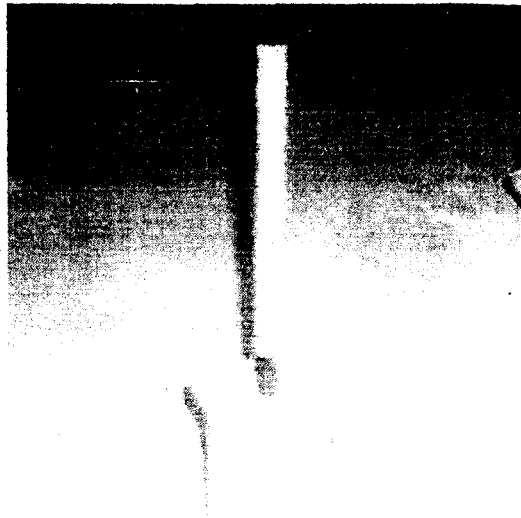
Figure 4.4: Adjustment of the bar verticality

52
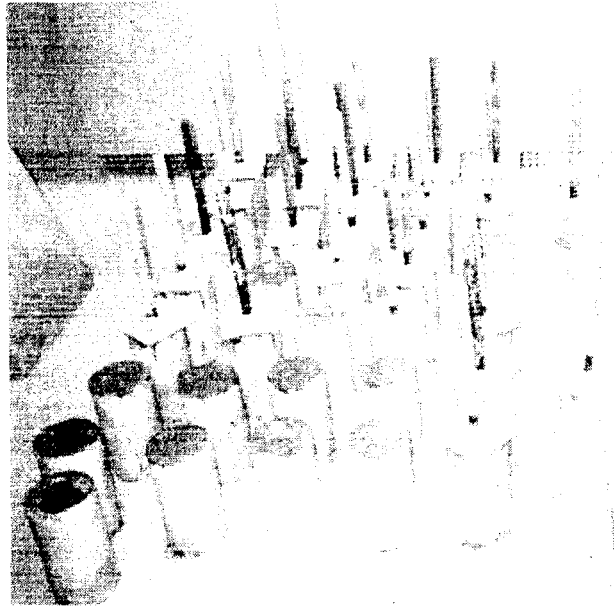
Figure 4.5: Concrete specimens after casting
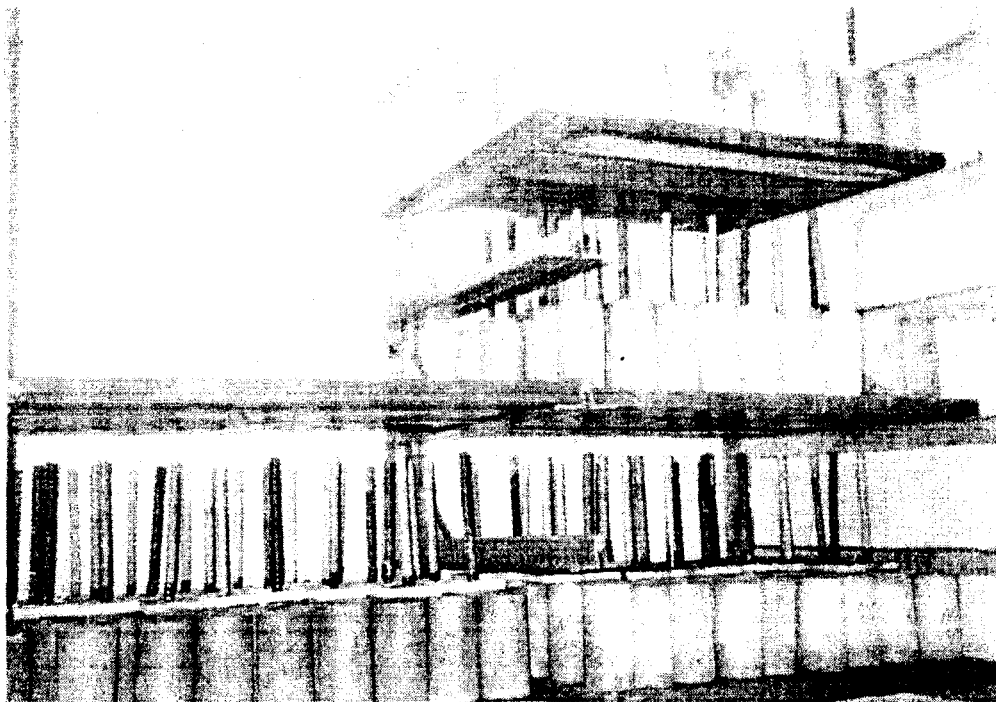
Figure 4.6: Concrete specimens in the curing room
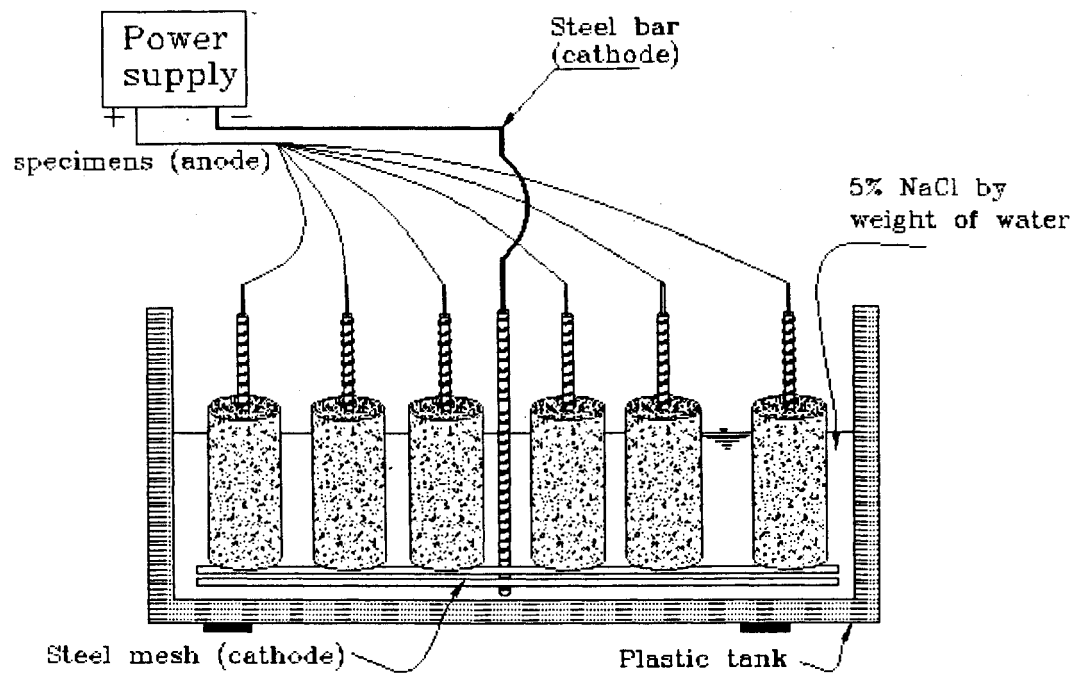
Figure 4.7: Schematic diagram of the accelerated corrosion test

Figure 4.8: Accelerated corrosion tank

54
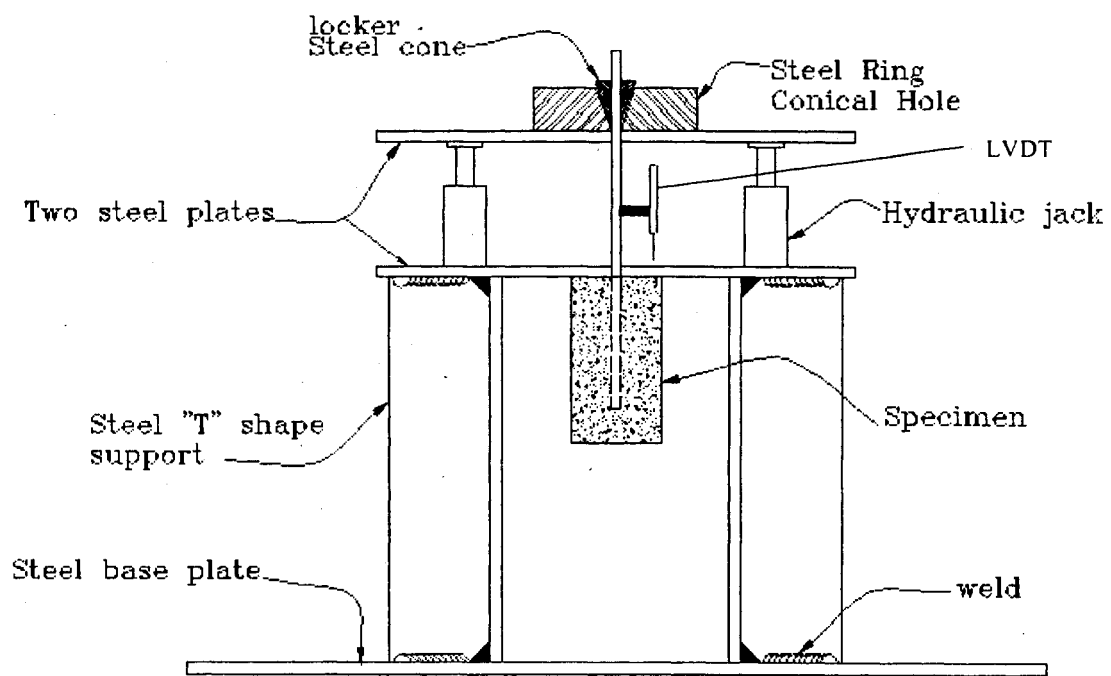
Figure 4.9: Pullout test setup

55

CHAPTER 5
TEST RESULTS

5.1 Introduction

The test results presented in this chapter are divided into three groups. The first group uses the current measurements to study the effect of different concrete types and the different steel types on corrosion initiation. The second group uses the pullout test to study the bond strength for different steel-concrete types, the study of the bond strength includes: uncorroded, pre-cracking, cracking, and severe corrosion stage. The third group shows the effect of corrosion on the bond strength for different degrees of corrosion with the percentage loss of the bar weight and the bar rib profile.

5.2 Current measurement results

5.2.1 Effect of steel types on the current measurements

Figures 5.1 through 5.12 show the relationship between the current in mA and the immersion time in days for NPC concrete (w/c = 0.52), NPC concrete (w/c = 0.32), S.F concrete, and F.A with the different steel types (regular carbon steel, epoxy-coated, and stainless steel bars) at different corrosion stages.

The epoxy-coated bars exhibited a sudden increase in the current readings compared to the stainless steel bars and the regular carbon steel bars for the two tested concrete types NPC concretes (w/c = 0.52 and 0.32) (Fig. 5.3 and 5.6). The current readings of the epoxy-coated bars changed from an average value of 3.4 mA to a maximum of 490 mA within 5 days, and from an average value of 1.2 mA to a maximum of 350 mA within 6 days with NPC concrete (w/c = 0.52), and NPC concrete (w/c = 0.32), respectively.

The epoxy-coated bars showed the lowest current readings before cracking during the whole period of the immersion time compared to the stainless steel bars and the regular carbon steel bars. The current readings of the epoxy-coated bars before cracking recorded an average value of 3.2, 1.3, 0.4, and 0.2 mA with NPC concrete (w/c = 0.52), NPC concrete (w/c = 0.32), S.F concrete, and F.A concrete respectively.

The stainless steel bars and the regular carbon steel bars showed similarity in reaching pre-cracking, cracking, and severe corrosion stages. For both stainless steel bars and regular carbon steel bars, NPC concrete (w/c = 0.52) recorded an average of 9, 17, and 19 days to reach pre-cracking, cracking, and severe corrosion stages respectively. While NPC concrete (w/c = 0.32) recorded an average of 25, 28, and 39 days to reach pre-cracking, cracking, and severe corrosion stages respectively. Also for both stainless steel bars and regular carbon steel bars S.F concrete recorded an average of 56, 66, and 90 days to reach pre-cracking, cracking, and severe corrosion stages respectively while F.A concrete recorded an average of 56, 66, and 93 days to reach pre-cracking, cracking, and severe corrosion stages respectively (Table 5.1).

The current readings for the stainless steel bars and regular carbon steel bars changed from an average value of 48 mA to a maximum value of 390 and 510 mA (for stainless steel bars and regular carbon steel bars, respectively) within 13 days, and from an average value of 20 mA to a maximum value of 325 mA within average of 16 days when using NPC concrete (w/c = 0.52) and, NPC concrete (w/c = 0.32) respectively (Fig. 5.3 and 5.6). On the other hand, the current readings for the same bars changed from an average value of 3.5 mA to a maximum value of 160 and 250 mA (for stainless steel bars and regular carbon steel bars, respectively) within 90 days, and from an average value of 1.6 mA to a maximum value of 134 mA within average of 91 days when using S.F concrete and, F.A concrete, respectively (Fig. 5.9 and 5.12).

The current passing through the stainless steel bars and the regular carbon steel bars started with a low level at an early age then rapidly increased after a certain time. The

57

current recorded an average initial value of 50, 17, 4.5, and 2.5 mA for stainless steel bars with NPC concrete (w/c = 0.52), NPC concrete (w/c = 0.32), S.F concrete, and F.A concrete respectively, and an average initial value of 45, 17, 4, and 2.2 mA for regular carbon steel bars with NPC concrete (w/c = 0.52), NPC concrete (w/c = 0.32), S.F concrete, and F.A concrete respectively. The current was rapidly increased because of the concrete cover cracking which left the steel bars without protection.

The current-immersion time relationship in most of the cases for the three different steel types showed an initial decrease in the current followed by sudden increase. The decrease of current for the first few days is an indication of the formation of the passive film around the reinforcing steel bar, which protect the steel from corrosion complying with previous researches Cornet et al. (1968). The sudden increase in the current was observed to coincide generally with the specimen cracking. In other words, the rate of corrosion of the steel bars was very slow at first, until depassivation of the steel occurred when corrosion started, and then the rate of corrosion increased significantly.

For epoxy-coated bars only severe corrosion stage was recorded, since a sudden cracking was observed across the specimen passing through the embedded end of the bar (Fig. 5.13), this sudden cracking was due to corrosion concentration around the uncoated embedded end of the bar. The surface of the cross-sectional area of the embedded end was left uncoated after cutting the bar to the required length. Hence, the corrosion products accumulated and concentrated in a small area trying to occupy more space, which caused vertical expansion and exerted a tension force leading to separate the lower part of the concrete specimen from the upper part at the embedded end of the bar.

The epoxy-coated bars embedded in NPC concretes (w/c = 0.52 and 0.32), were monitored for a maximum period of two months until severe corrosion occurred in all of the specimens. The results of the epoxy-coated bars embedded in S.F concrete and F.A concrete were not included in this research because the corrosion did not occur for a period of more than 6 months.

5.2.2 Effect of concrete types on current measurements and time-induced corrosion

Figures 5.14 through 5.20 show the relationship between the current in mA and the immersion time in days for regular carbon steel, epoxy-coated, and stainless steel bars, with the four different concrete types [NPC concrete (w/c = 0.52), NPC concrete (w/c = 0.32), S.F concrete, and F.A concrete] at different corrosion stages.

As expected, NPC concrete (w/c = 0.52) demonstrated the highest current values in the early stages of the test, approximately 48 mA with the regular carbon steel bars, 50 mA with the stainless steel bars, and 3.6 mA with the epoxy-coated bars, followed by NPC concrete (w/c = 0.32), approximately 20 mA with the regular carbon steel bars, 18 mA with the stainless steel bars, and 1.8 mA with in the epoxy-coated bars. Silica fume concrete demonstrated lower initial current reading than both NPC concretes (w/c = 0.52 and 0.32), approximately 4.5 mA with the regular carbon steel bars, and 5 mA with the stainless steel bars, but still higher than F.A concrete which showed the lowest initial current readings, approximately 2.5 mA with the regular carbon steel bars, and 2.6 mA with the stainless steel bars.

The initial lower current passing through the concrete specimens is an indication of the higher resistivity of the concrete. Permeability of the concrete is the main factor influencing the concrete resistivity, higher w/c ratio results in a higher permeability concrete than lower w/c ratio concrete, since the excess water in the concrete matrix occupies more voids (Neville 1981). On the other hand, the concrete with silica fume or fly ash as a supplementary cementing material exhibit lower permeability than the NPC concrete (Mehta 1981).

Supplementary cementing materials such as silica fume or fly ash improves the concentration of the hydration products, especially around aggregate particles and acts as the nucleation site for the calcium hydroxide crystals so it will be widely distributed in the

matrix rather than accumulating in water filled pores and around the aggregates. also the pozzolanic reaction that results from the supplementary cementing materials produces calcium-silicate-hydrate gel, which is dense, so it can fill more space for the same equal mass (Sarkar and Aitcin 1987, Berry and Molhotra 1987, Larbi 1993).

The maximum current reading corresponding to severe corrosion stages in all steel types was higher in higher permeability concrete (NPC concrete (w/c = 0.52)) than less permeability concrete (F.A and S.F concrete). The maximum current readings corresponding to severe corrosion stage for NPC concrete (w/c = 0.52) were 522 mA, 490 mA, and 380 mA for regular carbon steel bars, epoxy-coated bars, and stainless steel bars, respectively. while the maximum current readings corresponding to severe corrosion stage for NPC concrete (w/c = 0.32) were 330 mA, 350 mA, and 320 mA for regular carbon steel bars. epoxy-coated bars, and stainless steel bars, respectively. Also. the maximum current readings corresponding to severe corrosion stage for S.F concrete were 250 mA and 160 mA when using regular carbon steel bars and stainless steel bars respectively, while the maximum current readings corresponding to severe corrosion stage for F.A concrete was 134 mA for both regular carbon and stainless steel bars (Fig. 5.14. 5.17 and 5.20).

Normal Portland cement concrete with w/c ratio of 0.52 took 2 and 3 days to reach severe corrosion stage from the pre-cracking stage when using regular carbon steel bars and stainless steel bars, respectively, while NPC concrete (w/c = 0.32) took 11 and 13 days to reach severe corrosion stage from pre-cracking stage for regular carbon steel bars and stainless steel bars, respectively. Also, S.F concrete took 22 and 25 days from the pre-cracking stage to the severe corrosion stage when using regular carbon steel bars and stainless steel bars respectively, while F.A concrete took 25 and 29 days to reach severe corrosion stage from pre-cracking stage when using regular carbon steel bars and stainless steel bars respectively. The improvement for using low w/c ratio in concrete was clear in using NPC concrete (w/c = 0.32), since it provides 4 to 5-times better corrosion protection than using NPC concrete (w/c = 0.52). Also the improvement for using supplementary

cementing materials in low w/c ratio concrete was clear in using F.A and S.F concretes, they provided an average of 2-times better corrosion protection than using NPC concrete (w/c = 0.32).

5.3 Pullout test results

The pull out test was performed using a specially designed loading frame with manually operated hydraulic jacks. After establishing the specified level of corrosion, the specimen was removed from the accelerated corrosion tank and the pullout test was performed. One LVDT was hooked between the top surface of the concrete specimen and the loaded end of the steel bar to measure the relative displacement between them. The bond stress was calculated by dividing the ultimate pullout force over the surface area of the embedded part of the bar. The displacement was plotted against the bond stress to demonstrate the relationship of bond stress-slip for different concrete types and different steel types for uncorroded specimens. The displacement was also plotted against bond stress for the corroded specimens to demonstrate the effect of different degrees of corrosion on bond strength. The percentage the of weight loss for the corroded bars as well as the degradation of the rib height was measured and recorded against the bond stress to demonstrate the effect of corrosion with different concrete types and different steel types on bond stress. Tables 5.2 to 5.5 present the results of the pullout test for the different steel-concrete types.

5.3.1 Bond stress-slip relationships for uncorroded specimens

The bond stress-slip relationships for the uncorroded bars (0 corrosion level) are evaluated for the different steel types (epoxy-coated bars, regular carbon steel bars, and stainless steel bars) and for different concrete types [NPC concrete (w/c = 0.52), NPC concrete (w/c = 0.32), S.F concrete, and F.A concrete]. The effect of each steel and concrete types on the bond stress is demonstrated in the following sections.

5.3.1.1 Effect of steel types on bond stress-slip relationship

Figures 5.21 through 5.24 show the relationship between the bond stress in Mpa and the slip in mm for NPC concrete (w/c = 0.52), NPC concrete (w/c = 0.32), S.F concrete, and F.A with the different steel types (regular carbon steel, epoxy-coated, and stainless steel bars) at different corrosion stages.

As seen from the results, the epoxy-coated bars show the lowest bond stress compared to the regular carbon steel bars and stainless steel bars for all concrete types. For example, the epoxy –coated bars show an average of 14.6 and 8.6 % less in bond stress than regular carbon steel bars and stainless steel bars respectively when using NPC concrete (w/c = 0.52) (Fig 5.21). While they show an average of 22.3 and 7.4 % less in bond stress than regular carbon steel bars and stainless steel bars respectively when using F.A concrete (Fig 5.24).

The stainless steel bars demonstrated slightly higher bond stress than the epoxy-coated bars but still lower than the regular carbon steel bars for all concrete types. The stainless steel bars show an average of 10 % less in bond stress than regular carbon steel bars when using normal Portland cement concrete, while they show an average of 13 % less in bond stress than regular carbon steel bars when using concrete with supplementary cementing materials (F.A and S.F concrete)

5.3.1.2 Effect of concrete types on bond stress-slip relationship

Figures 5.25 to 5.27 show the relationship between the bond stress in Mpa and the slip in mm for regular carbon steel, epoxy-coated, and stainless steel bars with the four different concrete types [NPC concrete (w/c = 0.52), NPC concrete (w/c = 0.32), S.F concrete, and F.A concrete] at different corrosion stages.

Normal Portland cement concrete with w/c ratio of 0.32 exhibited the highest bond strength than the other concretes; it showed 47, 79, and 82 % higher in bond strength than F.A, S.F, and NPC concrete (w/c = 0.52), respectively when using epoxy-coated bars (Fig. 5.25). Also it showed 35, 54, and 84 % higher in bond strength than F.A, S.F, and NPC concrete (w/c = 0.52), respectively when using regular carbon steel bars (Fig. 5.26). Meanwhile when using stainless steel bars, NPC concrete (w/c = 0.32) showed 35, 45, and 66 % higher in bond strength than F.A, S.F, and NPC concrete (w/c = 0.52), respectively (Fig. 5.27).

The bond strength for F.A concrete was higher than S.F and NPC concrete (w/c = 0.52) but still lower than NPC concrete (w/c = 0.32); it showed 22, and 24 % higher in bond strength than S.F, and NPC concrete (w/c = 0.52), respectively when using epoxy-coated bars (Fig. 5.25). Also it showed 14, and 36 % higher in bond strength than S.F, and NPC concrete (w/c = 0.52), respectively when using regular carbon steel bars (Fig. 5.26). Furthermore, when using stainless steel bars, F.A concrete showed 7, and 23 % higher in bond strength than S.F, and NPC concrete (w/c = 0.52), respectively (Fig. 5.27).

Silica fume concrete exhibited higher bond stress than NPC concrete (w/c = 0.52) and lower bond stress than each NPC concrete (w/c = 0.32) and F.A concrete for all steel types. Silica fume concrete showed 2, 19, and 15 % higher in bond strength than NPC concrete (w/c = 0.52) when using epoxy-coated bars, regular carbon steel bars, and stainless steel bars, respectively (Figs. 5.25, 5.26, and 5.27).

5.3.2 Effect of different degrees of corrosion on bond strength

5.3.2.1 Corrosion observation

The three types of steel embedded in the four concrete types were carefully checked for the corrosion effects, the results of the observation were as follows:-

- Fly ash concrete as well as silica fume concrete showed less number of cracks (in the cracking stage and severe corrosion stage) than NPC concrete (w/c = 0.32) and NPC concrete (w/c = 0.52), their cracks were usually one or two, started from the top of the concrete cylinder and extended approximately 50 mm down, while both NPC concretes (w/c = 0.32 and 0.52) showed more cracks (four to six cracks), started from the top of the concrete cylinder and extended up to the end of the embedded bar.

- When using NPC concrete (w/c = 0.52), some concrete was adhering on the bar's surface after the pullout tests were performed, while less concrete was adhering when using NPC concrete (w/c = 0.32). The steel bars embedded in F.A concrete and S.F concrete did not have any concrete adhering on their surface even when using regular carbon steel bars.

- Regular carbon steel bars showed less damage with no surface voids compared to stainless steel bars, also the ribs of the regular carbon steel bars were slightly damaged (Fig. 5.28). The stainless steel bars were totally damaged after the severe corrosion stage, the bar surface showed lots of voids and no indication of the ribs as seen in Figure 5.29. The rust color for the stainless steel bars was dark black different than that of regular carbon steel rust color, which was brown.

5.3.2.2 Bond stress-slip relationship for different degrees of corrosion

The bond strengths for the regular carbon steel and stainless steel bars were evaluated in each concrete type with four different degrees of corrosion (0 corrosion stage, pre-cracking stage, cracking stage, and severe corrosion stage). The results compared for the four degrees of corrosion are based on the crack width; 0 corrosion stage started after three months of curing and before placing the specimens in the corrosion tank, pre- cracking stage considered when the current started to increases but before any cracking occurred.

Cracking stage started when the first crack occurs in the concrete specimen, and severe corrosion stage considered when any crack extended up to 4 mm. Table 5.2 to 5.5 present the results of the bond strength for each degree of corrosion for both regular carbon steel and stainless steel bars.

5.3.2.2.1 Effect of different degrees of corrosion on bond strength

Figures 5.30 to 5.37 show the bond stress-slip relationship for different degrees of corrosion for regular carbon steel and stainless steel bars embedded in each concrete type. As seen from the figures, in all concrete types and steel types the pre-cracking stage represented the highest bond strength than the other stages. For example when using F.A concrete with regular carbon steel bars (Fig. 5.36), the pre-cracking stage showed 4, 46, and 66% higher in bond strength than 0 corrosion, cracking, and severe corrosion stages respectively. Also when using S.F concrete with stainless steel bars (Fig. 5.35), the pre-cracking stage showed 16, 52, and 76% higher in bond strength than 0 corrosion, cracking, and severe corrosion stages respectively.

In all concrete types and steel types, 0 corrosion stage showed higher bond strength than both the cracking stage and the severe corrosion stage, and lower than the pre-cracking stage. For example it showed 2.5 and 7 times higher in bond strength than cracking and severe corrosion stages, respectively when using NPC concrete (w/c = 0.32) with regular carbon steel bars (Fig. 5.32). Also when using NPC concrete (w/c = 0.52) with stainless steel bars 0 corrosion stage showed 7 and 13 times higher in bond strength than cracking and severe corrosion stages, respectively (Fig. 5.31)

Cracking stage exhibited higher bond stress than severe corrosion stage and lower bond stress than each 0 corrosion and pre-cracking stage for all concrete types and steel types. For example it showed 80, 128, 16 and 17 % higher in bond strength than that of severe corrosion stage when using NPC concrete (w/c = 0.52), NPC concrete (w/c = 0.32), S.F

concrete, and F.A concrete respectively with stainless steel bars (Figs 5.31, 5.33, 5.35 and 5.37).

As mentioned earlier, fly ash concrete and S.F concrete showed one or two cracks, which started from the top of the concrete cylinder and extended approximately 50 mm down, leaving 110 mm from the embedded bar confined with uncracked concrete. On the other hand, NPC concrete (w/c = 0.32) and NPC concrete (w/c = 0.52) have the cracks extended up to the total length of the embedded bar. For this reason, the bond strength for F.A and S.F concrete specimens was higher than NPC concrete (w/c = 0.32) even at the severe corrosion stage. For example the bond strength for regular carbon steel bars in severe corrosion stage was 3.5 and 3.11 when using F.A and S.F respectively, while it was 1.11 and 0.61 when using NPC concrete (w/c = 0.32) and NPC concrete (w/c = 0.52) respectively.

In both regular carbon steel bars and stainless steel bars embedded in any concrete type, the pre-cracking stage exhibited slightly higher bond strength than 0 corrosion stage (as mentioned earlier). This result agrees with the previous researches (Maslehuddin et al 1990 and Amleh 2000). The initial rusty layer (occurs in the pre-cracking stage) that enveloping the bar surface, adds more cohesiveness and friction with the surrounding concrete which definitely increases the bond strength.

5.3.2.2.2 Effect of steel type and concrete type on bond strength in different degrees of corrosion

Figures 5.38 to 5.43 show the effect of using regular carbon steel bar and stainless steel bars with different concrete types in each corrosion stage. At the severe corrosion stage and cracking stage (Fig. 5.40 to 5.43) for both regular carbon steel bars and stainless steel bars, F.A concrete exhibit the highest bond strength than the other used concrete [for example; 1.1, 3 and 6 times higher in bond strength than S.F concrete, NPC concrete (w/c = 0.32), NPC concrete (w/c = 0.52), respectively when using regular carbon steel bars at

severe corrosion stage (Fig. 5.42)], followed by S.F concrete [for example; 3 and 5 times higher in bond strength than NPC concrete (w/c = 0.32) and NPC concrete (w/c = 0.52), respectively when using regular carbon steel bars at severe corrosion stage(Fig. 5.42)] then NPC concrete (w/c = 0.32) which showed higher bond strength than NPC concrete (w/c = 0.52) [for example; 2 times higher in bond strength than NPC concrete (w/c = 0.52) when using regular carbon steel bars at severe corrosion stage(Fig. 5.42)].

At pre-cracking stage, for both regular carbon steel bars and stainless steel bars (Fig. 5.38 and 5.39), NPC concrete (w/c = 0.32) shows the highest bond strength than the other used concrete [for example; 1.4, 1.5 and 1.2 times higher in bond strength than F.A concrete, S.F concrete and NPC concrete (w/c = 0.52), respectively when using regular carbon steel bars (Fig. 5.38)], followed by F.A concrete [for example; 1.1 and 1.3 times higher in bond strength than S.F concrete and NPC concrete (w/c = 0.52), respectively when using regular carbon steel bars (Fig. 5.38)] then S.F concrete which showed higher bond strength than NPC concrete (w/c = 0.52) [for example; 1.2 times higher in bond strength than NPC concrete (w/c = 0.52) when using regular carbon steel bars (Fig. 5.38)].

In all concrete types, regular carbon steel bars show higher bond strength than stainless steel bars in all corrosion stages. For example at cracking stage for F.A concrete (Fig. 5.40 and 5.41); the regular carbon steel bars was 9 % higher in bond strength than the stainless steel bars. The difference in the bond strength values between the two bars are more significant in 0 corrosion stage than that of the corroded stages. At 0 corrosion stage the effect of surface friction is considered between the two bars, while the corrosion products decrease the surface friction for both of them as corrosion continues to take place.

5.3.3 Effect of mass loss on bond strength

The mass loss of the steel reinforcing bar was obtained as the difference between the mass of the corroded bar (after removal of the loose corrosion product) from its mass before

corrosion. The effect of the different degrees of corrosion (calculated as a percentage of mass loss) on the bond strength was calculated for each concrete and steel type.

Figures 5.44 to 5.49 show the relationship between the bond strength in MPa and different degrees of corrosion (as a percentage of mass loss) for different concrete and steel types, the figures demonstrate the relationship for each concrete type with the regular carbon steel bars and stainless steel bars, and each steel type with the different concrete types.

As seen from the figures, in all concrete and steel types, the bond strength increased with very small increase of the percentage of mass loss, [for example the bond strength increased by 6% and 9% with 0.34 and 0.71 percentage of mass loss when using regular carbon steel bars and stainless steel bars respectively with NPC concrete (w/c = 0.52) (Fig. 5.44)], and then decreases with further increase of the mass loss [for example the bond strength decreased by 3.4 and 7.1 times with 3.75 and 4.49 percentage of mass loss when using regular carbon steel bars and stainless steel bars respectively with NPC concrete (w/c = 0.52) (Fig. 5.44)]. The reason for the first increase of the bond strength was the formation of a very thin rusty layer around the bar, which increases the concrete-steel friction. Furthermore, with the increase in the corrosion products, a friable layer formed around the bar leading to a significant decrease of the bond strength due to the loss of the surface friction and the degradation of the ribs height.

Fly ash concrete and S.F concrete exhibited constant bond strength at high percentage of mass loss, these bond strength are considerably high compared to that of NPC concrete (w/c = 0.52) and NPC concrete (w/c = 0.32), for example with regular carbon steel bars, the bond strength at high percentage of mass loss was 3.5 and 2.7 MPa when using F.A and S.F concretes, respectively (Figs 5.46 and 5.47), while it was 1.1 and 0.6 MPa when using NPC concrete (w/c = 0.32) and NPC concrete (w/c = 0.52) respectively with the same steel bars (Figs 5.44 and 5.45). The reason for that was related to the uncracked lower part of the specimen which does not exists in both NPC concretes (w/c = 0.52 and 0.32) as mention before.

5.3.4 Effect of loss of rib profile on bond strength

The ribs height were measured after the corrosion took place, and after cleaning the bars according to ASTM G1-90, The rib profile loss of the steel reinforcing bar was obtained as the difference between rib height of the corroded bar (after removal of the loose corrosion product) from its height before corrosion. The effect of the rib height degradation for both F.A concrete and S.F concrete was not clear and could not be added to the charts, since the bars in their specimens corroded from the top only within a small cracked section.

Figures 5.50 to 5.53 show the relationship between the bond strength in MPa and different degrees of loss in rib profile for different concrete and steel types, the figures demonstrate the relationship for each concrete type with the regular carbon steel bars and stainless steel bars, and each steel type with the NPC concrete (w/c = 0.32) and NPC concrete (w/c = 0.52).

The relationship shows slight increase in the bond strength with a very small decrease of the rib profile loss, followed by a considerable decrease of the bond strength with the increase loss of the bar profile. For example the bond strength increased by 4 and 10 % with 9 and 9.5 percentage of rib profile loss, while it decreased by 47 and 152 % with 22 and 31 % of bar profile loss when using regular carbon steel bars and stainless steel bars respectively with NPC concrete (w/c = 0.32).

Table 5.1: Corrosion times for different concrete and steel types at different corrosion stages

Concrete type	Corrosion time (days)								
	Regular carbon steel bars			Epoxy-coated bars			Stainless steel bars		
	Pre-cracking stage	Cracking stage	Severe corrosion	Pre-cracking stage	Cracking stage	Severe corrosion	Pre-cracking stage	Cracking stage	Severe corrosion
NPC concrete (w/c =0.52)	9	17	19	–	–	22	9	16	19
NPC concrete (w/c =0.32)	25	28	38	–	–	58	25	28	41
F.A Concrete (w/c =0.32)	56	66	91	–	–	–	56	66	95
S.F Concrete (w/c =0.32)	56	66	88	–	–	–	56	66	91

70

Table 5.2: Bond test data for NPC concrete (w/c = 0.52) for different steel types at different corrosion stages

Specimen No.	Steel bar type	Corrosion stage	Average crack number	Maximum crack width (mm)	% Weight loss	% Rib profile loss	Slip at maximum load (mm)	Bond strength (MPa)
1	Regular carbon steel bars	0 Corrosion	0	0	0	0	0.76	4
2			0	0	0	0	0.83	4.1
3			0	0	0	0	0.79	3.63
4		Pre-cracking	0	0	0.34	9.6	0.87	4.35
5		Cracking	1	0.1	3.41	13.6	0.4	1.54
6			2	0.1	6.51	28.8	0.3	0.94
7			2	0.1	3.75	22.7	0.35	1.2
8		Severe corrosion	6	4	7.44	40.95	0.31	0.7
9			5	5	8.67	54.5	0.27	0.61
10	Epoxy coated bars	0 Corrosion	0	0	0	-	0.8	4.56
11			0	0	0	-	0.75	3.5
12			0	0	0	-	0.74	3.47
13		Severe corrosion	Splitting horizontal crack	-	-	-	0.75	3.59
14				-	-	-	0.7	3.3
15				-	-	-	0.71	3.15
16				-	-	-	0.72	3.3
17				-	-	-	0.77	4.19
18				-	-	-	0.79	4.4
19	Stainless steel bars	0 Corrosion	0	0	0	0	0.6	2.66
20			0	0	0	0	0.69	3.23
21			0	0	0	0	0.7	3.83
22		Pre-cracking	0	0	0.71	8	0.67	4.16
23			0	0	0.64	9	0.72	4
24		Cracking	2	0.1	4.49	48.4	0.2	0.54
25			2	0.1	5	20	0.2	0.77
26		Severe corrosion	7	4	10.26	71.2	0.2	0.35
27			7	4.5	10.58	77.3	0.2	0.3

Table 5.3: Bond test data for NPC concrete (w/c = 0.32) for different steel types at different corrosion stages

Specimen No.	Steel bar type	Corrosion stage	Average crack number	Maximum crack width (mm)	% Weight loss	% Rib profile loss	Slip at maximum load (mm)	Bond strength (MPa)
28	Regular carbon steel bars	0 Corrosion	0	0	0	0	0.93	7.55
29			0	0	0	0	0.85	5.36
30			0	0	0	0	0.92	7.1
31		Pre-cracking	0	0	0.93	22.74	0.84	5.13
32			0	0	0.64	9	0.87	7.93
33		Cracking	1	0.1	1.86	28.8	0.28	3
34			1	0.1	2.2	31	0.25	2.7
35		Severe corrosion	3	4	3.72	45.48	0.2	1.76
36			4	4	5.27	59.07	0.32	1.11
37	Epoxy coated bars	0 Corrosion	0	0	0	-	0.86	6.5
38			0	0	0	-	0.84	5.52
39			0	0	0	-	0.93	6.39
40		Severe corrosion	Splitting horizontal crack	-	-	-	0.8	5.15
41				-	-	-	0.94	6.61
42				-	-	-	0.9	6.42
43				-	-	-	0.85	6.24
44				-	-	-	0.85	6
45				-	-	-	0.86	6.35
46	Stainless steel bars	0 Corrosion	0	0	0	0	0.95	6.37
47			0	0	0	0	0.86	6
48			0	0	0	0	0.8	5.16
49		Pre-cracking	0	0	0.45	9.54	0.85	6.93
50			0	0	0.89	11.8	0.92	6.4
51		Cracking	1	0.1	2	48.66	0.3	1.6
52			1	0.1	1	31.8	0.3	2.5
53		Severe corrosion	4	5	7.05	68.22	0.25	0.7
54			-	-	-	-	-	-

Table 5.4: Bond test data for S.F concrete for different steel types at different corrosion stages

Specimen No.	Steel bar type	Corrosion stage	Average crack number	Maximum crack width (mm)	% Weight loss	% Rib profile loss	Slip at maximum load (mm)	Bond strength (MPa)
82	Regular carbon steel bars	0 Corrosion	0	0	0	-	0.6	5.1
83			0	0	0	-	0.71	4.89
84			0	0	0	-	0.85	7.79
85		Pre-cracking	0	0	0.93	-	0.65	5.55
86			0	0	0.93	-	0.82	5.4
87		Cracking	1	0.1	3.8	-	0.35	2.7
88			1	0.1	-	-	0.5	3.54
89		Severe corrosion	2	4	1	-	0.4	3.11
90			2	4.5	3.41	-	0.34	2.82
91	Epoxy coated bars	0 Corrosion	0	0	0	-	0.55	4
92			0	0	0	-	0.55	4.37
93			0	0	0	-	0.5	3.57
94		Severe corrosion	Splitting horizontal crack	-	-	-	-	-	-
95				-	-	-	-	-	-
96				-	-	-	-	-	-
97				-	-	-	-	-	-
98				-	-	-	-	-	-
99				-	-	-	-	-	-
100	Stainless steel bars	0 Corrosion	0	0	0	-	0.67	5.74
101			0	0	0	-	0.6	5
102			0	0	0	-	0.5	4.4
103		Pre-cracking	0	0	0.64	-	0.52	5.1
104			0	0	0.64	-	0.61	5.4
105		Cracking	1	0.1	0.64	-	0.36	3.35
106			1	0.1	3.4	-	0.33	3.25
107		Severe corrosion	2	4	3.5	-	0.3	3
108			2	4	3.4	-	0.29	2.9

Table 5.5: Bond test data for F.A concrete for different steel types at different corrosion stages

Specimen No.	Steel bar type	Corrosion stage	Average crack number	Maximum crack width (mm)	% Weight loss	% Rib profile loss	Slip at maximum load (mm)	Bond strength (MPa)
55	Regular carbon steel bars	0 Corrosion	0	0	0	-	0.69	5.45
56			0	0	0	-	0.73	5.59
57			0	0	0	-	0.67	5.31
58		Pre-cracking	0	0	0.31	-	0.75	5.82
59			0	0	0.4	-	0.7	5.47
60		Cracking	1	0.1	0.81	-	0.5	3.98
61			1	0.1	0.48	-	0.55	4.5
62		Severe corrosion	1	4	4.03	-	0.45	3.5
63			1	4	1.86	-	0.49	3.54
64	Epoxy coated bars	0 Corrosion	0	0	0	-	0.55	4.38
65			0	0	0	-	0.49	4.35
66			0	0	0	-	0.57	4.69
67		Severe corrosion	Splitting horizontal crack	-	-	-	-	-	-
68				-	-	-	-	-
69				-	-	-	-	-
70				-	-	-	-	-
71				-	-	-	-	-
72				-	-	-	-	-
73	Stainless steel bars	0 Corrosion	0	0	0	-	0.5	4.65
74			0	0	0	-	0.44	3.43
75			0	0	0	-	0.45	4.7
76		Pre-cracking	0	0	0.44	-	0.65	5.33
77			0	0	0.5	-	0.67	5.45
78		Cracking	1	0.1	0.96	-	0.4	3.66
79			1	0.1	0.9	-	0.5	4.1
80		Severe corrosion	2	4.5	1.92	-	0.4	3.14
81			2	4	3	-	0.42	3.8

74
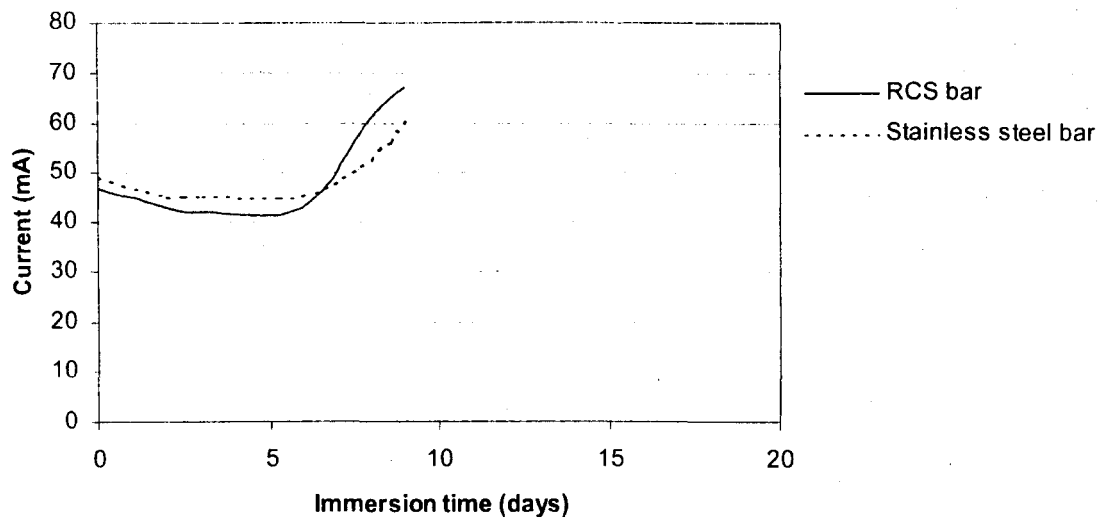
Figure 5.1: Current readings for NPC concrete (w/c = 0.52) specimens with different steel types for pre-cracking stage
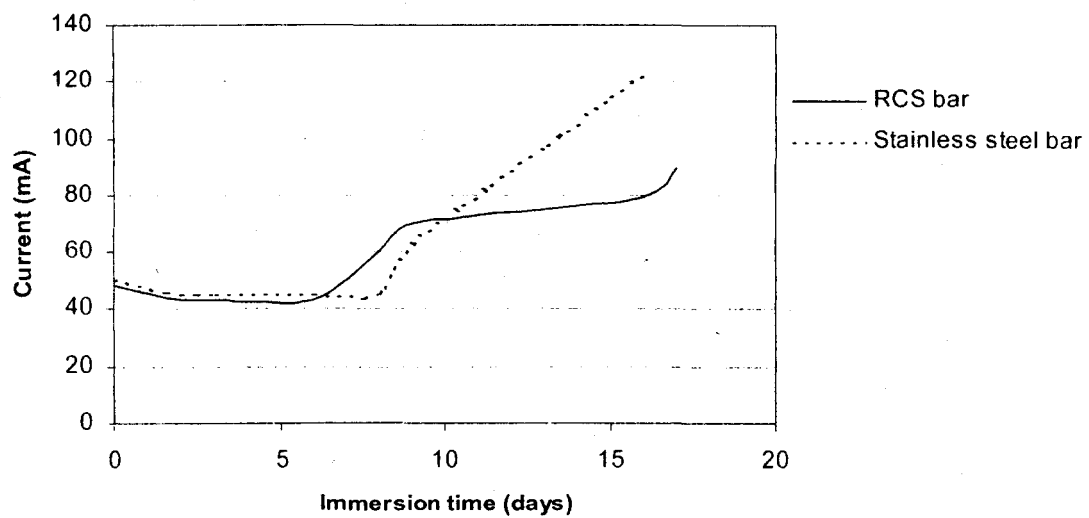
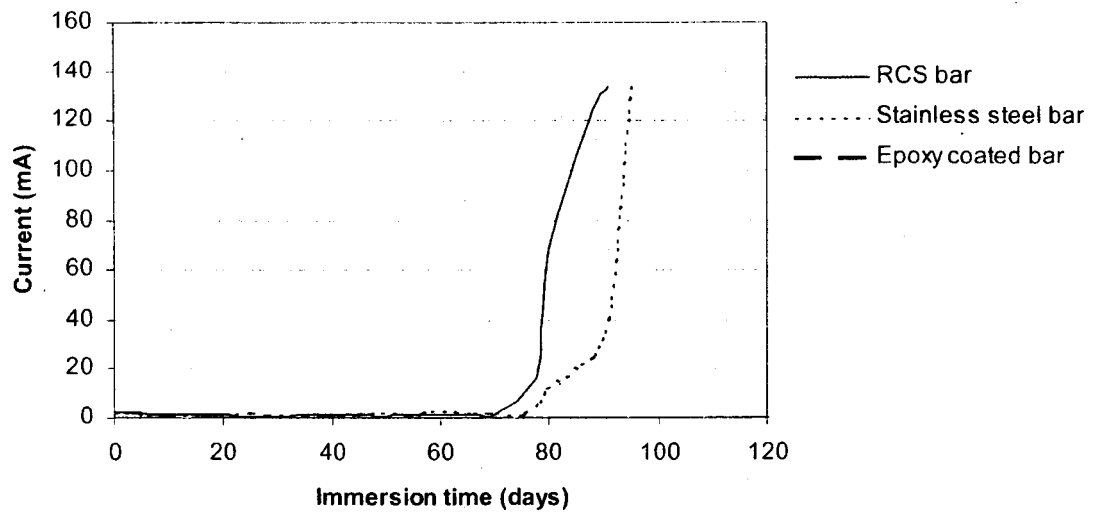**Figure 5.2**: Current readings for NPC concrete (w/c = 0.52) specimens with different steel types for cracking stage

75
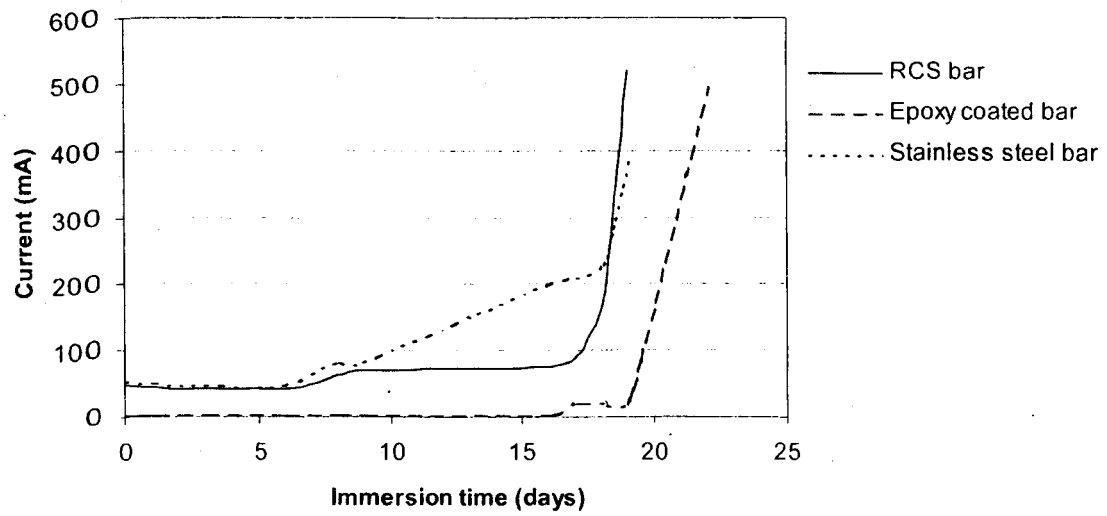
Figure 5.3: Current readings for NPC concrete (w/c = 0.52) specimens with different steel types for severe corrosion stage
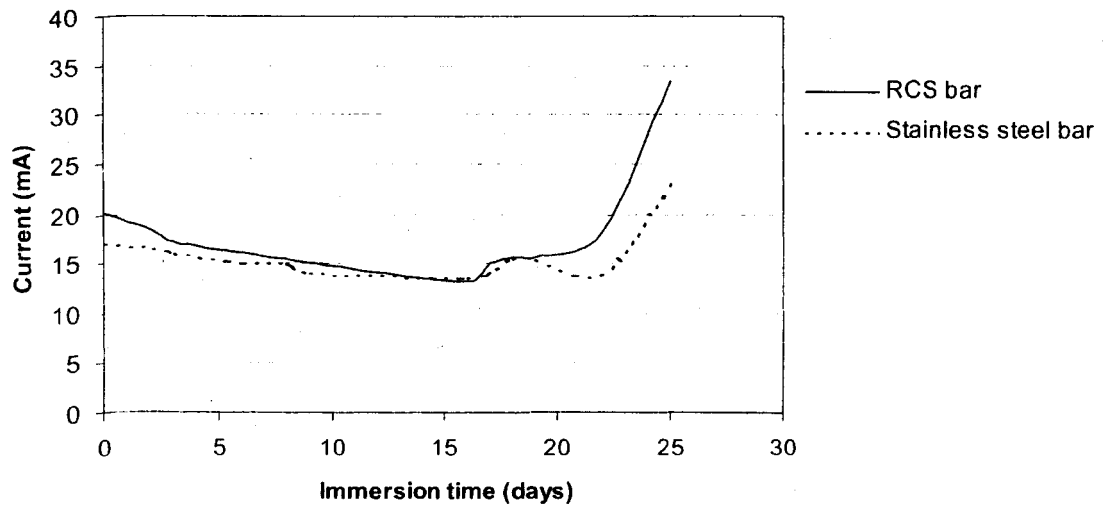
Figure 5.4: Current readings for NPC concrete (w/c = 0.32) specimens with different steel types for pre-cracking stage
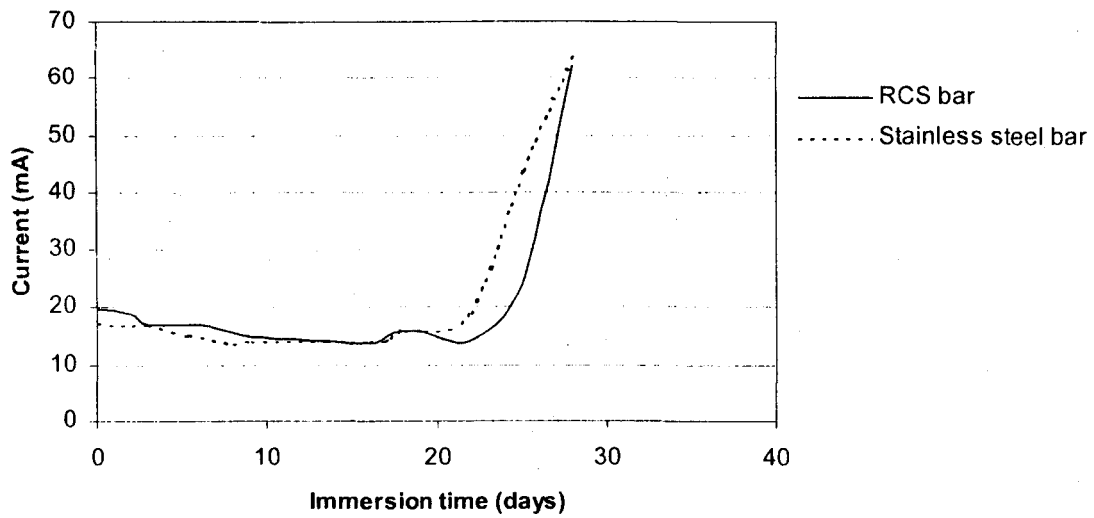
Figure 5.5: Current readings for NPC concrete (w/c = 0.32) specimens with different steel types for cracking stage
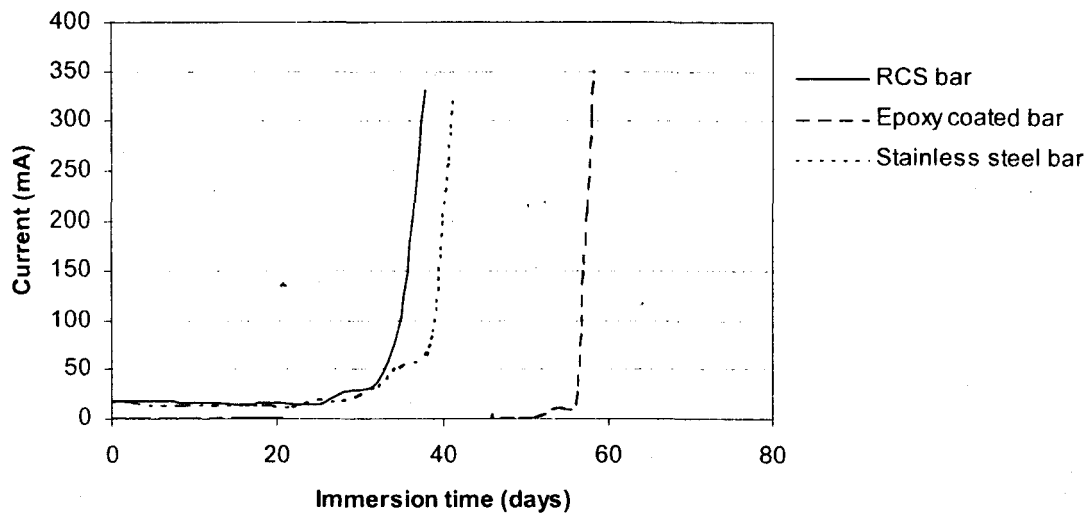
Figure 5.6: Current readings for NPC concrete (w/c = 0.32) specimens with different steel types for severe corrosion stage

77
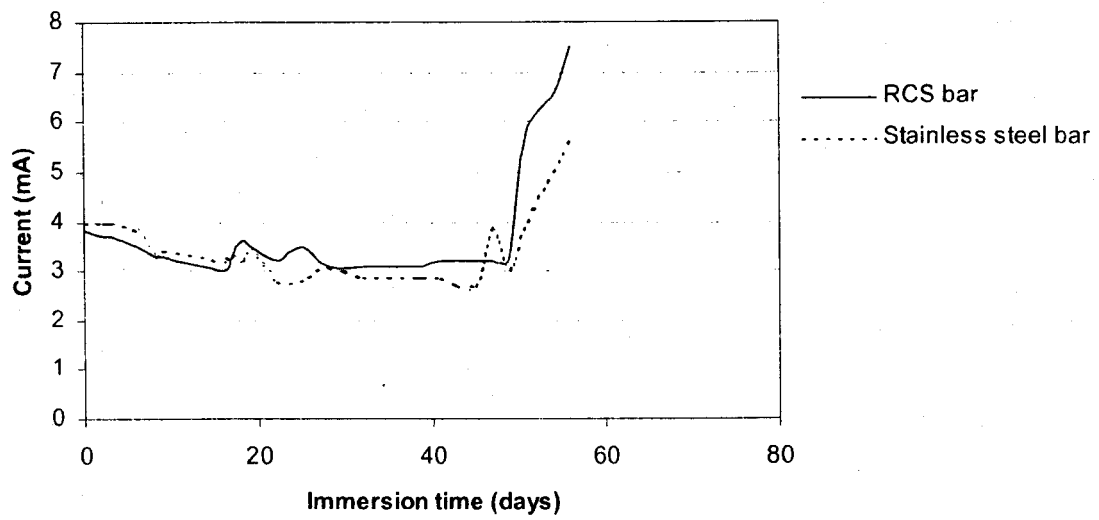
Figure 5.7: Current readings for S.F concrete specimens with different steel types for pre-cracking stage
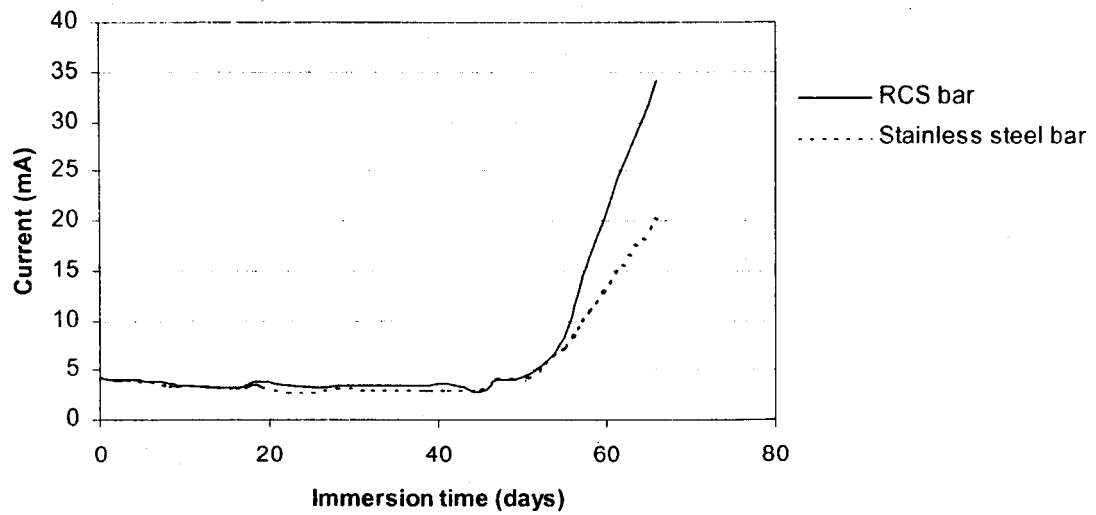
Figure 5.8: Current readings for S.F concrete specimens with different steel types for cracking stage
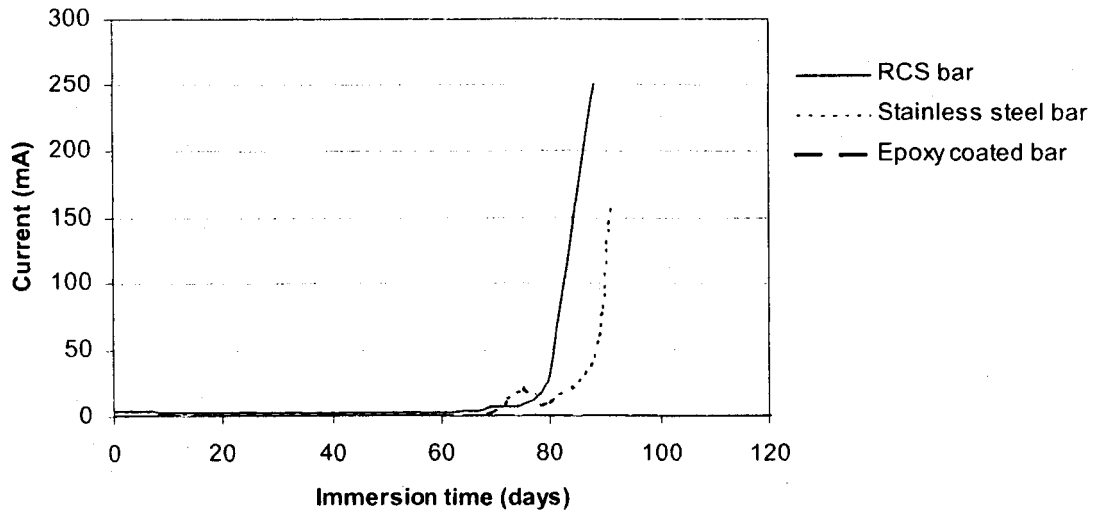
Figure 5.9: Current readings for S.F concrete specimens with different steel types for severe corrosion stage
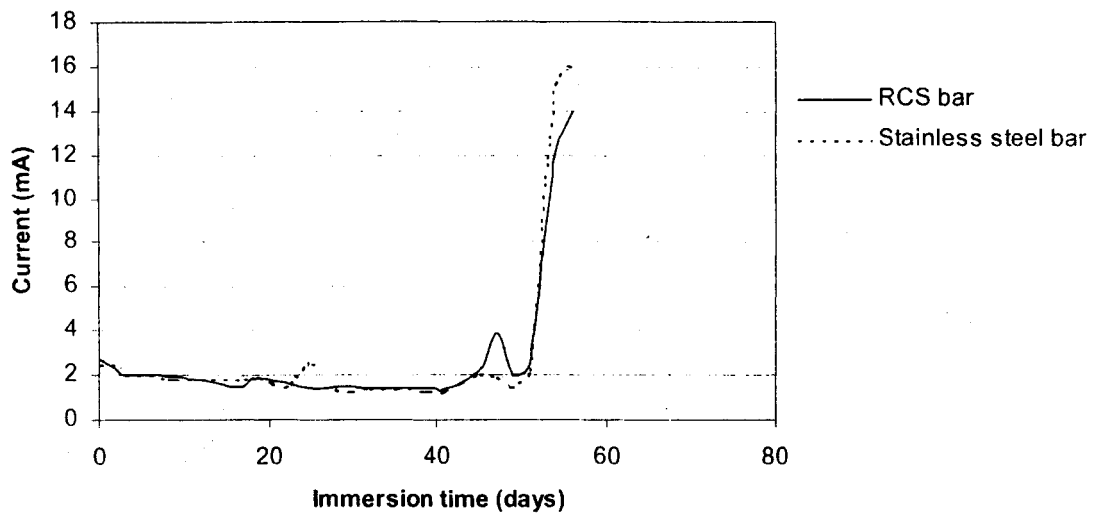
Figure 5.10: Current readings for F.A concrete specimens with different steel types for pre-cracking stage

79
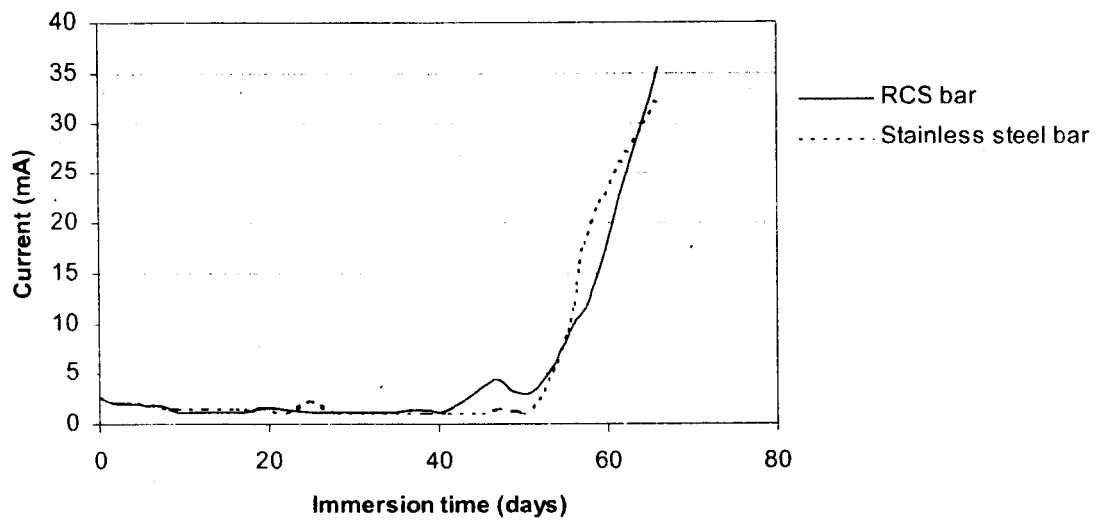
Figure 5.11: Current readings for F.A concrete specimens with different steel types for cracking stage

Figure 5.12: Current readings for F.A concrete specimens with different steel types for severe corrosion stage

80
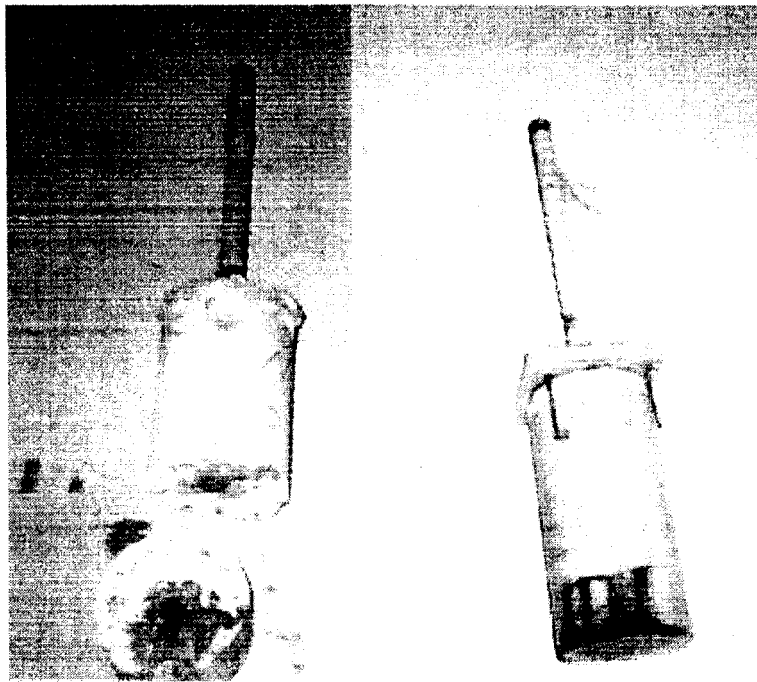
Figure 5.13: Epoxy coated bar corroded specimens
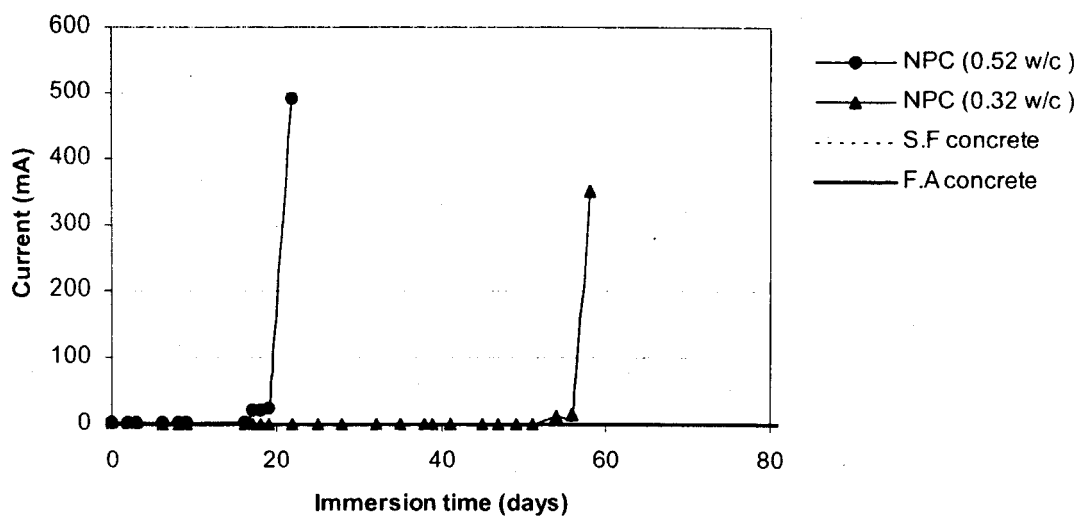
Figure 5.14: Current reading for different concretes for epoxy coated steel bar for severe corrosion stage

81
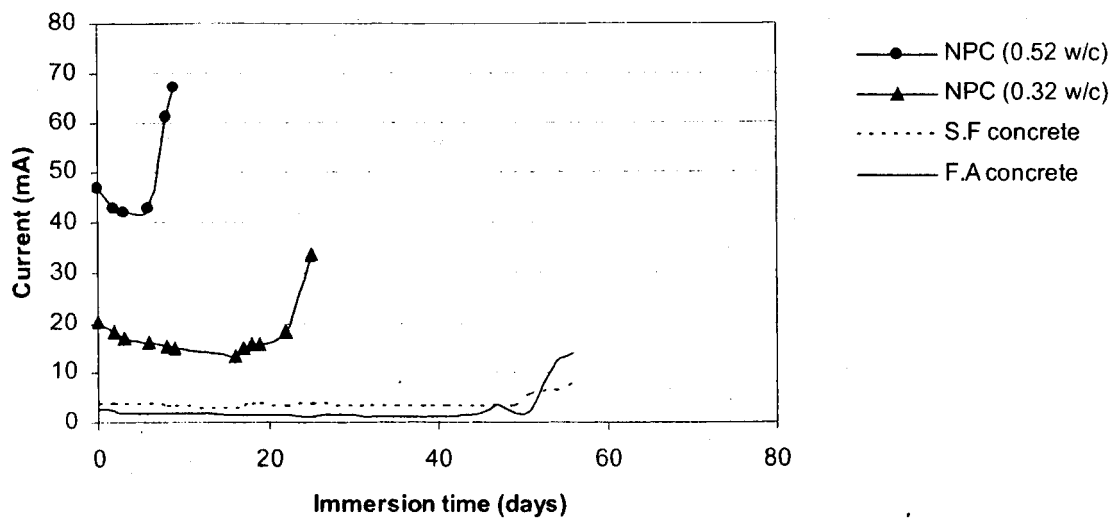
Figure 5.15: Current reading for different concretes for regular carbon steel bar for pre-cracking stage
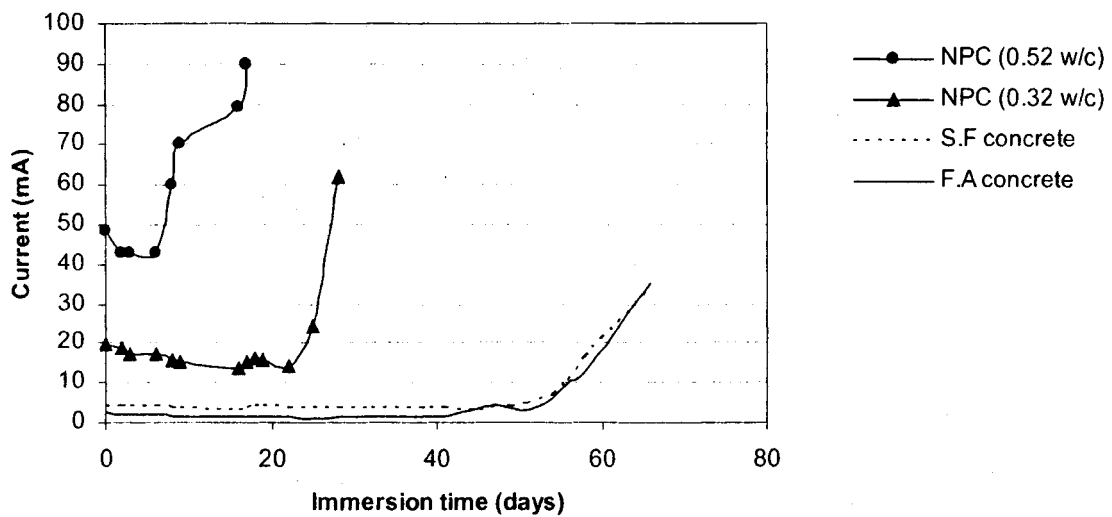
Figure 5.16: Current reading for different concretes for regular carbon steel bar for cracking stage

82
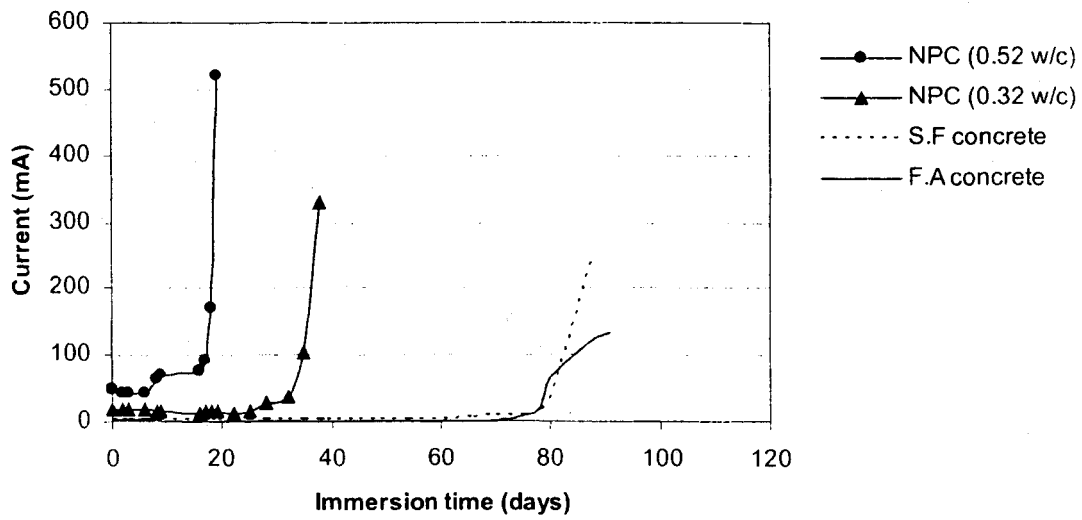
Figure 5.17: Current reading for different concretes for regular carbon steel bar for severe corrosion stage
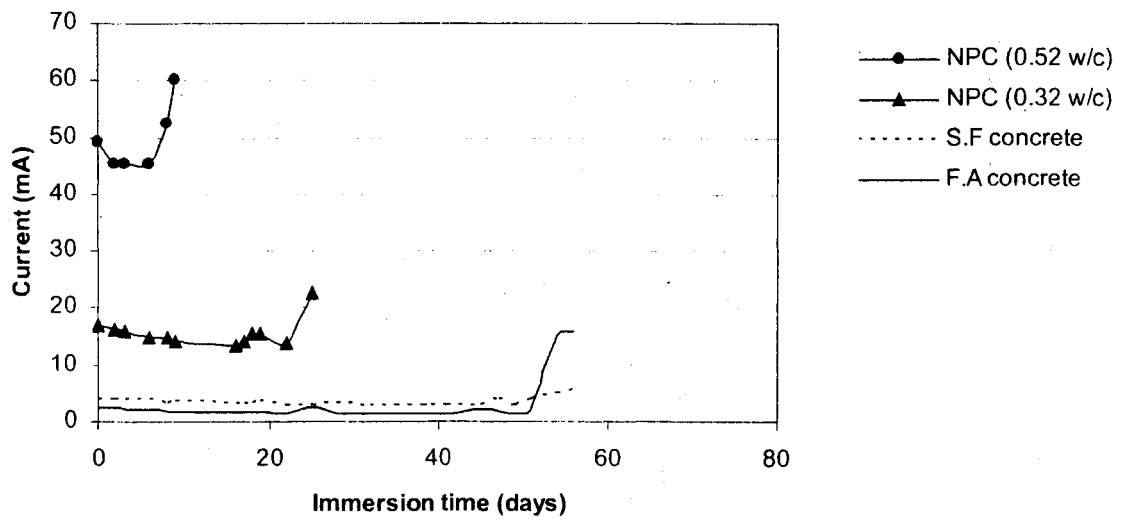
Figure 5.18: Current reading for different concretes for stainless steel bar for pre-cracking stage

83
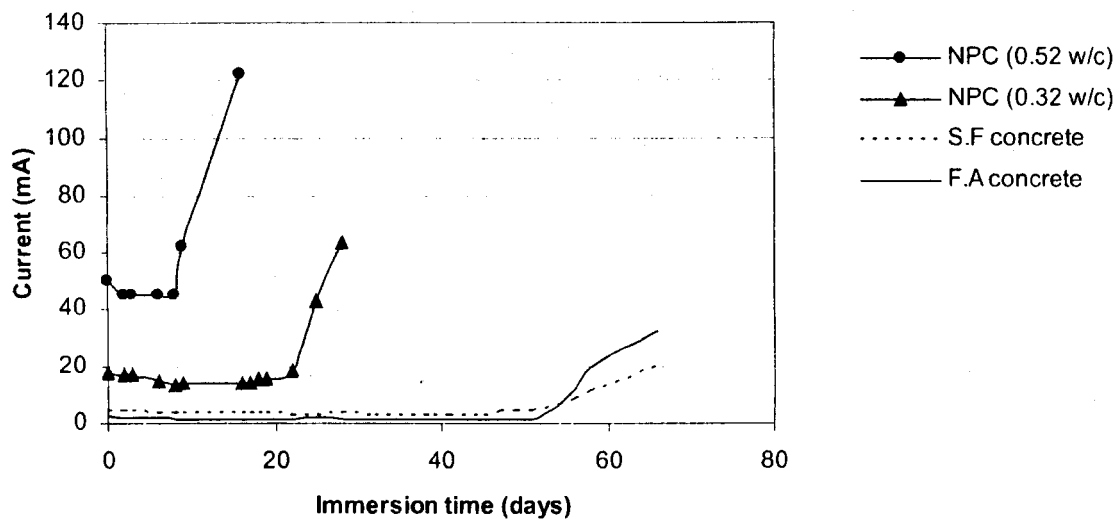
Figure 5.19: Current reading for different concretes for stainless steel bar for cracking stage
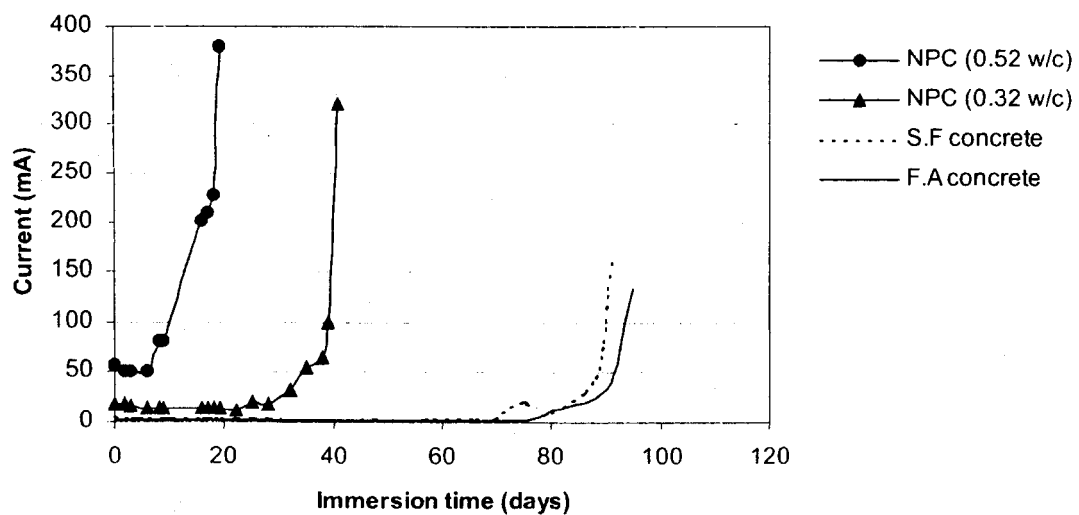
Figure 5.20: Current reading for different concretes for stainless steel bar for severe corrosion stage

84
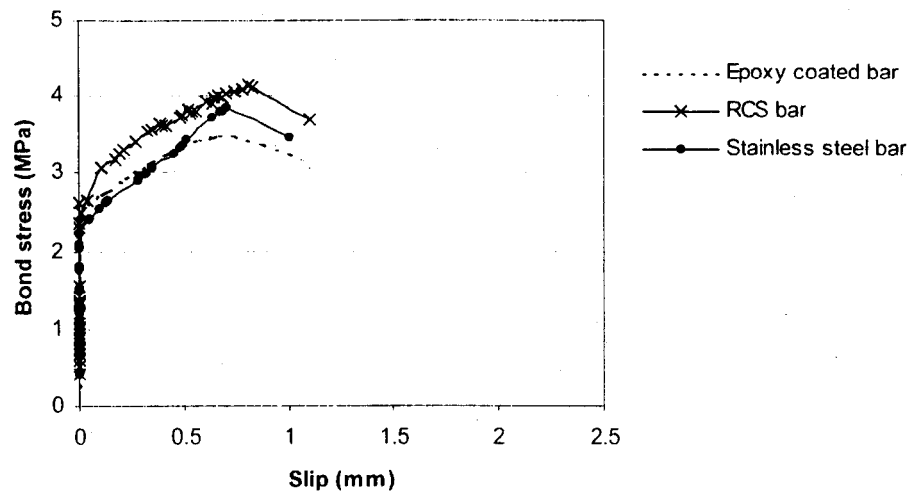
Figure 5.21: Variation of bond stress with slip for 0.52 normal concrete mix with different steel types (0 corrosion stage)
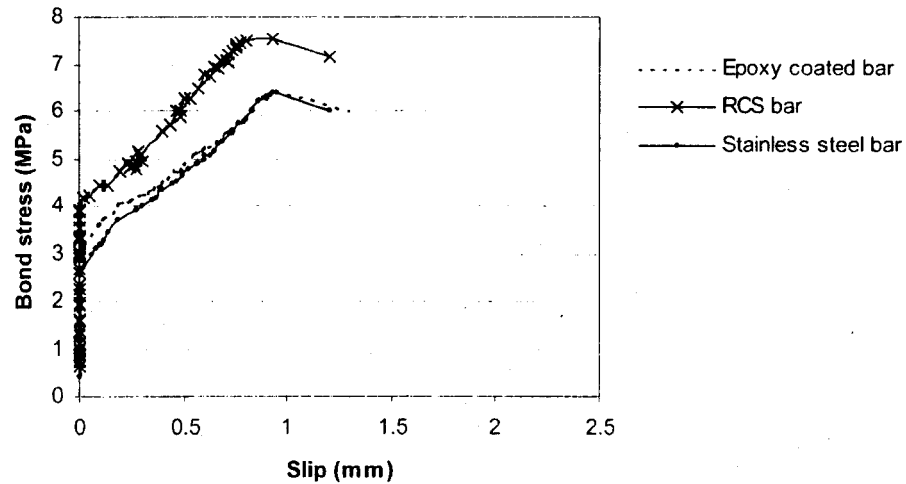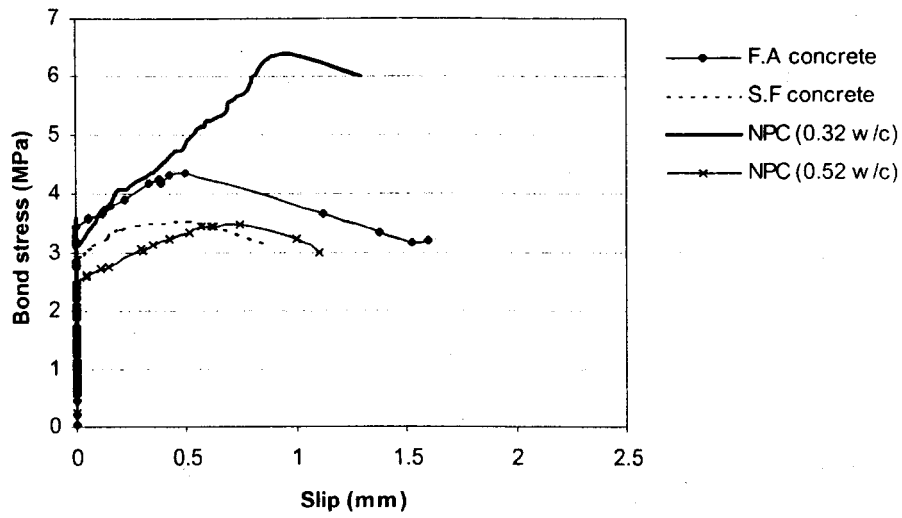

Figure 5.22: Variation of bond stress with slip for 0.32 normal concrete mix with different steel types (0 corrosion stage)

85
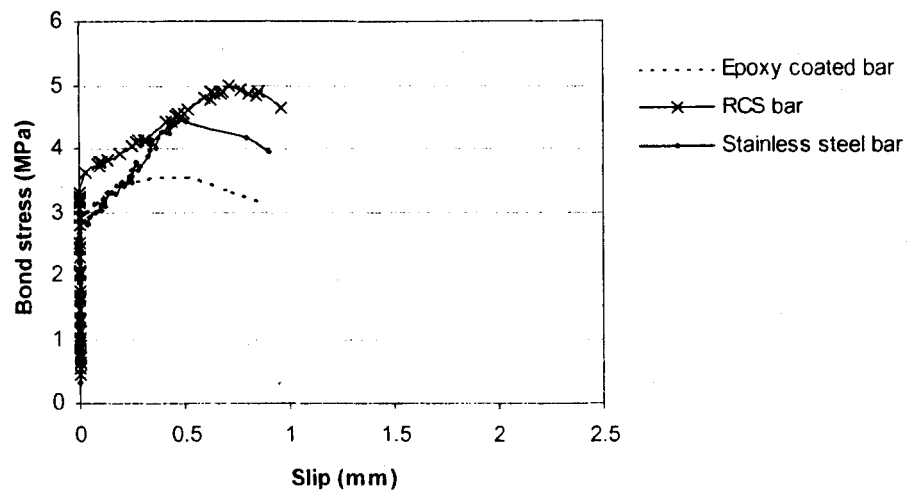
Figure 5.23: Variation of bond stress with slip for silica fume concrete mix with different steel types (0 corrosion stage)
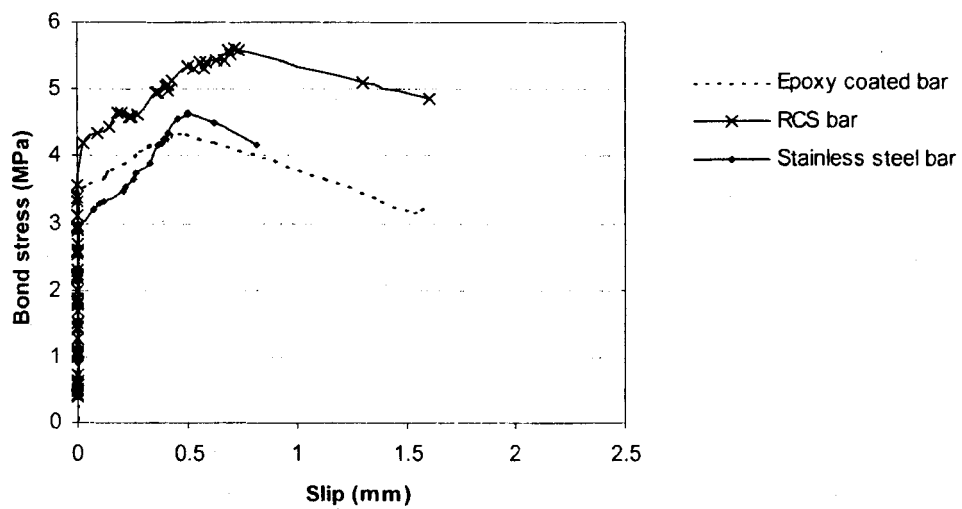
Figure 5.24: Variation of bond stress with slip for sundance fly ash concrete mix with different steel types (0 corrosion stage)

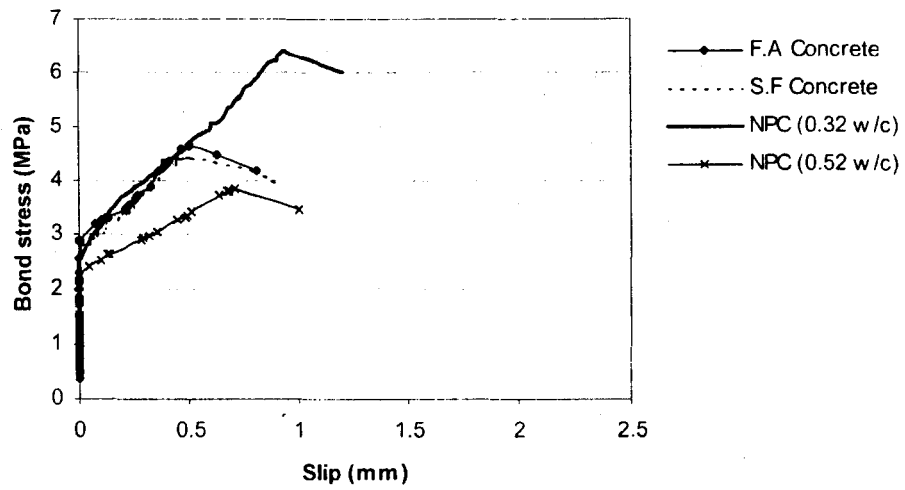**Figure 5.25**: Variation of bond stress with slip for epoxy-coated bar for different concretes (0 corrosion stage)
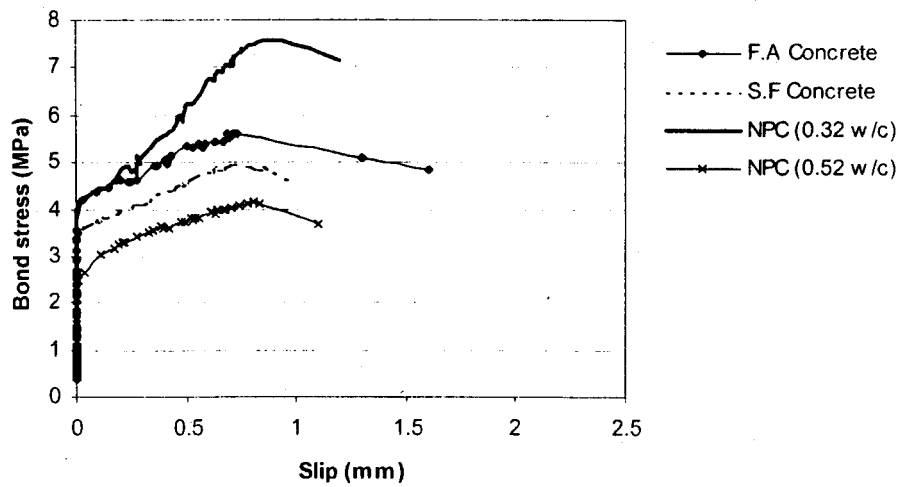
Figure 5.26: Variation of bond stress with slip for regular carbon steel bar for different concretes (0 corrosion stage)

87

Figure 5.27: Variation of bond stress with slip for stainless steel bar for different concretes
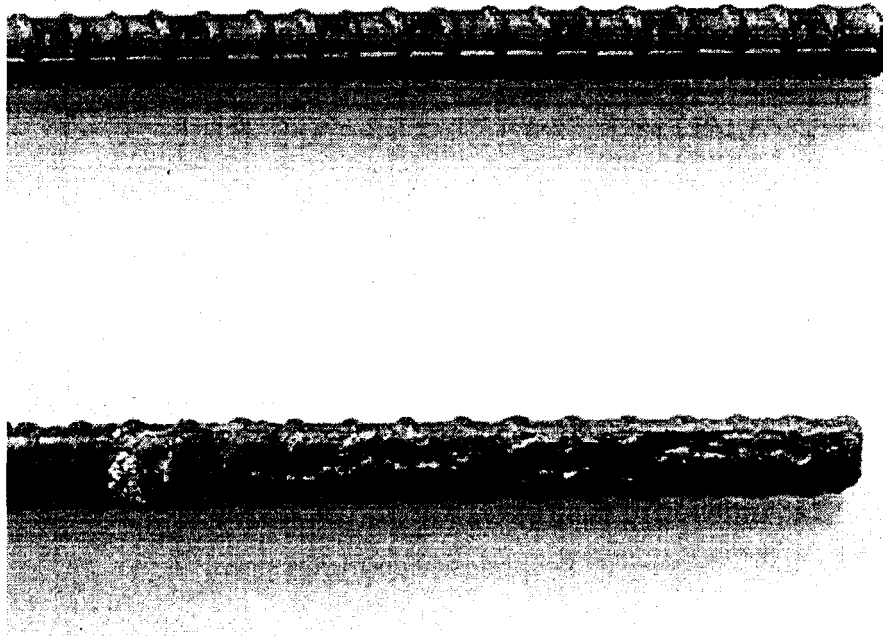(0 corrosion stage)

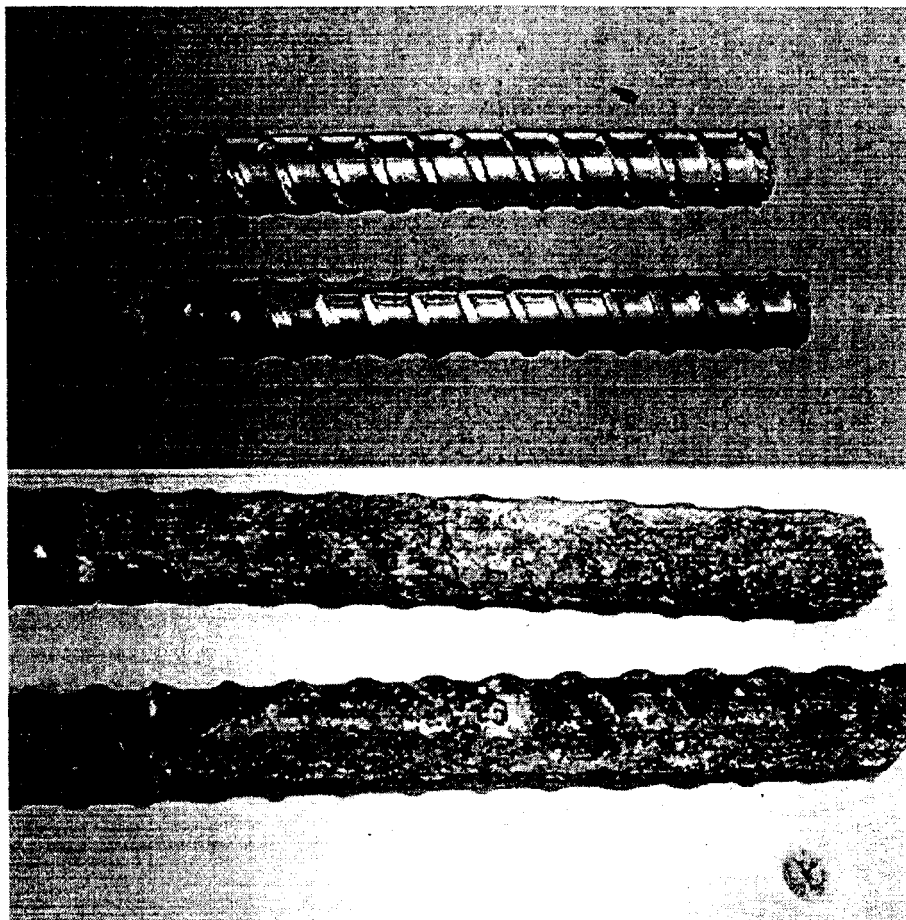**Figure 5.28**: Effect of corrosion on regular carbon steel bars

88

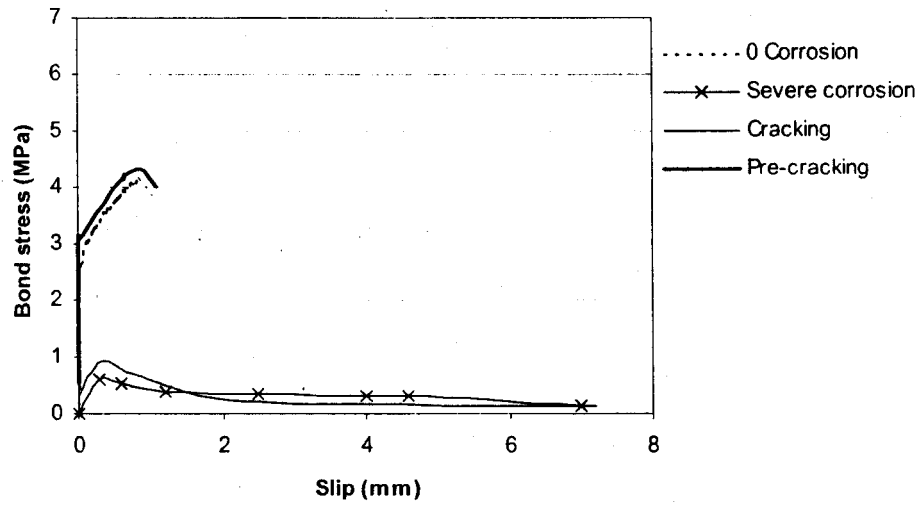**Figure 5.29:** Effect of corrosion on stainless steel bars

Figure 5.30: Relationship between bond strength and degrees of corrosion for NPC concrete (w/c = 0.52) with regular carbon steel bar
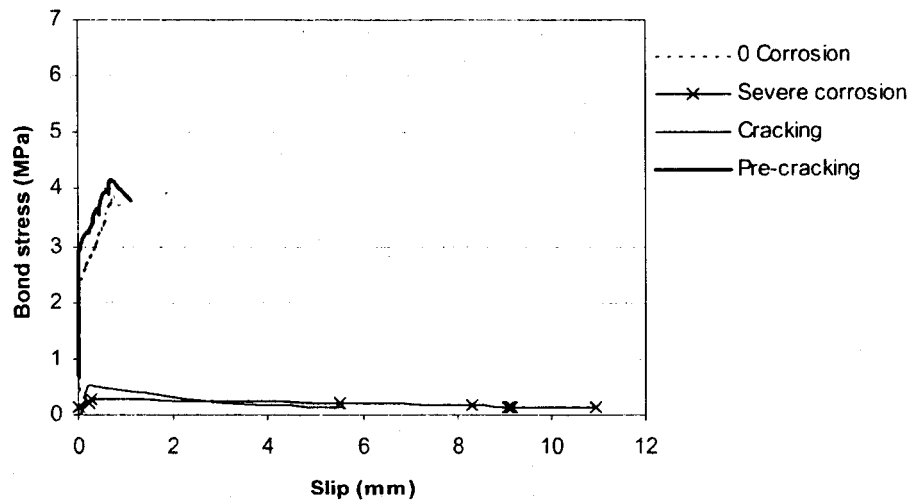

Figure 5.31: Relationship between bond strength and degrees of corrosion for NPC concrete (w/c = 0.52) with stainless steel bar
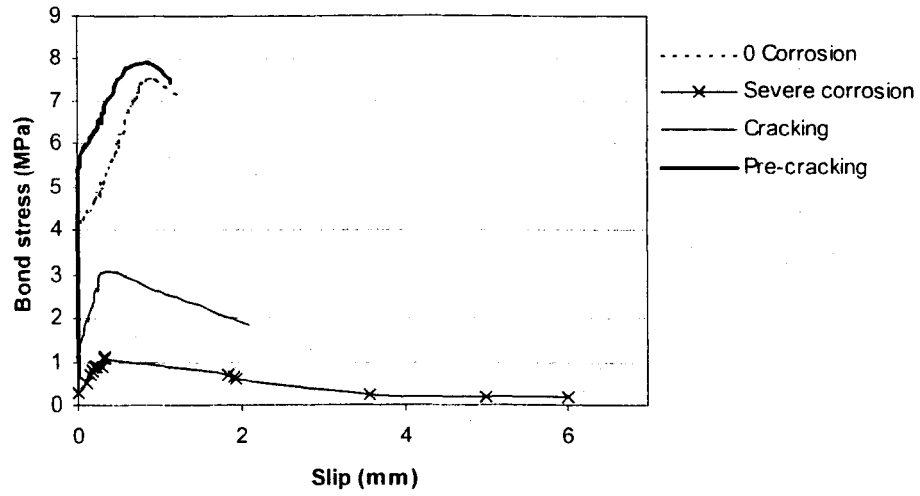
90

Figure 5.32: Relationship between bond strength and degrees of corrosion for NPC concrete (w/c = 0.32) with regular carbon steel bar
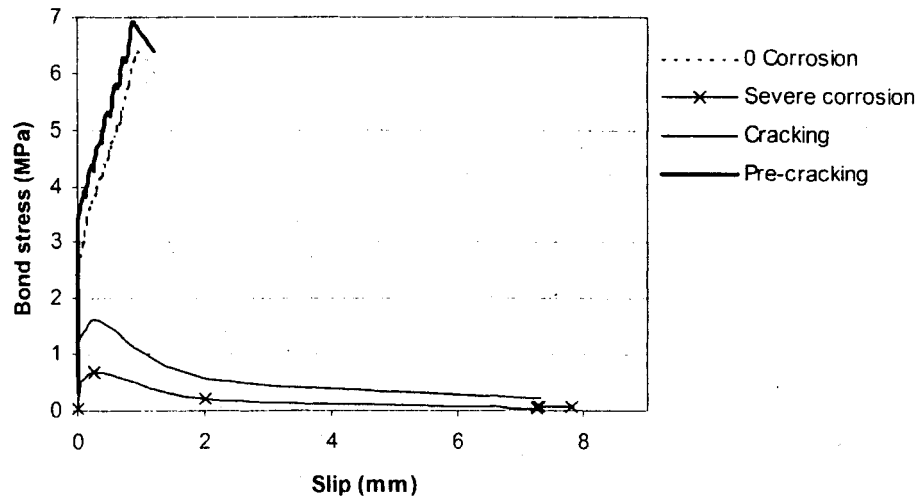

Figure 5.33: Relationship between bond strength and degrees of corrosion for NPC concrete (w/c = 0.32) with stainless steel bar
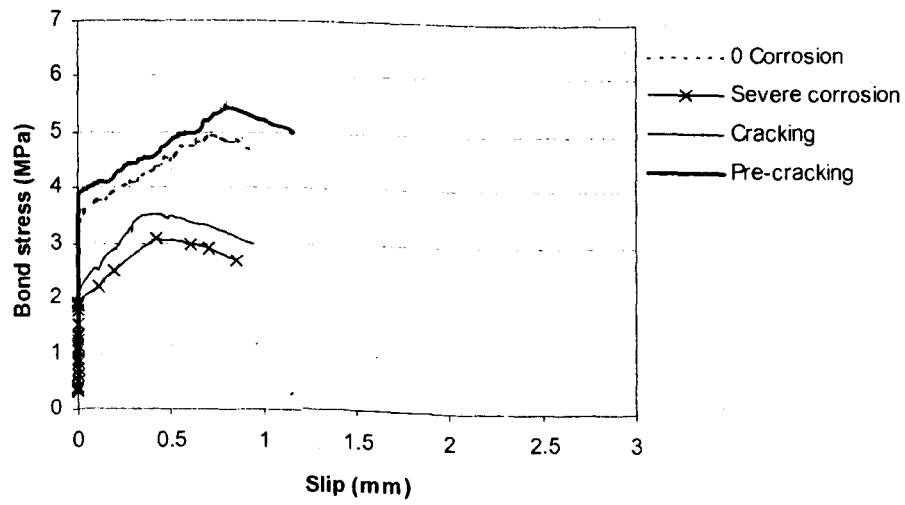
91

Figure 5.34: Relationship between bond strength and degrees of corrosion for S.F concrete with regular carbon steel bar
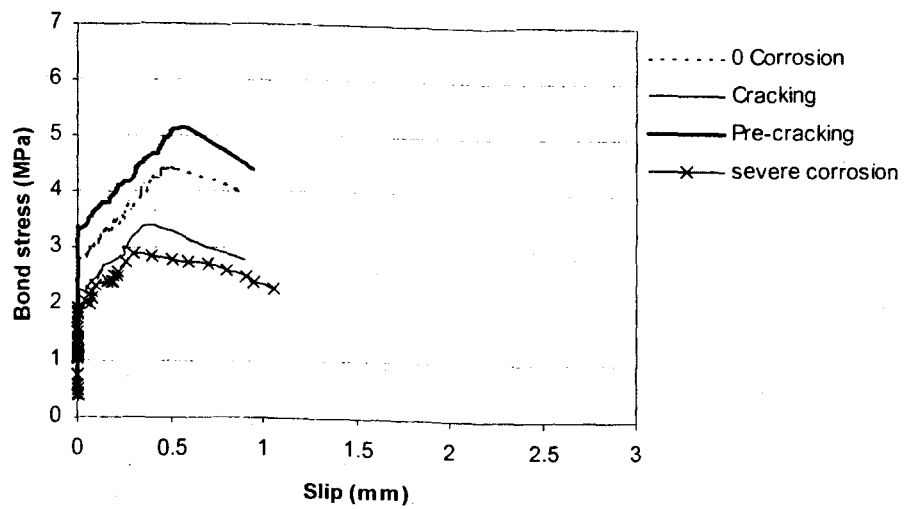

Figure 5.35: Relationship between bond strength and degrees of corrosion for S.F concrete with stainless steel bar
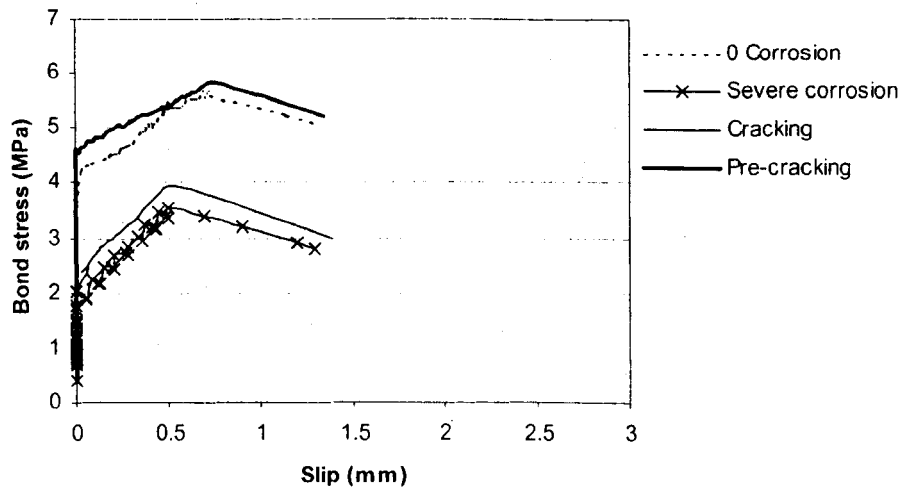
92

Figure 5.36: Relationship between bond strength and degrees of corrosion for fly ash concrete with regular carbon steel bar

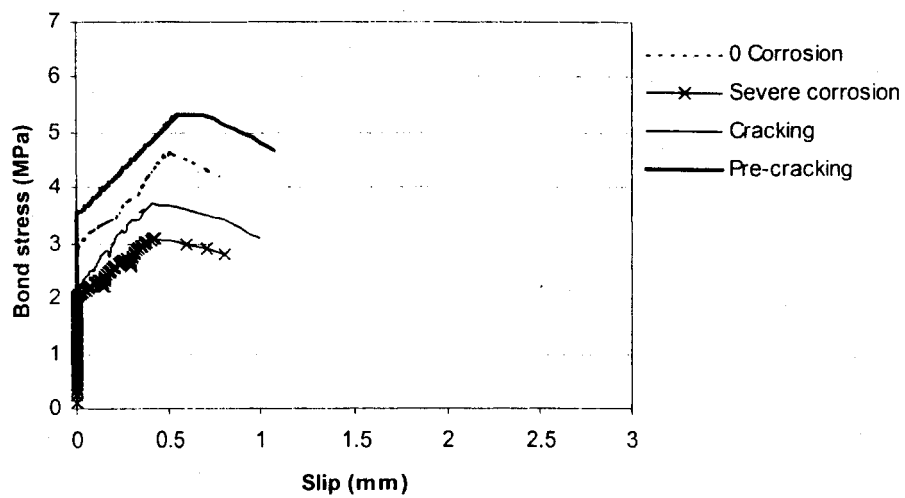**Figure 5.37**: Relationship between bond strength and degrees of corrosion for fly ash with concrete stainless steel bar

93

Figure 5.38: Relationship of bond stress-slip characteristics for pre-cracking stage for regular carbon steel bars in different concrete types

Figure 5.39: Relationship of bond stress-slip characteristics for pre-cracking stage for stainless steel bars in different concrete types
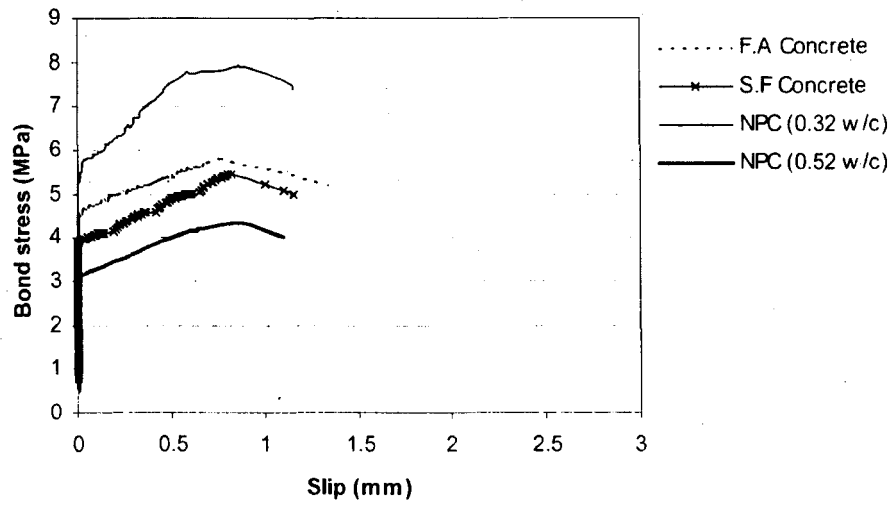
94
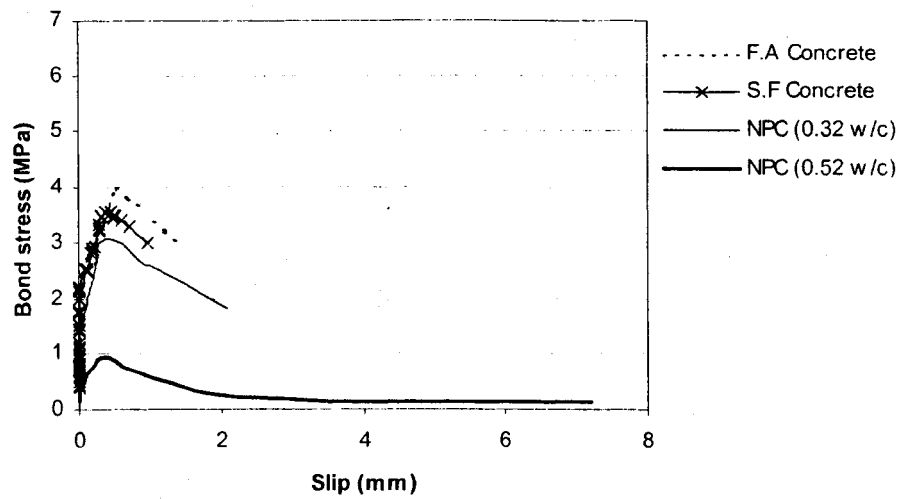
Figure 5.40: Relationship of bond stress-slip characteristics for cracking stage for regular carbon steel bars in different concrete types
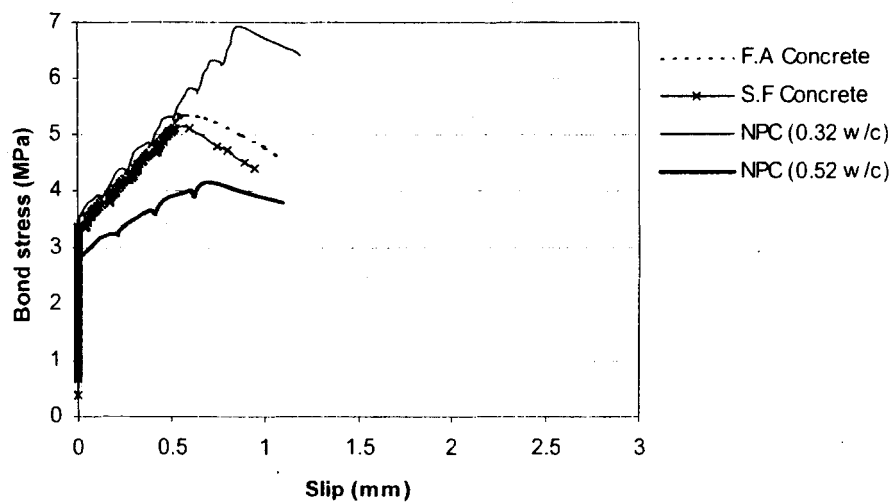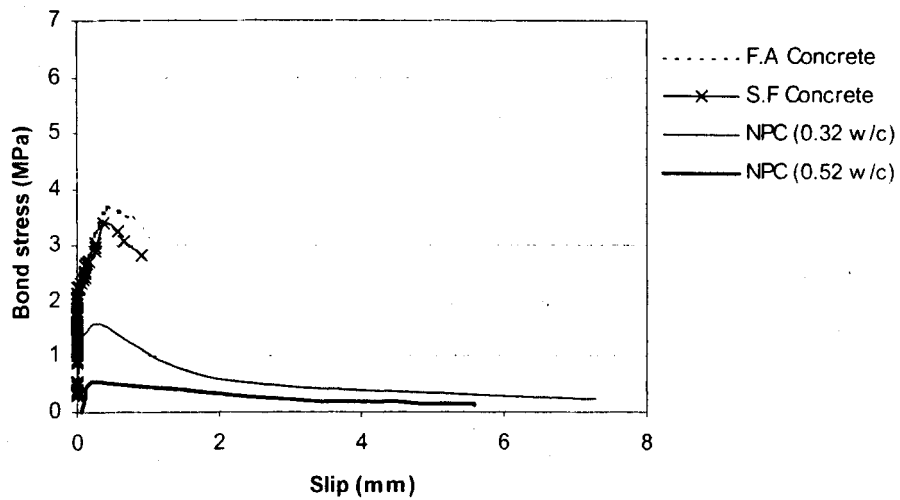

Figure 5.41: Relationship of bond stress-slip characteristics for cracking stage for stainless steel bars in different concrete types

95
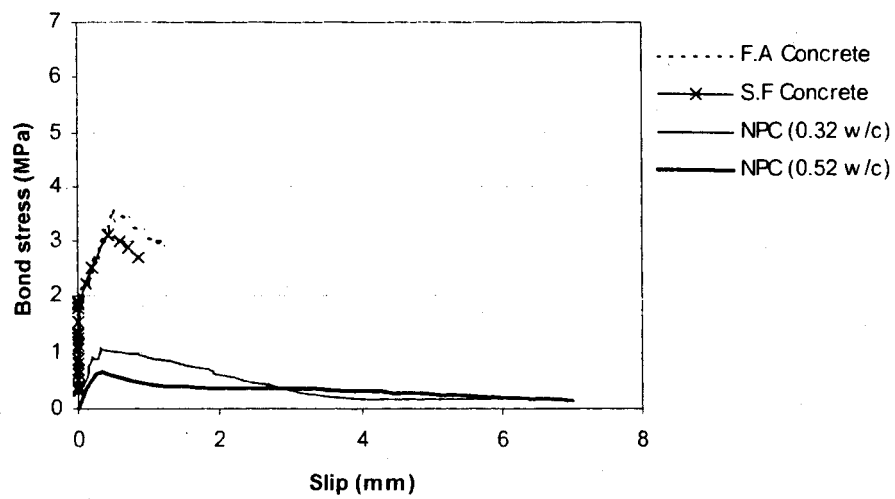
Figure 5.42: Relationship of bond stress-slip characteristics for severe degree of corrosion for regular carbon steel bars in different concrete types
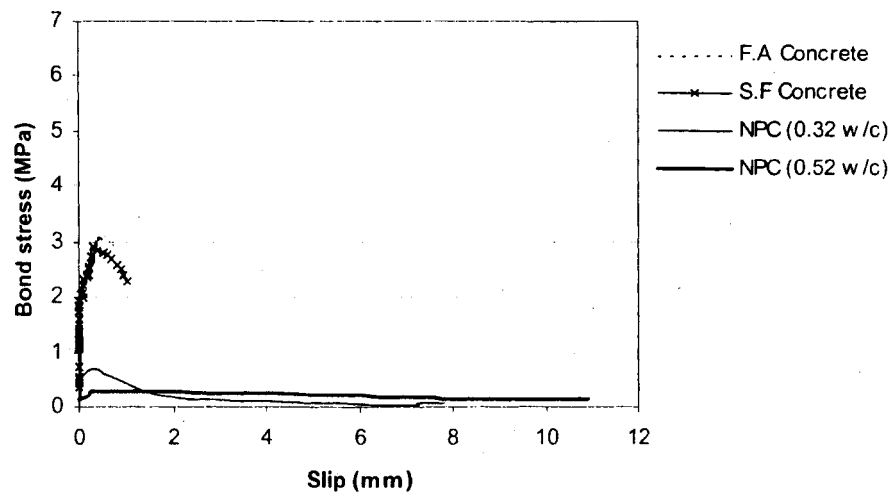
Figure 5.43: Relationship of bond stress-slip characteristics for severe degree of corrosion for stainless steel bars in different concrete types
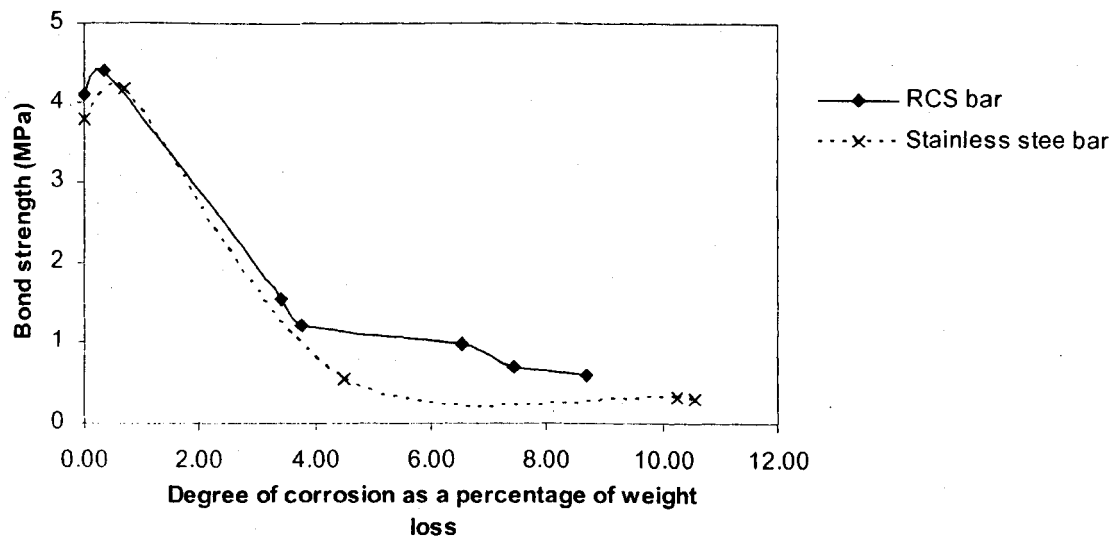
Figure 5.44: Relationship between bond strength and different degrees of corrosion for NPC concrete (w/c = 0.52)
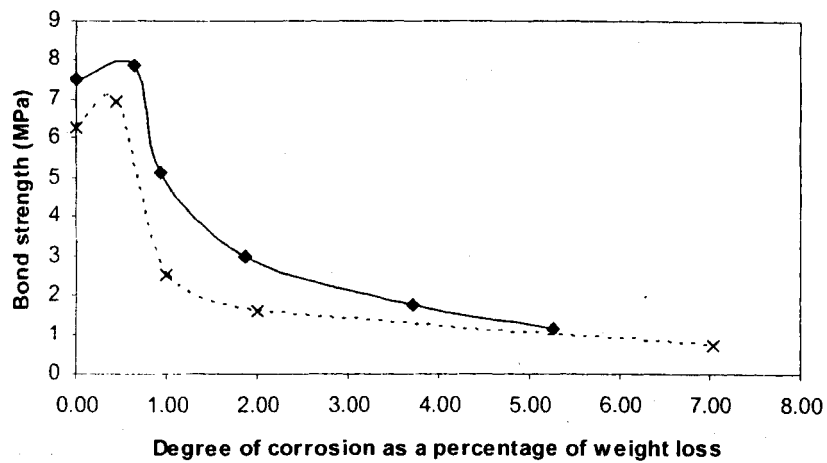
Figure 5.45: Relationship between bond strength and different degrees of corrosion for NPC concrete (w/c = 0.32)

97
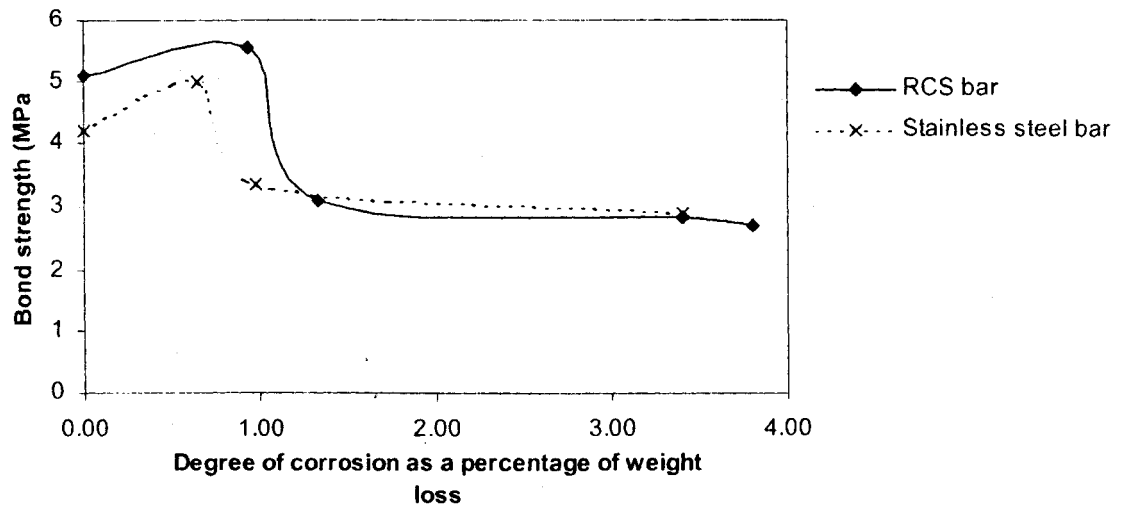
Figure 5.46: Relationship between bond strength and different degrees of corrosion for silica fume concrete
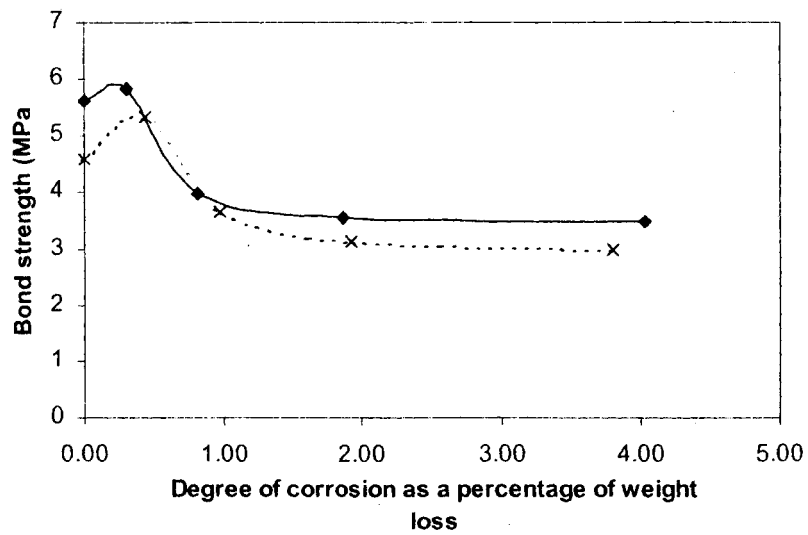
Figure 5.47: Relationship between bond strength and different degrees of corrosion for fly ash concrete

98
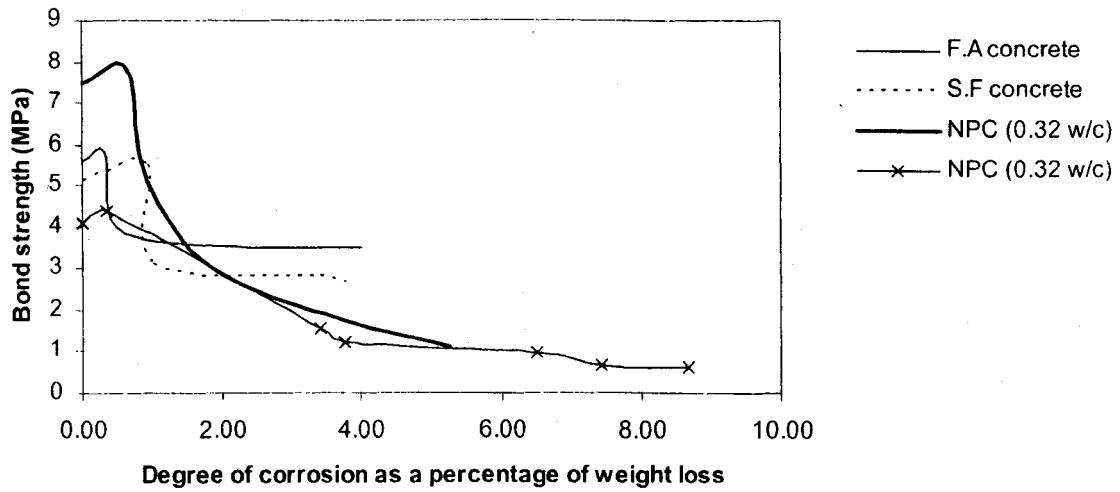
Figure 5.48: Relationship between bond strength and different degrees of corrosion for regular carbon steel bars in different concrete types
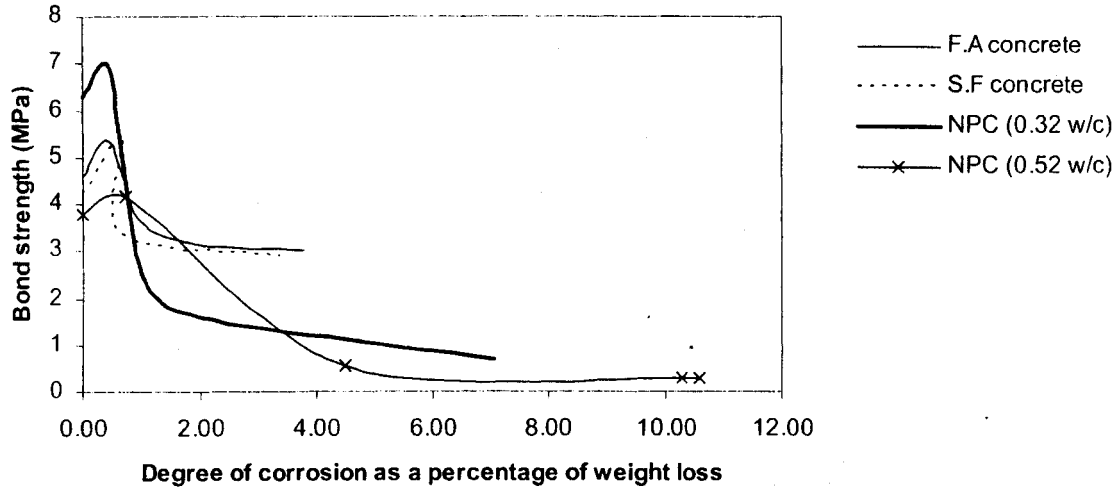
Figure 5.49: Relationship between bond strength and different degrees of corrosion for stainless steel bars in different concrete types

99
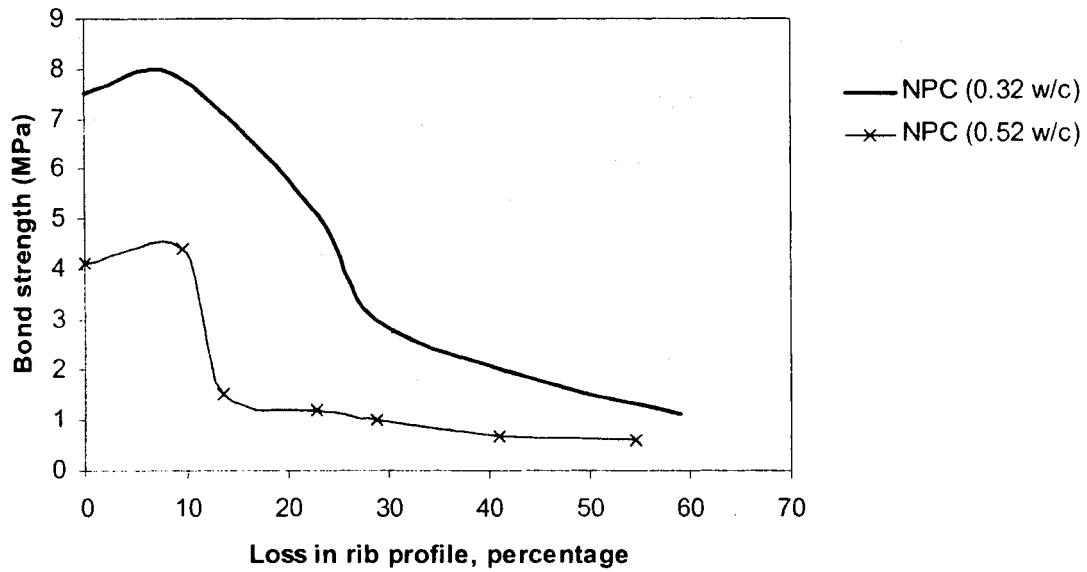
Figure 5.50: Effect of loss of rib profile on bond strength for regular carbon steel bars in two concrete types
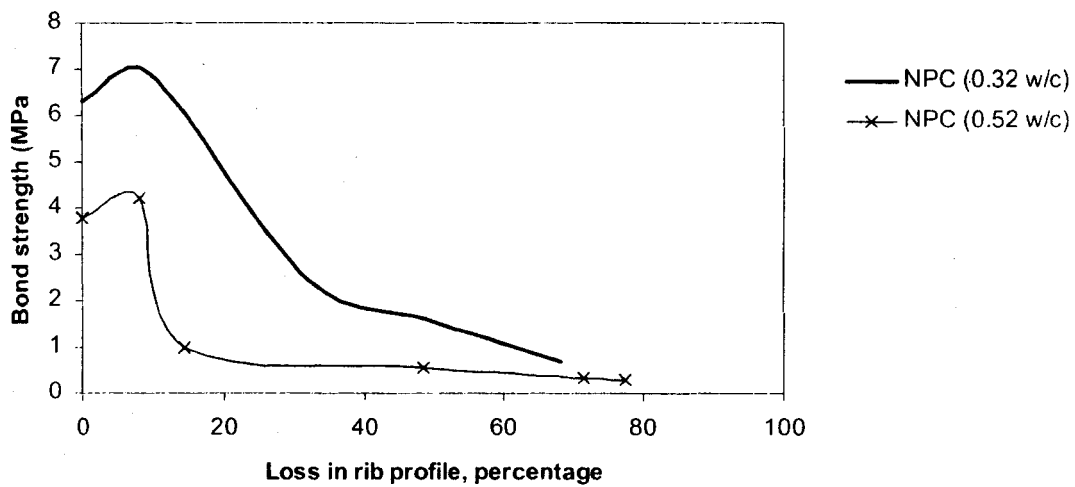
Figure 5.51: Effect of loss of rib profile on bond strength for stainless steel bars in two concrete types

100
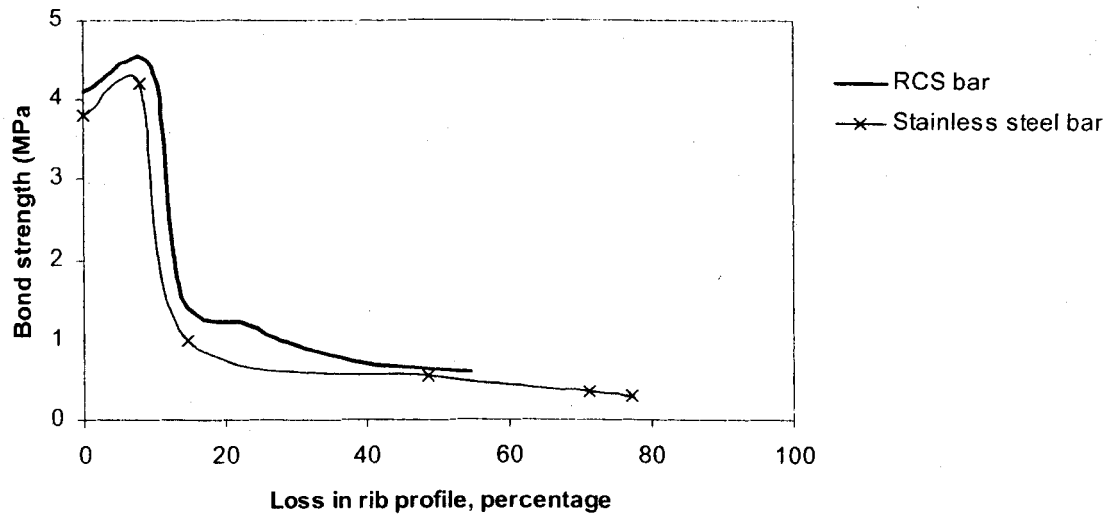
Figure 5.52: Effect of loss of rib profile on bond strength for NPC concrete (w/c = 0.52) for both normal and stainless steel bars
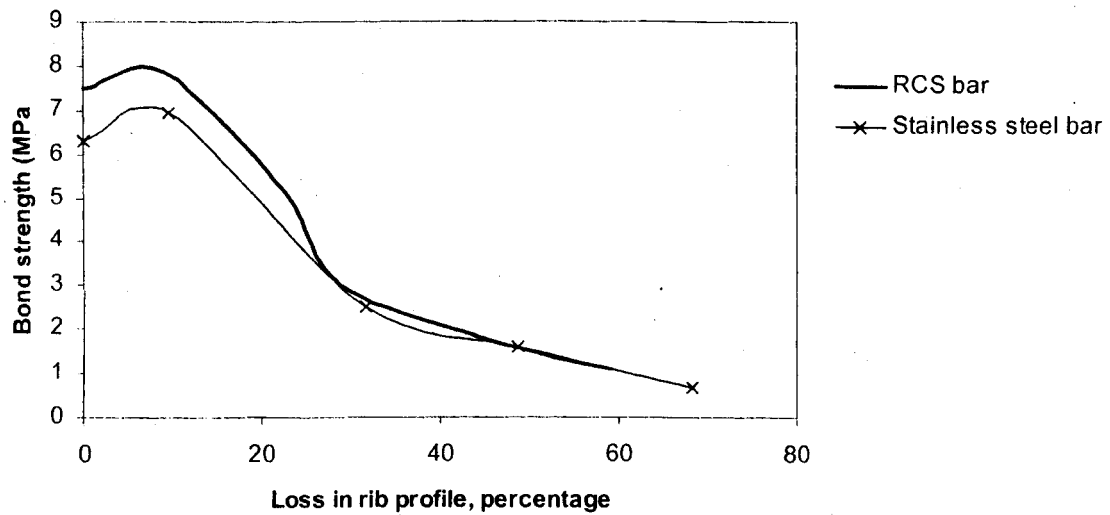
Figure 5.53: Effect of loss of rib profile on bond strength for NPC concrete (w/c = 0.32) for both normal and stainless steel bars

101

CHAPTER 6
CONCLUSIONS AND RECOMMENDATIONS

6.1 Conclusions

- A sudden cracking across the concrete specimen was observed when testing the epoxy-coated bars with uncoated embedded end under the accelerated corrosion test. This sudden cracking resulted from the concentrating of the corrosion products around the uncoated embedded end of the bar which caused vertical expansion and exerted a tension force leading to separate the lower part of the concrete specimen from the upper part at the embedded end of the bar.

- Under the accelerated corrosion test, the epoxy-coated bars show the lowest current readings during the whole period of the immersion time (before the crack initiation) compared to the stainless steel bars and the regular carbon steel bars [3.2, 1.3, 0.4, and 0.2 mA average current reading before crack initiation for NPC concrete (w/c = 0.52), NPC concrete (w/c = 0.32), S.F concrete and F.A concrete]. Also the epoxy-coated bars exhibit a sudden increase in the current reading compared to the other used steel bars for the two tested concrete types NPC concretes (w/c = 0.52 and 0.32). The current readings of the epoxy-coated bars changed from an average value of 3.4 mA to a maximum of 490 mA within 5 days, and from an average value of 1.2 mA to a maximum of 350 mA within 6 days with NPC concrete (w/c = 0.52), and NPC concrete (w/c = 0.32) respectively. The low current reading of the epoxy-coated bars compared to the other used bars implies to the superior effect of the coated bars in corrosion resistance, while the sudden increase of the epoxy-coated bars current shows the seriousness of the concrete cracking due to the corrosion concentration in uncoated small area.

- Both of the stainless steel bars and regular carbon steel bars reached pre-cracking, cracking, and severe corrosion stages around the same times [9, 17, and 19 days to reach pre-cracking, cracking, and severe corrosion stages respectively when using NPC concrete (w/c = 0.52). While 25, 28, and 39 days to reach pre-cracking, cracking, and severe corrosion stages respectively when using NPC concrete (w/c = 0.32)]. The time taken by both of the stainless steel bars and regular carbon steel bars to reach sever corrosion stage was shorter than that of the epoxy-coated bars. This could be due to a higher resistivity of coated bars than the uncoated bars.

- During monitoring the current reading for the three steel types under the accelerated corrosion test, an initial decrease in the current for sometimes followed by a sudden increase was observed. The initial current increase was an indication of the formation of the passive film around the reinforcing steel bar, which protect the steel from corrosion, while the followed current decrease indicated to the steel depassivative resulted from the specimens cracking which lead to the increase in the corrosion rate [complying with the previous researches Cornet et al. (1968), Al-Sulaimani et al (1990), Amleh and Mirza (1999), and others].

- Normal Portland Cement concrete (w/c = 0.52) showed the highest current reading at the early age and at the severe corrosion stage [48, 50 and 3.6 mA with the regular carbon, stainless steel, and the epoxy-coated bars respectively in the initial current reading] during monitoring the current reading for the three steel types under the accelerated corrosion test, followed by NPC concrete (w/c = 0.32) [20, 18 and 1.8 mA with the regular carbon, stainless steel, and the epoxy-coated bars respectively in the initial current reading]. Also, S.F concrete showed lower initial current reading and lower severe corrosion current reading than both NPC concrete (w/c = 0.52) and NPC concrete (w/c = 0.32) [4.5, 5 and 0.4 mA with the regular carbon, stainless steel, and the epoxy-coated bars respectively in the initial current reading] but still higher than F.A concrete which has the lowest initial and severe corrosion current reading [2.5, 2.6 and 0.2 mA with the regular carbon, stainless

1 0 3

steel, and the epoxy-coated bars respectively in the initial current reading]. The lower current reading in F.A and S.F concretes compared to that of NPC concretes (w/c = 0.32 and 0.52) signifies the beneficial effect in using supplementary cementing materials in concrete to protect the reinforcing bars from corrosion. Also, the low current reading in NPC concrete (w/c = 0.52) compared to that of NPC concrete (w/c = 0.32) signifies the beneficial effect in using low w/c ratio in concrete to protect the reinforcing bars from corrosion.

- When testing the bond strength for the uncorreded bars, the epoxy-coated bars showed the lowest bond strength compared to the regular carbon steel bars and stainless steel bars for all concrete types [For example, the epoxy –coated bars show an average of 14.6 and 8.6 % less in the bond stress than the regular carbon steel bars and the stainless steel bars respectively when using NPC concrete (w/c = 0.52)]. The stainless steel bars demonstrated higher bond strength than the epoxy-coated bars but still lower than the regular carbon steel bars for all concrete types [For example, the stainless steel bars show an average of 7% less in the bond strength than the regular carbon steel bars when using NPC concrete (w/c = 0.52)]. This shows the preference in using the regular carbon steel bars than the stainless steel and the epoxy-coated bars in enhancing the concrete-steel bond strength.

- When testing the bond strength for the uncorreded bars. NPC concrete (w/c = 0.32) showed the highest bond strength than the other used concretes for all steel types: it showed 47, 79, and 82 % higher in bond strength than F.A, S.F, and NPC concrete (w/c = 0.52), respectively when using epoxy-coated bars. Also, it showed 35, 54, and 84 % higher in bond strength than F.A, S.F, and NPC concrete (w/c = 0.52), respectively when using regular carbon steel bars. Meanwhile, when using stainless steel bars, NPC concrete (w/c = 0.32) showed 35, 45, and 66 % higher in bond strength than F.A, S.F, and NPC concrete (w/c = 0.52). respectively. Fly ash concrete showed higher bond strength than S.F and NPC concrete (w/c = 0.52). it showed 22, and 24 % higher in bond strength than S.F, and NPC concrete (w/c =

0.52), respectively when using epoxy-coated bars. Also, it showed 14, and 36 % higher in bond strength than S.F, and NPC concrete (w/c = 0.52), respectively when using regular carbon steel bars. Furthermore, when using stainless steel bars. F.A concrete showed 7, and 23 % higher in bond strength than S.F, and NPC concrete (w/c = 0.52), respectively. Silica fume concrete exhibited higher bond stress than NPC concrete (w/c = 0.52) for all steel types. Silica fume concrete showed 2, 19, and 15 % higher in bond strength than NPC concrete (w/c = 0.52) when using epoxy-coated bars, regular carbon steel bars, and stainless steel bars. respectively.

- The use of supplementary cementing materials in concrete decrease the cracks number due to corrosion. The cracks of the fly ash and silica fume concrete due to the corrosion of embedded bars were usually one or two cracks, while the cracks for both NPC concretes (w/c = 0.32 and 0.52) were between four to six cracks.

- The effect of accelerated corrosion on the regular carbon steel bars was less than that on the stainless steel bars at the same corrosion stage. The regular carbon steel bars showed less damage with no surface voids compared to stainless steel bars, also, the ribs of the regular carbon steel bars were slightly damaged. On the other hand, the stainless steel bar surface was totally damaged after the severe corrosion stage, with lots of voids and no indication of the ribs.

- The bond strength in the pre-cracking stage is slightly higher than that in 0 corrosion stage for both regular carbon steel bars and stainless steel bars embedded in any concrete type (for example when using F.A concrete with regular carbon steel bars, the pre-cracking stage showed 4% higher in bond strength than 0 corrosion stage. Also, when using S.F concrete with stainless steel bars, the pre-cracking stage showed 16% higher in bond strength than the 0 corrosion stage). These results agree well with previous researches (Maslehuddin et al 1990 and

1 0 5

Amleh 2000). The initial rusty layer (occurs in the pre-cracking stage) that enveloping the bar surface, adds more cohesiveness and friction with the surrounding concrete which definitely increases the bond strength.

- In all corrosion stages, the regular carbon steel bars showed higher bond strength than the stainless steel bars for all concrete types. For example at cracking stage for F.A concrete the regular carbon steel bars was about 9 % higher in bond strength than the stainless bars. The difference in the bond strength values between the two bars are more significant in 0 corrosion stage than that of the corroded stages. At 0 corrosion stage the effect of surface friction is considered between the two bars, while the corrosion products decrease the surface friction for both of them as corrosion continues to take place. This demonstrate to the preference in using the regular carbon steel bars than the stainless steel in enhancing the concrete-steel bond strength even after several degrees of corrosion take place in the steel bar.

- Although the F.A concrete showed less bond strength than NPC concrete (w/c = 0.32), it is better to use fly ash in concrete to obtain the best concrete to protect the steel bars from corrosion.

6.2 Recommendations

- It is recommended for further investigation to measure the chloride ion content at the steel reinforcing level, this is because the percentage of the chloride ion content at the bar level indicates to the corrosion activity in the steel reinforcing.

- It is recommended to measure the steel reinforcing tensile strength after the corrosion takes place, the corrosion products could severely affect the steel reinforcing tensile strength due to the corrosion concentration in some areas.

- It is highly recommended for further investigation to do more testing to calculate the effective developing lengths for the regular carbon and stainless steel bars after certain degrees of corrosion takes places.

REFERENCES

- Abadjiev, F. Panayotov, K. and Pelrov. S., (1993), "Influence of condensed silica fume as admixture to concrete on the bond to the reinforcement," Construction and Buiding Materials. 7(1), 41-4.

- Abdulaziz A. Bubshait and BassamTahir. , (1997), "effect of silica fume on the concrete-steel bond," Building Research and information, Volume 25 Number 6, pp.68-73

- ACI committee 408., (1991), "State of the art report: Bond under cyclic loads." Journal of the American concrete institute, No. 88-M68, pp. 669-673.

- Almusalam Abdullah, A. Al-Gahtani Ahmad S., Aziz Abdur Rauf and Rasheeduzzafar., (1995), "effect of reinforcement corrosion on bond strength. Construction and Building Material", Vol. 10. No.2, pp. 123-129.

- Al-Sulaimani, G J. Kaleemullah M, Basunbul I A, & Rasheeduzzafar. , (1990), " Influence of corrosion and cracking on bond behavior and strength of reinforced concrete members," Proceedings American Concrete Institute. Vol 87, No. 2, pp. 220-231.

- Amleh, L. and Mirza, M.S., (1999), "Corrosion Influence on Bond Between Steel and Concrete,"ACI Structural Journal, May – June, pp. 415-423.

- Amleh, L., (2000), "Bond deterioration of reinforcing steel in concrete due to corrosion," Ph.D thesis department of Civil Engineering and Applied Mechanics. Mc Gill University

- ASTM C 227-97a. , (2001), "Standard Test Method for Potential Alkali Reactivity of Cement-Aggregate Combinations," (Mortar-Bar Method).

- ASTM C 234. , (1991), "Standard Test Method for Comparing Concrete on the Basis of the Bond Developed with Reinforcing," American Society for Testing and Materials.

- Auyeung, Yubun, Balaguru, P., and Chung, Lan. , (2000), "Bond Behavior of Corroded Reinforcement Bars," ACI journal. No. 97-M28, pp. 214-220.

- Aziz, A.R., (1994), "Reduction in Bond and the Strength of Slabs due to Corrosion of Reinforcement," Thesis for Master of Science. King Fahd University of Petroleum and Minerals. Dhahran, Saudi Arabia.

- Berry, E.E. and Malhotra V.M., (1987), "Fly Ash in Concrete, Supplementary Cementing Materials for Concrete," Canada Center for Minerals & Energy Technology, pp. 37-166.

- Cabrera J. G., and Ghodussi, P., (1992), "Effect of reinforcement corrosion on the strength of steel concrete bond." Proc mt. Conf. On Bond in Concrete- from research to practice. Riga, Latvia. pp. 10.11-10.24.

- Cairns J. and Ramli Abdullah., (1994), "Fundamental Tests on the Effect of an Epoxy Coating on Bond Strength," ACI Journal /July- August No. 91-M32. pp. 331-338.

- Cao H.T.and Sirivivatnanon V., (1991), "Corrosion of steel in concrete with and without silica fume," Cement and concrete research.Vol 21,pp.316-324.

- Choi, Oan. Chul, Lee, Woong Se., (2002), "Interfacial bond analysis of deformed bars to concrete." ACI journal, No. 99-S75, pp. 750-755.

- Cleary, D. B., and Ramirez, J. A., (1989), "Bond of Epoxy Coated Reinforcing Steel in Concrete Bridge Decks," Report No. CE-STR-89- 2. School of Engineering, Purdue University, Feb., pp. 127

- Cornet, I..Ishikawa, T., and Bresler, B., (1968), "Materials Protection", Vol.7, No.3, pp.44-47.

- Darwin, David, and Ebeneze, K. Graham., (1993), "Effect of Deformation Height and Spacing on Bond Strength of Reinforcing Bars," AC! Structural Journal, V. 90, No. 6, Nov-Dec, pp. 646-657.

- David W., (1941), "Bond Stress in Concrete Pullout Specimens," American Concrete Institute, Vol 13, No.1, September, pp. 37-50.

- Edwards A.D., Jannopoulos P.J., (1978), "Local bond stress-slip relationship under repeated loading," magazine of Concrete research 30(103). pp. 62-72.

- Ferguson P.M., (1966), "Bond stress: the state of art," Report by ACI committee 408. ACI Journal 63(11), 408. 1-408.22.

- Ferguson P.M., Turpin R.D.,Thompson J.N., (1954), "Minimum bar spacing as function of bond and shear strength," ACI Journal 50(10), 869-88.

- Gjorv, O.E., Monteiro, PJM. AND Mehta, P.K., (1990). "Condensed-silica fume on the steel-concrete bond," ACI Materials Journal, pp. 573.

- Goldman, A. and Bentur, A., (1993), "Effects of Pozzolanic and Non-Reactive Microfillers on the Transition Zone in High Strength Concrete," Interfaces in Cementitious Composites, RILEM, J.C. Maso, Ed., Published by E & FN Spon, London, pp. 53-61.

- Hamad B.S., (1995), "comparative Bond Strength of Coating and Uncoated Bars with different Rib Geometries," ACI Journal, No. 64-62, pp. 579-590.

- Khedr, S.A. and Abu-Zeid, M.N., (1994), "Characteristics of silica fume concrete," Journal of Materials in Civil Engineering, 6(3), 357-75.

- Kimura, Hideka, and Jirsa, James., (1992), "Effects of Bar Deformation and Concrete Strength on Bond of Reinforcing Steel to Concrete," PMFSEL Report No. 92-4, Phil M. Ferguson Structural Engineering Laboratory, University of Texas at Austin.

- Larbi, J.A., (1993), "Microstructure of the Interfacial Zone Around Aggregate Particles in Concrete," Heron, Vol.38, No.1, pp. 69.

- Leroy A., Lutz, and Peter Gergely.,(1967), "Mechanics of Bonds and Slip of Deformed Bars in Concrete," ACI Journal ,No. 64-62, pp. 711-721.

- Lutz, Leroy A.; Gérgely, Peter; and Winter, George.,(1966), "Mechanics of Bond and Slip of Deformed Reinforcing Bars in Concrete," Research Report No. 324, Department of Civil Engineenng, Cornell University, Ithaca, New York.

- Maslehuddin M., Ibrahim M. Allam, Ghazi J. Al. Sulaimani, Abdulaziz L. Al-Mana, and Sahel N. Abdulijauwad., (1990), "Effect of rusting of reinforcing steel on its Mechanical Properties and bon with Concrete," ACI Journal ,No. 87-M53, pp. 496-500.

- Mehta, P.K., (1981), "Studies on Blended Portland cement Containing Santorin Earth," Cement and Concrete Research, Vol.11, No.4, pp. 507-518.

- Mehta, P.K., (1986), "Concrete Structure, properties and Materials," prenticeHall Inc., New Jersy, Chapters 2 and 6.

- Morita S., Kaku T., (1979), "Splitting bond failures of large deformed reinforcing bars," ACI Journal 76(1), pp. 93-110.

- Neville, A.M., (1981),"Properties of Concrete," 3rd Edition, Pitman Publishing Ltd., London, Chapter 1.

- Park, R., and Paulay, T., (1975), "Reinforced Concrete Structure," Ultimate strength design of reinforced concrete structures, vol. 1, printed by the University of Canterbury for extension study seminars conducted for practicing structural engineers in New Zealand.

- Rehm G., (1968), "The basic principles of the bond between steel and concrete." Cement and Concrete Association, Translation No. 134, London, pp.66.

- Rehm, G., (1961), "Uber die Grunlagen des Verbundes Zwischen Stahl und Beton," Deutscher Ausschuss für Stahlbeton, Heft 138, Wilhelm Ernest und Sohn, Berlin

- Sarkar, S.L. and Aitcin, P.C., (1987), "Comparative Study of the Microstructures of Normal and Very High-Strength Concerts Cement," Concrete and Aggregates, Board Vol.32, 1953, pp. 285-297.

- Soretz, S., and Holzenbein, H., (1979), "Rib Dimension Influence on Bond and Bendability," ACI journal. Proceedings V. 76, pp. 87-91.

- Task Group Bond Models., (2000), "Bond of reinforcement in concrete." State of the art report.

- Welch G.B.and Patten B.J.F., (1967), "Reduction in concrete-Steel Bond with Horizontally Embedded Reinforcement,"UNCIV Report No R-8, university of New South Wales, pp 26.